Volume 19, Number 6
December, 1965

SOVIET ATOMIC ENERGY

АТОМНАЯ ЭНЕРГИЯ
(ATOMNAYA ENERGIYA)

TRANSLATED FROM RUSSIAN

CONSULTANTS BUREAU

PHYSICAL CHEMISTRY

RESEARCH IN SURFACE FORCES

Academician B. V. Deryagin, Editor

Volume 1:

"This volume is a welcome addition as a work of reference for research workers in the field of surface chemistry."
—Journal of Scientific Industrial Research

The 29 reports in this collection were presented at the conference on surface forces held at the Institute of Physical Sciences of the Academy of Sciences of the USSR. Following an introductory paper, the remaining 28 presentations cover results of investigations (theory and practice) on surface forces in various systems, their properties, and methods of investigations carried out by Soviet scientists. The editor, who has contributed to nearly half the papers in this volume, is an academician of the Academy of Sciences of the USSR, and is also organizer and permanent Director of the Laboratory of Surface Phenomena at the Institute. A Special Research Report translated from Russian.

CONTENTS: Introduction • General problems in surface forces • Polymer adhesion • Surface forces in thin liquid films • Surface effects in dispersed systems • Surface forces in aerosols.

190 pages CB 1963 $27.50

Volume 2: Three-Dimensional Aspects of Surface Forces

Consists of 38 of the papers read at the Second Conference on Surface Forces (Institute of Physical Chemistry, Academy of Sciences, November 1962). The selection of papers makes this a monograph on the three-dimensional aspects of surface forces. Consideration is given to general problems in surface forces and surface effects, as well as to the effects of these forces on the processes occurring at solid–liquid interfaces, at interfaces between these phases and gases, and on the properties of thin films. The collection is organized into five sections: Theoretical Problems (5 papers); Electrical Surface Forces (7 papers); Experimental Studies of the Properties of Thin Films (11 papers); Surface Phenomena in Dispersed and Porous Systems (6 papers); Surface Phenomena in Adhesion and Friction (9 papers). A Special Research Report translated from Russian.

Approx. 290 pages CB 1966 $27.50

(c/b) CONSULTANTS BUREAU 227 West 17th Street, New York, New York 10011

Declassified and Approved For Release 2013/03/15 : CIA-RDP10-02196R000700020006-0

SOVIET ATOMIC ENERGY

A translation of **ATOMNAYA ÉNERGIYA,**
a publication of the Academy of Sciences of the USSR

Volume 19, Number 6 December, 1965

CONTENTS

Annual Subscription: $95 **Single Issue: $30** **Single Article: $15**

CONTENTS (continued)

NOTE

The Table of Contents lists all material that appears in Atomnaya Énergiya. Items originally published in English or generally available in the West are not included in the translation and are shown in brackets. Whenever possible, the English-language source containing the omitted items is given.

The Russian press date (podpisano k pechati) of this issue was 12/6/1965. Publication therefore did not occur prior to this date, but must be assumed to have taken place reasonably soon thereafter.

THE DEVELOPMENT OF ACCELERATORS IN NOVOSIBIRSK*

GENERAL REVIEW OF THE PROJECT

(UDC 621.384.60)

G. I. Budker

Translated from Atomnaya Énergiya, Vol. 19, No.
pp. 497-498, December, 1965
Original article submitted October 15, 1965

Part of the program of the Institute of Nuclear Physics, Siberian Division of the Academy of Sciences, USSR, devoted to accelerators, consists in the development of plasma accelerators, iron-free pulsed accelerators, facilities with colliding particle beams and special accelerator facilities for industry.

The Institute for Nuclear Physics has existed in Siberia since 1961, but operations were commenced several years earlier in Moscow in the Laboratory for New Methods of Acceleration, I. V. Kurchatov Institute of Atomic Energy, from which the Novosibirsk Institute was subsequently organized.

Operations on plasma accelerators are undertaken with facilities for investigating the so-called stabilized electron beam. The basic idea of these operations consists in an attempt to utilize the powerful field of the self-focussing closed relativistic electron beam for retaining the accelerated ions in orbit. These operations are proceeding more slowly than would be desired. At present it can only be reported that we have produced a closed beam of relativistic electrons at 130 A. At the present time the assembly of the high-voltage internal injector on a spiral ridge apparatus is completed and during next year we are hoping to increase several times the magnitude of the circulating current. This makes it possible to proceed with a study of the phenomenon of constriction of the beam into a narrow cord.

Operations on iron-free accelerators are being concentrated principally around single-turn accelerators with shaping of the magnetic field by the form of the conducting surfaces, which should be accomplished by virtue of the small thickness of the skin layer as a result of operating the accelerator on short pulses.

At the previous conference we spoke about certain accelerators being started-up in Novosibirsk. Moreover, a number of models have been tested for planning electron accelerators, including accelerators with colliding proton beams.

As a result of these operations, confidence has built-up that for our type of laboratory the installation of high-energy iron-free proton accelerators is certainly more reasonable than the installation of iron proton accelerators. Certain experimental advantages of iron-cored accelerators by no means compensate for the many-fold increase of the cost in comparison with the cost of iron-free accelerators.

However, we have ceased development of a project for an iron-free proton accelerator of 500-1000 GeV with a field of 200 kgauss and also an iron-free accelerator with colliding proton beams of $2 \cdot 12$ GeV associated with advances in the creation of superconductors. It may prove that during the time of construction of the high-energy pulsed accelerator the technology and manufacture of superconducting materials will attain such a level that iron-free pulsed accelerators might depreciate due to absolescence as they are constructed. In the solution of this problem we are standing at the crossroads.

Lately, we have obtained extremely satisfactory results in the development of accelerators for industrial purposes. Recently, we have started up an electron accelerator of the high-voltage transformer type with a tube operating at the commercial frequency of 50-60 cps, with an electron energy of 1.5 MeV and a beam intensity of 25 kW extracted in air. The efficiency of the accelerator exceeds 90%. The outside of the accelerator is a tank with a diameter of 1.2 m and a height of 2.0 m without any external high-voltage or electronic equipment whatsoever. In

* Report read by G. I. Budker at the International Conference on High-Energy Accelerators (Frascati, Italy).

the near future it is proposed to start up an accelerator of this same type with an energy of 3 MeV, and also a similar pulsed accelerator with considerably smaller dimensions. We are also proposing to utilize the accelerators as electron and positron injectors in a synchrotron.

At the present time, two colliding beam devices are operating in the Institute. Experiments are being carried out on the VÉP-1 electron-electron colliding beam apparatus concerned with the scattering of electrons by electrons at large angles. Experiments have only just commenced on the VÉPP-2 electron-positron colliding beam equipment, with a maximum energy of 2 · 700 MeV. An assembly is planned for light particles at high energies, and also colliding proton beam equipment.

In all the devices we do not combine in any way the injection energy with the limiting energy of the storage device. The energy of the injector is considerably lower. Acceleration up to the limiting energy is accomplished in the storage device by raising the magnetic field after accumulation of the particles. This will be managed quite inexpensively and it will complicate operation only trivially.

The experiments on colliding beams are being carried out under the direction of A. A. Naumov and the author of this paper.

OPERATIONAL STATUS OF THE VEP-1 ELECTRON STORAGE RINGS

G. I. Budker, N. A. Kushnirenko, A. A. Naumov,
A. P. Onuchin, S. G. Popov, V. A. Sidorov,
A. N. Skrinskii, and G. M. Tumaikin

Translated from Atomnaya Énergiya, Vol. 19, No. 6,
pp. 498-502, December, 1965

At the last accelerator conference in 1963, a report was given on the construction of the VEP-1 machine intended for electron-electron scattering experiments at energies up to 2 · 130 MeV [1]. By that time, the first experiments on electron storage in a single magnetic track had been carried out with the machine. In the work which has gone on during the past two years, it is possible to distinguish the following basic stages: simultaneous storage of electrons in the two tracks, an investigation of some of the interaction effects of the two beams [2], and measurements of the luminosity of the machine for electron-electron scattering in the angular range 45-90°.

The VEP-1 machine. A general sketch of the machine is shown in Fig. 1. Its basic elements are two paired, high-vacuum, magnetic tracks, a special B-2S electron synchrotron, an electron-optical channel, and a system for single-turn extraction of the beam from the accelerator and for injection into the storage rings [1, 3].

The radius of the storage ring magnetic tracks is 43 cm, and the aperture, 3 · 4 cm. Opposite the point of tangency of the orbits, slits have been made in the common portion of the magnet poles in order to extract the electrons scattered at the point of intersection of the beams. The median plane of the storage rings is vertical.

The storage ring resonators operate at the second harmonic of the electron rotational frequency. In addition to resonators and inflectors, each storage ring is equipped with several mechanical probes, a system for optical observation of the beam, plates for controlling the position and transverse dimensions of the beam, and apparatus for varying and measuring the frequency of the betatron oscillations of the particles. The problems of electron beam observation in a storage ring and of controlling the parameters of the beam are given in [4].

The energy at which the electrons are injected in the storage ring is 43 MeV. A special, iron-free, B-2S synchrotron with spiral electron storage [3] is used as an injector. The current extracted from the synchrotron beam in a pulse less than 5 nsec long is about 300 mA (more than 10^{10} particles). The energy spread does not exceed 0.2%. The accelerator pulse repetition rate is once every 15 sec.

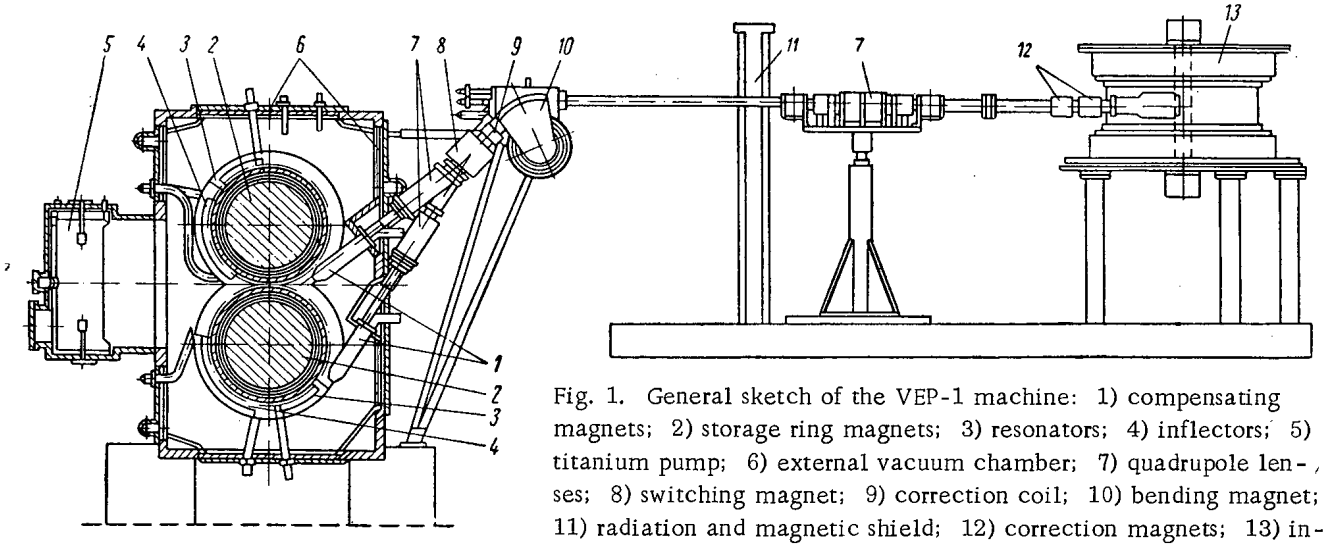

Fig. 1. General sketch of the VEP-1 machine: 1) compensating magnets; 2) storage ring magnets; 3) resonators; 4) inflectors; 5) titanium pump; 6) external vacuum chamber; 7) quadrupole lenses; 8) switching magnet; 9) correction coil; 10) bending magnet; 11) radiation and magnetic shield; 12) correction magnets; 13) injector – B-2S synchrotron.

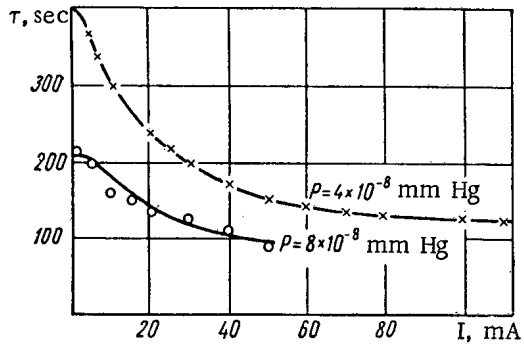

Fig. 2. Electron lifetime as a function of the amount of beam current; energy, 43 MeV; resonator voltage, 5 kV.

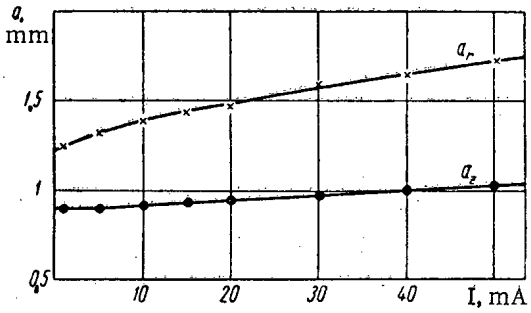

Fig. 3. Radial (a_r) and axial (a_z) dimensions of a bunch as a function of the amount of beam current; energy 43 MeV, $P = 8 \cdot 10^{-8}$ mm Hg.

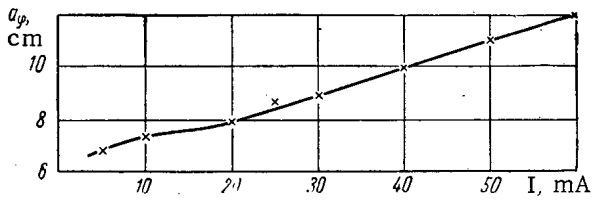

Fig. 4. Azimuthal dimension of a bunch as a function of the amount of beam current; energy, 43 MeV; resonator voltage, 5 kV.

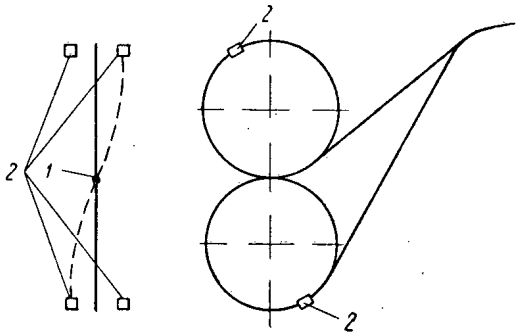

Fig. 5. Diagram of counter locations for recording electron-electron scattering at small angles: 1) point of intersection; 2) scintillation counters.

A great deal of the work with a beam in the storage rings was carried out at the injection energy. In that situation, each injector pulse was used for the addition of electrons into one of the tracks of the storage rings. Work at higher energies was broken down into cycles approximately 10 min long. Only half the cycle time was used for measurement; the rest of the time was taken up by electron storage and by variation of the magnetic field intensity in the tracks.

Electron storage. Despite the fact that one has managed to inject a current greater than 100 mA into the storage rings in a single pulse, the average injection pulse does not exceed 10 mA. The stability of the injection mode leaves room for improvement. The maximum current in either of the tracks of the storage rings has been 200 mA. A limitation is imposed by the instabilities which arise through interaction of the beam with the reasonator [5].

The dependence of electron lifetime in the storage rings on the amount of beam current is shown in Fig. 2 for an energy of 43 MeV.

A representation of the transverse dimensions of the beam at 43 MeV and their dependence on the amount of stored current is shown in Fig. 3. The measurements were made by means of a photomultiplier and a high-speed shutter, on which an image of the observed beam was projected, located in front of the photomultiplier. The results are in agreement with estimates of the deterioration of the vacuum in the beam because of compensation of its charge by ions of the residual gas.

The radial dimension of the beam is greater than the axial because of the contribution of radial phase oscillations. Their amplitude also increases with increasing beam current as can be seen from Fig. 4 which shows the dependence of azimuthal dimensions of a bunch on the amount of beam current. The measurements were made with a resolution of about 1 cm by means of an electron-optical converter. It is of interest to note that an artificial increase in transverse dimensions of the beam leads to a reduction of the phase dimensions of a bunch.

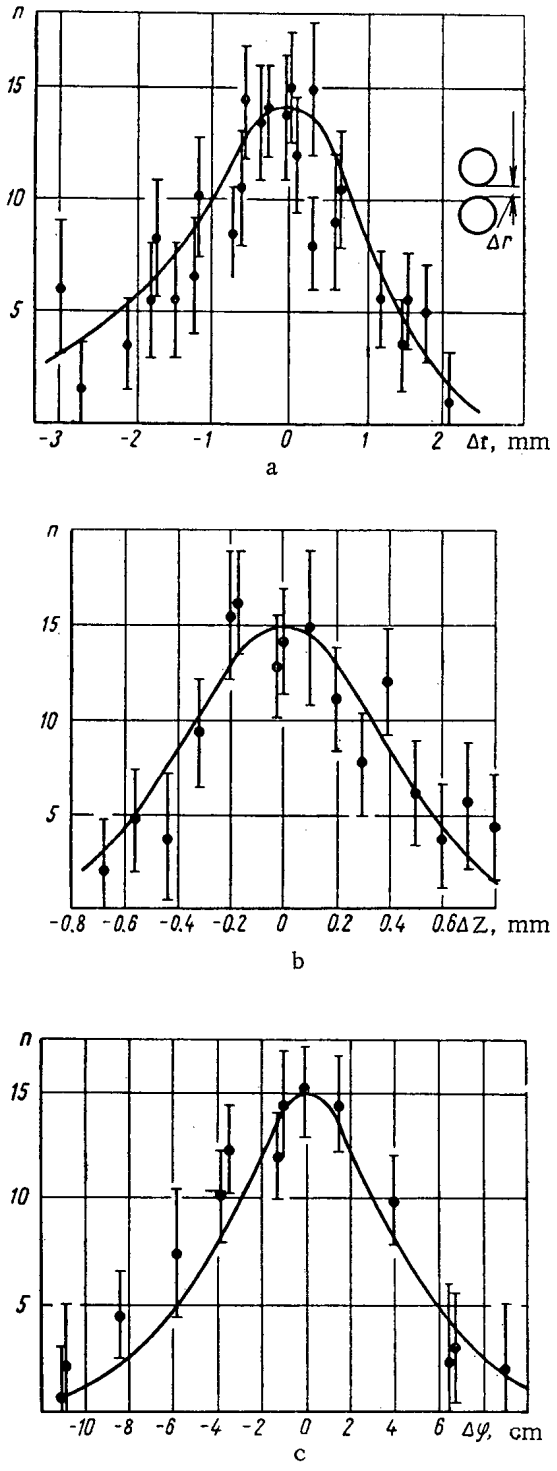

Fig. 6. Dependence of intersection efficiency on beam thinning in the radial (a) and axial (b) directions and on thinning out of bunches in phase (c). The number of counts per millicoulamp is plotted on the ordinate; measurements were made for approximately 15 mA currents in each beam; the solid lines are calculated curves; normalization was done at the maximum count.

With an increase in electron energy, the transverse beam dimensions are reduced. In our case, this leads to an increase in the role of the ADA effect and to a sharp reduction in beam lifetime. Artificial increase in the radial dimension of the beam saves the situation.

Luminosity measurements. The final adjustment of the machine, and check on the efficiency of the intersection process, is performed by observing electron-electron scattering at small angles. The large cross section for this process makes it possible to find the optimal operating conditions without significant expenditure of time while varying the numerous parameters of the machine.

The experimental geometry is shown in Fig. 5. Each magnetic track of the storage rings had two scintillation counters located at a quarter of a betatron oscillation from the point of intersection on the beam path. The counters were connected in pairs in two coincidence circuits with an effective resolving time $2\tau = 4.5$ nsec (the spacing between two bunches in orbit).

The counter system recorded pairs of electrons which were scattered at an angle of approximately 1.5°. The effective scattering cross section, integrated over the angle covered by the two pairs of counters, was $200/\gamma^2$ b, or 30 mb, 43 MeV electrons. The work was done at a background level (random coincidences) comparable to the magnitude of the signal. The background was measured by parallel coincidence circuits with a delay in one of the branches.

The number of counts in such a system, normalized to the integral of the product of the two beam currents over the time of measurement, can serve as a measure of the efficiency of the intersection process. A convenient unit of measurement for this integral is the coulamp (short for coulomb-ampere). In an hour of operation, the machine can produce up to 3 coulamps. The average current in each of the tracks is about 30 mA. Operation at higher currents is inefficient because of the rapid intensification of "intersection effects" [2].

In Fig. 6 are shown the results of measurements of the intersection efficiency as a function of beam displacements in the radial and axial directions and of phase separation of the bunches. The shape of the curves is in good agreement with data on bunch dimensions. The absolute value of the counts is several times less than expected. The discrepancy, apparently, can be attributed to the inaccuracies of the geometrical conditions of the experiment. A suggestion having to do with coherent oscillations of a special kind which reduce intersection efficiency is in disagreement with data on the effect of transverse beam dimensions on intersection efficiency. Independently of the fact that an increase in transverse dimensions might be produced by artificial excitation of betatron oscillations or by intersection effects [2], the ob-

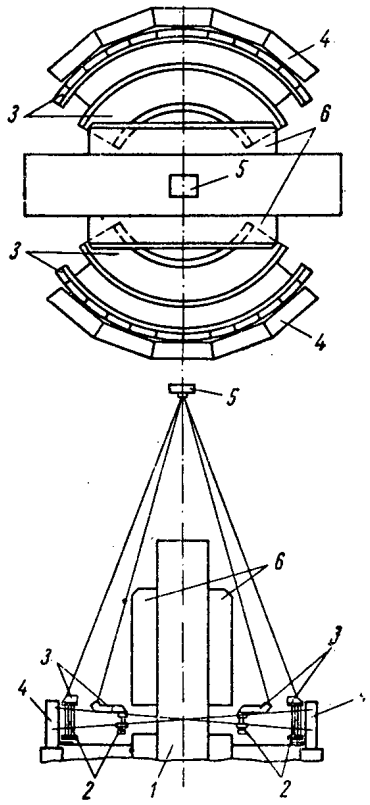

Fig. 7. Diagram of the arrangement of the detection system: 1) vacuum chamber; 2) spark chambers; 3) prisms; 4) scintillation counters; 5) camera; 6) magnet for upper track.

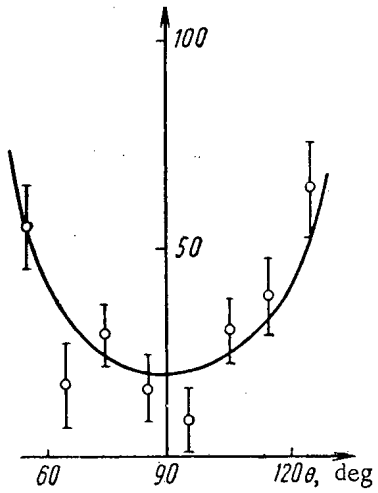

Fig. 8. Angular distribution of electron-electron scattering. A calculated curve for the Moeller cross section is shown.

served reduction in counting rate is in good agreement with calculations performed for "purely incoherent" dimensions.

The value of the luminosity, defined as the quotient of the division of the observed count rate by the effective cross section for the process, was, in order of magnitude, 10^{27} cm^{-2} · sec^{-1}. It agreed with the initial results of experiments on double bremsstrahlung observed in electron-electron scattering.

Initial electron-electron scattering experiments. In Fig. 7 is shown a diagram of an experiment to measure the angular distribution for electron-electron scattering in the range 45-90°. The detection system consisted of four cylindrical spark chambers with a vertical axis which passed through the point of intersection of the beams. A camera objective was located on the same axis; the prism system used had axial symmetry. A second coordinate of the track was measured by means of tilted mirrors which were located underneath the spark chambers.

Triggering of the spark chambers was accomplished by a coincidence circuit which was connected to two groups containing five scintillation counters each.

The solid angle of the detection system was limited by the aperture of the slit in the body of the storage ring magnet. The effective cross section of Moeller scattering, integrated over that solid angle, was $100/\gamma$ mb.

In the first experiments, performed at an electron energy of 43 MeV, the spark chamber system was triggered more than 300 times per coulamp; further, about 10 pictures corresponded to the detection of electron-electron scattering, which did not disagree with our ideas about the value for the luminosity of the machine. Test measurements with phase thinning of the electron bunches showed that the background did not exceed 10%. The result of preliminary analysis of the pictures is shown in Fig. 8. It is clear that the deviation from the calculated curve for electron-electron Moeller scattering does not exceed the statistical error.

At the present time, experiments at an electron energy of 100 MeV are getting under way on the machine.

LITERATURE CITED

1. V. N. Baier et al., Proceedings of the International Conference on Accelerators (Dubna, 1963) [in Russian], Moscow, Atomizdat (1964), p. 274.

2. G. N. Kulipanov, Experimental data on the interaction of beams at intersection [in Russian], Report Presented by the USSR at the International Conference on Accelerators, Frascati (1965).
3. E. A. Abramyan et al., see [1], p. 1065.
4. E. I. Zinin et al., System for control and monitoring parameters of the electron beams in the VEP-1 storage rings [in Russian], Report Presented by the USSR at the International Conference on Accelerators, Frascati (1965).
5. V. L. Auslender et al., Report Presented by the USSR at the International Conference on Accelerators, Frascati (1965).

OPERATIONAL STATUS OF THE VEPP-2 POSITRON-ELECTRON STORAGE RINGS

V. L. Auslender, G. A. Blinov, G. I. Budker,
M. M. Karliner, A. V. Kiselev, A. A. Livshits,
S. I. Mishnev, A. A. Naumov, V. S. Panasyuk,
Yu. N. Pestov, V. A. Sidorov, G. I. Sil'vestrov,
A. N. Skrinskii, A. G. Khabakhpashev, and I. A. Shekhtman

Translated from Atomnaya Énergiya, Vol. 19, No. 6,
pp. 502-505, December, 1965

The construction of the VEPP-2 machine planned for experiments with positron-electron interactions at energies up to 2 · 700 MeV has been reported [1]. In the work that has gone on in the past two years, the following fundamental stages can be pointed out: start-up of the synchrotron-injector; production of large electron currents in the storage rings; investigation of the instabilities associated with the beam-resonator interaction [2], and positron storage. At the present time, work is going forward with the VEPP-2 machine on a study of the interactions of the two beams and on measurement of the luminosity by positron-electron scattering at small angles.

VEPP-2 machine. An overall diagram of the machine is shown in Fig. 1. It consists of a B-3M synchrotron with external injector, high-vacuum magnetic storage rings, a system for single-turn extraction of the beam from the synchrotron and its injection into the storage rings, an electron-optical channel, and a converter for transforming an electron beam into a positron beam. All these elements have been described in detail [1, 3].

The special B-3M synchrotron used as accelerator-injector is operating at the present time at a reduced level with energies up to 200 MeV; the current extracted from the synchrotron beam in a pulse less than 20 nsec long reaches 100 mA (more than 10^{10} particles); the energy spread does not exceed 0.2%; the repetition rate of the acceleration pulses is ~3 Hz. Work on the start-up of the B-3M synchrotron is the subject of a report presented at the conference on accelerators in 1963 [4].

The storage ring is a weak-focussing racetrack with four identical straight sections. The radius of the equilibrium orbit is 150 cm, the length of the straight sections, 60 cm, and the chamber aperture is 8 · 14 cm². Two straight sections are used for the injection of electrons and positrons; a high-frequency resonator is located in the third, and the straight section opposite the resonator is intended for experimental work.

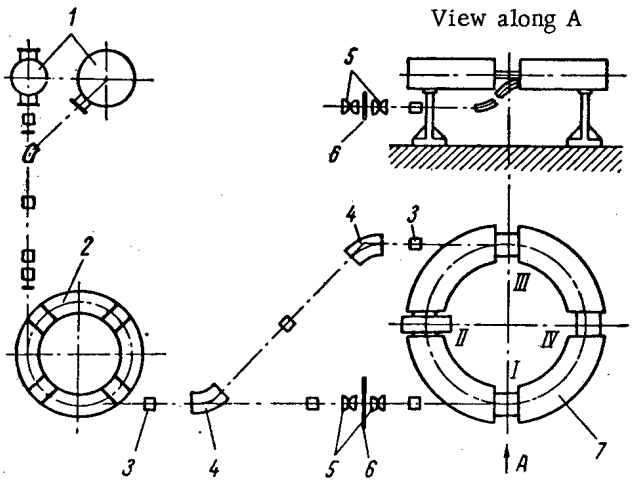

Fig. 1. General diagram of the VEPP-2 machine: 1) injectors; 2) B-3M synchrotron; 3) quadrupole lenses; 5) parabolic lenses; 4) bending magnets; 6) converter; 7) storage ring.

The high-frequency system of the storage ring operates at the first harmonic of the particle rotational frequency, 25.1 MHz. The resonator is coaxial, half-wave, and highly loaded by a two-disc condenser; Q is about 4000. At the present time, a 20 kW high-frequency generator is being used which delivers voltages up to 35 kV to the resonator.

In each quadrant, the two internal windings of the electromagnet coil are supplied individually, which ensures displacement of the median plane in each quadrant by ±1 cm. The actual position of the orbit is adjusted by shunting the appropriate quadrants. To control the relative position of the electron and positron orbits in the vertical, in quadrants not having inflector plates, "separating plates" have been installed

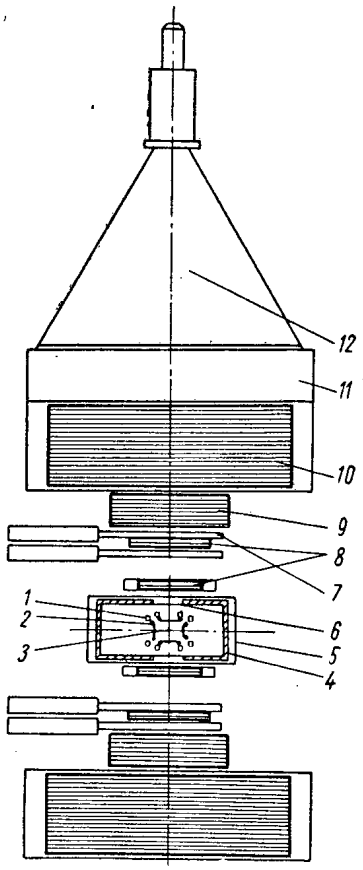

Fig. 2. Vertical section of the collision region and detection system; 1) current windings; 2) electrostatic quadrupole; 3) colliding beams; 4) internal vacuum chamber; 5) external vacuum chamber; 6) "window"; 7) scintillation counter; 8) "thin" spark chambers; 9) shower chamber; 10) range chamber; 11) shield; 12) scintillation counter.

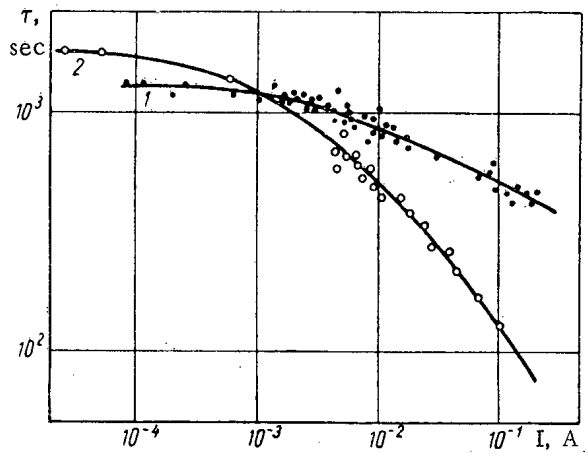

Fig. 3. Electron lifetime as a function of the amount of beam current: 1) 100 MeV; 2) 200 MeV.

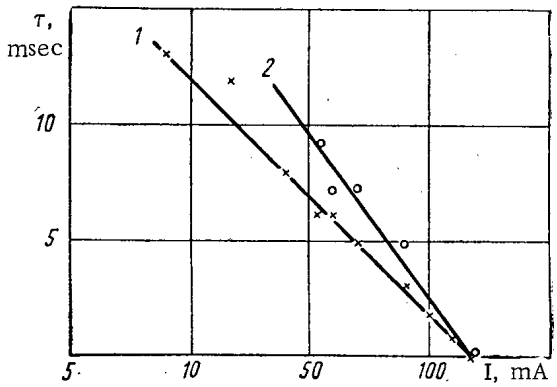

Fig. 4. Dependence of damping time on beam current with (1) and without (2) ions present.

on which dc voltages up to 50 kV can be applied making it possible to control the collision angle of the electron and positron beams at the point of intersection to 10^{-2} rad, and also to separate the beams for storage.

By means of eight current windings located in the straight section where the beams collide (Fig. 2), it is possible to control the frequency of betatron oscillations in the range $\Delta\nu \approx 0.1$, and also to produce a frequency dependence on the radius $(d\mu/dR) \approx 0.03$ (quadratic nonlinearity) and amplitude of the betatron oscillations $[d\mu/d(a^2)] \approx 0.04$ (cubic nonlinearity). In the same straight section, an electrostatic quadrupole has been installed making it possible to separate the betatron oscillation frequencies of the electron and positron beams by $\Delta\nu \approx 0.05$. (The numerical data given refers to an electron energy of 100 MeV.) In the rest of the system, control and monitoring of beam parameters is similar to that used for the VEP-1 machine [5].

The long lifetime of the beam makes it possible to decouple the operating energy of the storage ring from the injection energy. The required operating energy is established by an increase in the magnetic field after storage.

Electron storage. The basic work in studying the process of injection into the storage ring was carried out at 100 MeV. This energy corresponds to a radiation damping time of about 1 sec for the betatron oscillations, which also determines the selected repetition rate for the injection cycle, 0.5 Hz. The electron storage rate achieved on the machine was approximately 30 mA per injection pulse.

An electron current of about 0.5 A (10^{11} particles) was obtained in the storage ring. Limitations arose because of the instabilities that were reproduced by beam-resonator interactions [2]. Transverse beam instabilities were not observed.

If the betatron oscillation frequencies are well removed from dangerous resonance values, the electron lifetimes for the natural dimensions of the machine and for currents greater than 1 mA are determined mainly by the ADA effect [6]. The dependence of electron lifetime on the amount of beam current is shown in Fig. 3. The lifetime is 450 sec for a current of 100 mA and an energy of 100 MeV. The curves were obtained at a vacuum of approximately $3 \cdot 10^{-8}$ torr, which was obtained without baking the chamber. After baking, the lifetime was more than 3 h for small currents. Then the energy of the stored beam was increased to 550 MeV for a resonator voltage of 20 kV. The increased beam energy caused intense outgassing from the walls of the storage ring vacuum chamber which was reduced by extended treatment.

When working with intense electron beams in the VEPP-2 storage ring, an interesting phenomenon was observed. When beam betatron oscillations occurred in a time which was much less than the natural radiation damping time. In Fig. 4, the dependence of damping time on the amount of stored current is shown with and without ions present. A dependence of damping time on betatron oscillation frequencies far from dangerous resonances was not observed within the limits of accuracy of the measurements. It is possible that this effect is associated with resonance excitation of electromagnetic oscillations in vacuum chamber elements.

Positron storage. The electron beam is converted into a positron beam by a tungsten foil located in the focal plane of two "parabolic" lenses; the foil thickness is about one radiation unit [1]. For a focal distance of 10 cm, the beam diameter at the converter foil is not greater than 1 mm. Inclusion of the lenses increases the injection efficiency about 20 times.

Work is going on with 200 MeV electrons and 100 MeV positrons. The positron storage rate that has been achieved is about 0.3 μA per injection pulse, corresponding to a conversion coefficient efficiency of 10^{-5}. The maximum positron current recorded in the storage ring was 0.4 mA (10^8 particles).

At the present time, work is being done on increasing the positron storage rate.

Experimental arrangements. In order to carry out experiments involving the investigation of positron-electron interactions, a system of spark chambers has been assembled which covers a solid angle of $2 \cdot 0.7$ sr about the vertical direction.

First along the path of escaping particles (see Fig. 2) are spark chambers with thin plates for the determination of the flight angle of the particles and the coordinates of the interaction point. A magnetic field directed along the line of the beam intersection permits one to determine the sign of the charge on the detected particles. It will be possible to determine the type of particle by the nature of its interactions with the material in the plates of the "shower" and "range" spark chambers. A rather complicated system of mirrors makes it possible to use a single camera.

Triggering of the entire spark chamber system is produced by four scintillation counters $40 \cdot 40$ cm^2 in size connected in a coincidence circuit. An anticoincidence counter $120 \cdot 120$ cm^2 acts as a shield against cosmic radiation. Between this counter and the chambers, there is a layer of lead 20 cm thick.

At an energy of $2 \cdot 300$ MeV and storage ring currents of $1 \cdot 100$ mA^2, such a chamber system enables one to detect several positron-electron elastic scattering events per hour. The same order-of-magnitude counting rate is expected for π-meson pairs at the maximum of the cross section curve corresponding to the formation of the intermediate ρ-meson.

For adjusting beam intersection in the storage ring, for measuring luminosity and controlling it afterward during operation, a system has been set up to measure positron-electron scattering at small angles similar to the one used with the VEP-1 machine [7]. The scintillation counters in this system, located in the injection straight section of the storage ring, are planned for detection of positron-electron pairs which have undergone scattering at approximately 1.5°.

To reduce overloading by the intense electron beam, the positron counter is shielded by lead and separated into two individual counters located 10 cm from one another along the beam path and connected in coincidence. A preliminary study of background conditions indicates a satisfactory state of affairs.

LITERATURE CITED

1. V. L. Auslender et al., Proceedings of the International Conference on Accelerators (Dubna, 1963) [in Russian], Moscow, Atomizdat (1964), p. 247.

2. V. L. Auslender et al., Phase instability of an intense electron beam in a storage ring [in Russian], Report Presented at the International Conference on Accelerators, Frascati (1965).
3. G. I. Budker et al., Proceedings of the International Conference on Accelerators (Dubna, 1963) [in Russian], Moscow, Atomizdat (1964), p. 1065.
4. G. I. Budker et al., Start-up of the B-3M synchrotron – an injector for the positron-electron storage ring [in Russian], Report Presented at the International Conference on Accelerators, Frascati (1965).
5. E. I. Zinin et al., System for control and monitoring electron beam parameters in the VEP-1 storage ring [in Russian], Report Presented at the International Conference on Accelerators, Frascati (1965).
6. C. Bernardini et al., Phys. Rev. Letters, 10, 407 (1963).
7. G. I. Budker et al., Operational status of the VEP-1 electron storage rings [in Russian], Report Presented at the International Conference on Accelerators, Frascati (1965).

A HIGH-CURRENT POSITRON SOURCE

G. I. Budker

Translated from Atomnaya Énergiya, Vol. 19, No. 6,
pp. 505-507, December, 1965

The method used for obtaining positrons with the BEPP-2 machine and other accelerators has an important defect – the low coefficient for conversion of the initial electron beam into the narrow, almost monochromatic, positron beam needed for injection into an accelerator or storage ring.

The method proposed below for obtaining almost monochromatic positrons in a narrow angular interval this failing and is a practical solution for the problem of positron storage. In addition, it offers the possibility of constructing positron accelerators or of converting existing accelerators into positron accelerators of the same intensity.

The essence of the method is that positrons, produced from a beam of electrons of relatively low energy (5-10 MeV) in a broad range of angles and energies, are slowed down in a special target to thermal or epithermal velocities, are extracted from the target by an electrical field, and are then accelerated to injection energy.

Special attention should be directed to positronium formation and the combination of gas molecules with positrons leading to removal of positrons from the system. By choice of gas, it is possible to make the formation of positronium during slowing down sufficiently small,because positronium is not formed at positron energies below a certain value (9 eV for argon). In those cases where an electric field is applied, the magnitude must be chosen so that the positron temperature is less than this threshold.

Even in noble gases, the positron enters into chemical combination with the gas, forming an ionized molecule. However, this process begins at energies below 1.5 eV. By chance coincidence of the numerical parameters, the time for slowing down from 9 to 1.5 eV because of elastic collisions of positrons with molecules is close to the annihilation lifetime for positrons so that one can neglect this effect. The presence of an electric field produces heating of the positron gas to several electron-volts, and the effect of molecule formation is additionally diminished.

There are two possible methods for carrying out this idea as well as a combination of the two.

The first method – a continuous one – involves an electric field applied to the target (gaseous, as a rule) so weak that the equilibrium positron energy will be below the threshold for positronium formation. This requirement defines a maximum positron drift velocity in the electric field which is independent of pressure. Because of mobility, the weak electric field draws the slow positrons to the edge of the target. In the case of gaseous targets, a sharp boundary is formed by differential pumping or by chilling. Since all the positrons approach the target boundary with practically zero energy, they form a parallel, monochromatic beam by further acceleration in a uniform electric field.

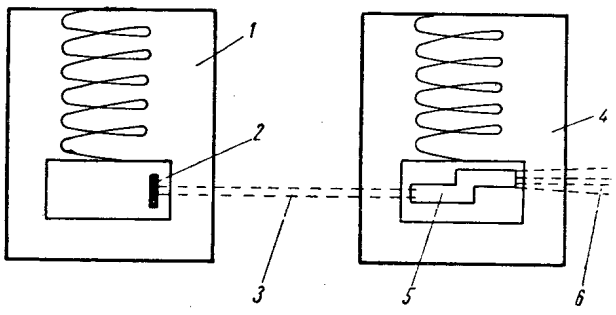

Fig. 1. Sketch of positron source: 1) accelerator; 2) electron source (cathode) at a voltage of $3 \cdot 10^6$ V; 3) 1 A electron beam emerging from accelerator and incident upon apparatus for converting electrons into 6 MeV positrons; 4) 3 MeV tandem accelerator; 5) apparatus for converting electrons into positrons, maintained at $3 \cdot 10^6$ V; 6) positron beam, accelerated to 3 MeV.

The target length and the gas pressure within it are determined by the fact that a positron must succeed in escaping from the target during its lifetime while moving in the gas with drift velocity. Since the positron drift velocity is fixed, the time to escape from the target is inversely proportional to target length. The positron lifetime in the target is inversely proportional to the density. By equating these times, it is possible to find the target thickness (g/mm^2) which is approximately equal to the slowing down distance for positrons with an energy of several hundred keV. By locating the target in a magnetic

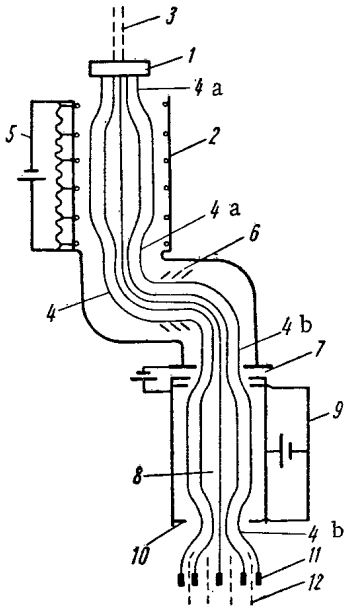

Fig. 2. Diagram of apparatus for converting electron to positrons; 1) solid converter; 2) gaseous target of the first kind; 3) 6 MeV electron beam; 4) magnetic field lines; 4a, 4b) magnetic mirrors; 5) potentiometer for longitudinal, extraction electric field; 6) system for producing a sharp pressure drop by pumping or chilling; 7) electrodes for accelerating slow positrons to 10 keV; 8) rarefied gaseous trap of the second kind; 9) electrostatic plugs for confining slow positrons; 10) system for rapid extraction and acceleration of stored positrons; 11) a system of magnetic louvers which close the magnetic field for the ejection of positrons into space; 12) positron beam.

trap which lengthens the path of fast neutrons, it is possible to slow down positrons with energies up to 500 keV and more in the same thickness. With an initial electron energy of 6 MeV, it is therefore possible to slow down a large part of the positrons emitted from the converter. The effective coefficient for the conversion of electrons into a narrow beam of positrons in this case is of the order of $3 \cdot 10^{-5}$. Its smallness is associated with the low initial electron energy and the correspondingly small number of positrons emitted from the converter. With increasing initial electron energy, the conversion coefficient rises sharply. In the case of a solid target, it is impossible to use the effect of a magnetic trap; however, the simplicity of a solid target as compared with a gaseous one is deserving of consideration. Unfortunately, in solids, the slowing down process, positron annihilation, and drift in an electric field are considerably less clear than in gases.

In the second, pulsed method, the target is located beforehand in a magnetic and electrostatic trap which captures fast positrons and does not emit slow ones. Initially, no extraction field of any kind is applied to the gaseous target. Positrons in the target are stored for a time of the order of their lifetime. This time is 1 msec at an argon pressure of 1 torr. Then the positrons are extracted from the target by a short, pulsed, longitudinal electric field. This makes it possible to increase the pulsed value of the positron current in the ratio of storage time to injection time. This ratio is large for linear accelerators and especially so for cyclic accelerators with one-turn injection.

To increase the storage time, it is necessary to make the target sufficiently rarefied. For practically reasonable values of length (1 m) and pressure which correspond to a lifetime of 1 msec, positrons with an energy of several tens of keV are slowed down in the target. Therefore, it is possible to consider a combination of the first and second methods where positrons with energies of the order of 500 keV are slowed down in a trap of the first kind with an extracting electric field and, being accelerated to 10 keV, arrive in a trap of the second kind where they are once again slowed down to thermal velocities and stored for 1 msec.

To illustrate the proposed method, we present a scheme for the combined method without discussing the problem of reasonable choices for the numerical values of the parameters.

We have two 3 MeV electron accelerators with a current of 1 A in a pulse 1 msec long. It is required to obtain a narrow, monochromatic beam of positrons with maximum intensity in a pulse $3 \cdot 10^{-8}$ sec long for single-turn injection into a synchrotron. Just such a problem is presented by our machine with colliding electron-positron beams, and the necessary equipment was set up. With the usual method of conversion, it is possible to obtain a positron current of the order of 10^{-6} A.

A diagram of the pertinent equipment is sketched in Fig. 1, and a diagram of the equipment for converting electrons into positrons is shown in Fig. 2.

The length of each trap is ~1 m. Pressure in the first trap is 100 torr (argon or xenon), in the second, it is less than 1 torr. The coefficient for the conversion of electrons in target 1 (see Fig. 2) into positrons with energies that could be slowed down in the gas, including positron capture in the magnetic traps, is of the order of $3 \cdot 10^{-5}$. Storage time in the second trap is of the order of 1 msec; the time required for injection into the synchrotron is $3 \cdot 10^{-8}$ sec; the ratio of the times is $3 \cdot 10^{4}$, and the conversion coefficient is ~1. Therefore the apparatus considered above makes it possible to inject a 1 A current of 3 MeV positrons which exceeds the electron current in ordinary synchrotrons and which matches the maximum electron current in the B-3M accelerator at the Institute of Nuclear Physics, Siberian Section, USSR Academy of Science.

For higher initial electron energies, the conversion coefficient rises sharply, and the positron current begins to be limited by the Langmuir law or by plasma phenomena.

We have developed a model of the electron-to-positron converter on which experiments will be begun in the near future.

Note added in proof. After this report was presented at the conference in Frascati, we discovered that a similar method for the production of narrow, monochromatic positron beams by slowing down fast neutrons in a gas was proposed by F. P. Denisov, P. A. Cherenkov, and A. M. Gromov at the end of 1964 (unpublished).

At the same time, we discovered that K. Robinson, in February 1965, put forward the idea of positron storage in a high-vacuum magnetic trap using radiation damping (Preprint CEAL-1016).

EXPERIMENTS ON CHARGE-EXCHANGE INJECTION OF PROTONS INTO A STORAGE RING

G. I. Budker, G. I. Dimov, A. G. Popov,
Yu. K. Sviridov, B. N. Suhkina, and I. Ya. Timoshin

Translated from Atomnaya Énergiya, Vol. 19, No. 6,
pp. 507-510, December, 1965

Charge-exchange injection of protons into a storage ring was achieved in August 1964 on an experimental machine, a diagram of which is shown in Fig. 1.

The first experiments were carried out on a weak-focussing storage ring with an aperture 8 · 4 cm and orbital radius of 42 cm. A hydrogen jet was used as an ionizing target which was directed along a radius from the center of the ring and which was switched on by means of an electrodynamic gate in a time of 300 to 600 μsec. The transverse dimension of the jet at the orbit was ~1 cm. The proton yield in the orbit rose with increasing jet density. Monitoring of the proton beam showed that it diverged after emerging from the ionizing target because of the latter's finite thickness, expanded radially to 1.7 cm after a quarter wave length of the radial betatron oscillations, and was focussed to the original transverse dimension in 3-4 mm more than a half wave length. The vertical transverse dimension of the beam in the first revolution (3-4 mm) was practically unchanged, and there was no noticeable loss of protons.

For charge-exchange injection into a storage ring without an accelerating field (quasi-betatron mode), the protons moved in a tightening spiral because of energy loss in the jet. Proton storage in this mode was observed by the luminous intensity of the hydrogen jet, which was detected by a photomultiplier, and also by broad-band induction electrodes and targets at the inner wall of the circular chamber. For 1 MeV protons and injection length of 20 μsec (100 revolutions), Fig. 2 shows oscillograms of the negative ion current in front of the neutralizing target (a), of the proton current from the ionizing target (b), of the luminous intensity of the jet (c), and of the proton current at the internal target (d). From the oscillogram of jet luminosity and from the corresponding induction electrode signals, it is clear that during the 100 revolutions when the beam was being introduced into the storage ring, the orbital current increased linearly and then remained constant for ~150 revolutions. During that time, the orbital radius was reduced (which was observed by means of vertical induction electrodes), but the beam had not yet reached the internal target. Then the beam struck the internal target. The charge incident on the internal target was 100 times greater than the charge in the proton beam during the first revolution. The signal amplitude from the induction electrodes during storage was also 100 times greater than the signal with a baffle introduced at the end of the first revolution. The accuracy of these measurements was ~10%. The photomultiplier signal, which recorded the jet luminosity, increased only by 40-50 times during storage, which is apparently associated with the difference in the transverse distribution of the stored proton current and of the current in the first revolution. Similar relationships were obtained for injection up to 250 revolutions. Thus the injection efficiency is close to 100% for charge-exchange injection in the quasi-betatron mode.

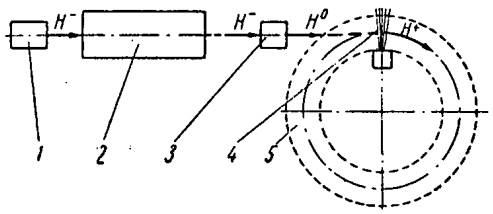

Fig. 1. Diagram of the machine for charge-exchange injection of protons into a storage ring: 1) source of negative hydrogen ions; 2) accelerator; 3) input gaseous target; 4) hydrogen jet in orbit; 5) storage ring.

Change-exchange injection of protons in the resonance mode was achieved for accelerating voltage amplitudes up to 6 kV and for a frequency multiplicity equal to one. In this mode, the accelerating hf-field compensates for the proton ionization energy loss. An oscillogram of the signal from the resonance induction electrodes is shown in Fig. 3 for the injection of 1 MeV protons in the resonance mode during 1500 revolutions (injection time, 300 μsec); the accelerating voltage was 1.5 kV. In Fig. 4, oscillograms are shown which are typical for capture in the resonance mode (energy,

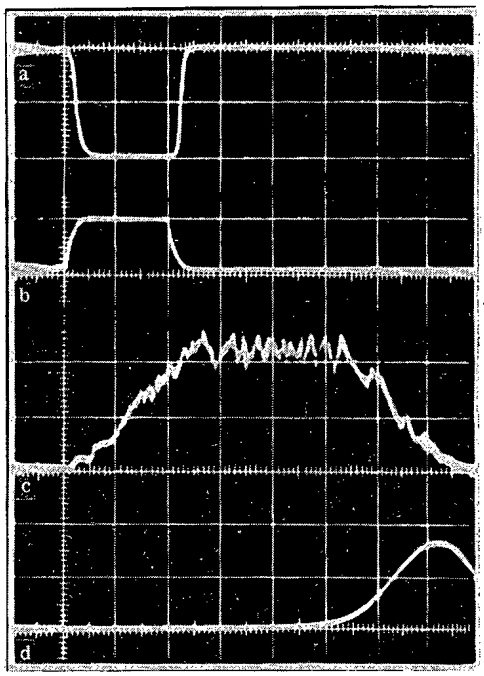

Fig. 2. Current oscillograms for proton injection into a storage ring in the quasi-betatron mode: a) current pulse in front of neutralizing target; b) proton current pulse on emergence from ionizing target; c) photomultiplier signal; d) proton current pulse from internal target. Horizontal scale, 10 μsec/cm.

1 MeV, injection time, 20 μsec). The first two oscillograms (see Figs. 4a, b) are the signals from the broad-band induction electrodes without accelerating voltage and with an hf accelerating field. A comparison of signal magnitudes shows that the linear density of the protons captured in the resonance mode, at the center of a bunch, is 1.5 times greater than the density of stored protons in the quasi-betatron mode. The third oscillogram (see Fig. 4c) shows the signal from the resonance induction electrodes, the fourth (see Fig. 4d) shows the signal from the inner target during storage in the resonance mode. A comparison of the latter oscillogram with the signal from the inner target during injection in the quasi-betatron mode (see Fig. 2) shows that an approximately constant particle loss occurs with capture in the resonance mode in contrast to the quasi-betatron mode. Further, the protons escape mainly in the inner portion of the ring (the signal from the outer target is many times less). Particle loss for resonance mode injection was 20-25%. In Fig. 5, oscillograms are shown of signals from the resonance induction electrode for proton storage in the resonance mode after 500 and 1000 revolutions (energy, 1 MeV). The storage current in the resonance mode increases linearly with time.

In our experiments, a hydrogen jet $\sim 10^{17}$ atom/cm^2 thick was used, the total cross section for proton loss because of scattering in hydrogen was $4.5 \cdot 10^{-22}$ cm^2/atom, and the effective number of injection revolutions allowing for the buildup in oscillations because of ionization energy loss in the jet was ~ 5000. For injection up to 1500 revolutions, the particle loss ought not to be more than a few percent, therefore we were unable to observe experimentally the increase in losses during storage. The constant 20-25% particle loss during injection in the resonance mode was in satisfactory agreement with the reduction in the azimuthal dimension of the separatrix because of energy loss.

In the initial experiments, a high-frequency source of negative hydrogen ions was used which had a maximum direct current of 21 μA at 400 W. The ion extraction system was probeless; the extraction voltage was 12 kV. A feature of such a source is the suppression of secondary electrons in the charge-exchange channel of the extracting electrode by a voltage of 250-300 V. With this source, a beam of negative hydrogen ions with intensity to 12 μA was obtained from the Van de Graaf accelerator. The beam was fed into the storage ring in pulses 1-300 μsec long

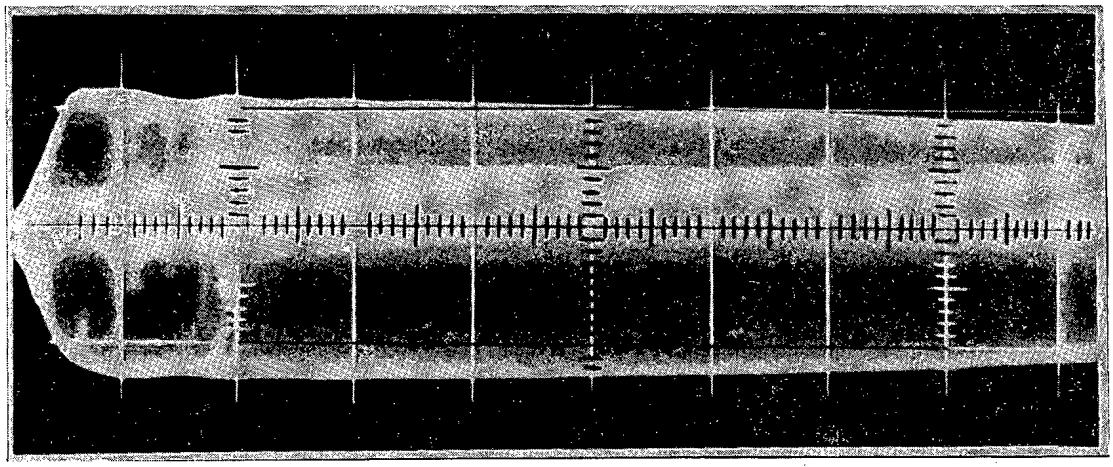

Fig. 3. Oscillogram of signal from induction electrodes for resonance mode injection. Horizontal scale, 500 μsec/cm.

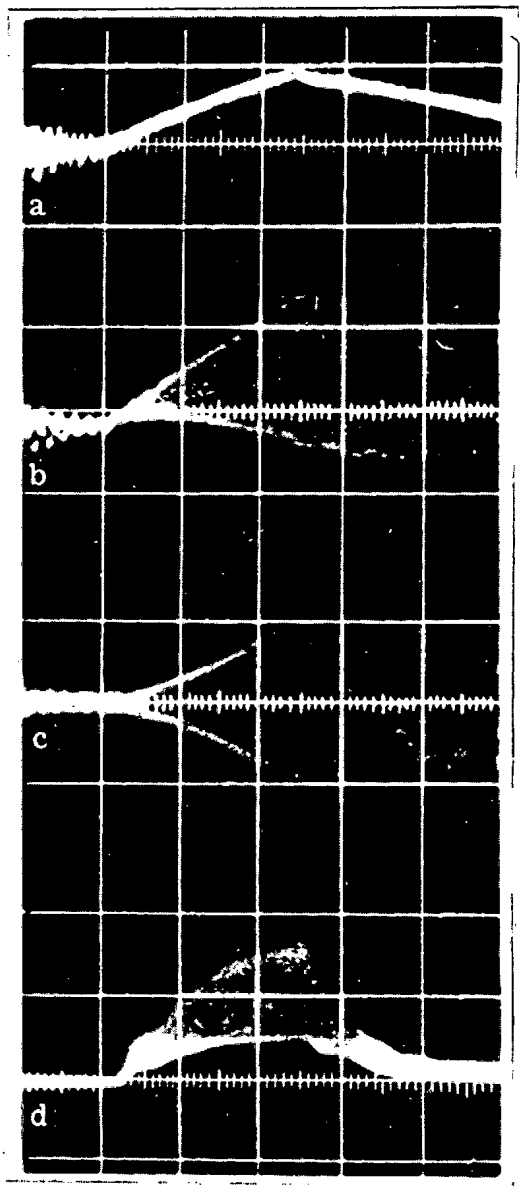

Fig. 4. Oscillograms typical of resonance mode capture. Horizontal scale, 10 μsec/cm.

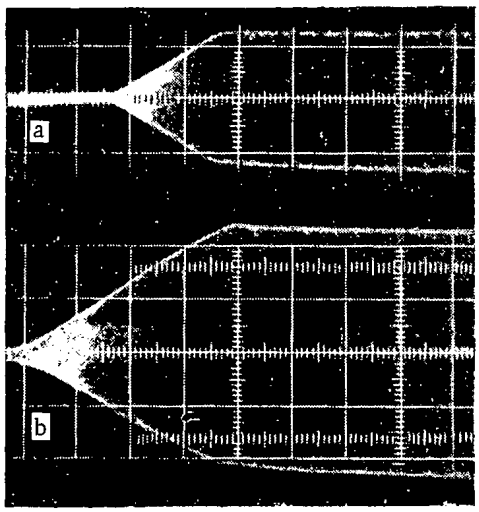

Fig. 5. Oscillograms typical of resonance mode proton capture after 500 (a) and 100 (b) revolutions. Horizontal scale 50 μsec/cm.

which were produced by means of a cutoff condenser installed in the ion duct. After focussing, the beam was introduced into a gaseous neutralization target 3-4 mm in cross section and having an angular aperture of $2 \cdot 10^{-3}$, which was made up in the form of a flow tube 5 cm long and 1 cm in diameter with associated diaphragms and differential pumping. The gas was delivered into the flow tube in separate pulses 1 msec long by means of an electromagnetic valve. The beam of atomic hydrogen from the target was introduced into orbit with an accuracy of ±1 mm in position and $2 \cdot 10^{-3}$ in angle. Energy stability was ±0.2%.

To obtain maximum atomic beam yield, we measured mass-spectroscopically the cross section for neutralization of negative hydrogen ions in a number of gases (H_2, N_2, C_2H_2, C_3H_8, CO_2, SF_6, CCl_2F_2) at energies of 1-1.5 MeV. It turned out that the maximum atomic beam yield depended slightly on the type of gas or the energy, and was 50-55%. In the neutralizing target, hydrogen or carbon dioxide gas was used with optimal thicknesses of $2.5 \cdot 10^{16}$ and $3 \cdot 10^{15}$ molecule/cm^2, respectively.

In order to store large currents, an arc source of negative hydrogen ions with currents to 1 mA and pulse length of 1 msec was installed in the Van de Graaf accelerator. With this source, a beam of negative ions with an intensity of 800 μA was obtained from the accelerator which made it possible to store 10^{12} protons (current, ~1 A) in the orbit of our machine.

Unfortunately, accelerator failure (breakdown of the compressed gas in the accelerating tube) delayed the performance of experiments on the storage of large proton currents although everything else had been made ready. Nevertheless, results of the preliminary experiments leave no doubt but that currents will be stored in the near future which will be limited by space charge.

CONCERNING THE POSSIBILITY OF A SELF-SUSTAINING THERMONUCLEAR REACTION IN A MIRROR MACHINE

(UDC 621.039.6 : 533.9)

D. V. Sivukhin

Translated from Atomnaya Énergiya, Vol. 19, No. 6,
pp. 510-517, December, 1965
Original article submitted February 20, 1965

An investigation is made of the energy balance in thermonuclear reactors of various types employing magnetic mirror trapping. Only the energy loss due to the escape of particles through the mirrors is taken into account. It is very likely that a self-sustaining thermonuclear reaction cannot be produced in such devices.

The experimental and theoretical investigations carried out to date do not yield a definite answer to the question of whether it is possible to obtain a self-sustaining thermonuclear reaction in a mirror machine. The main difficulty is usually taken to be the production in a trap of this kind of a stable plasma with the required temperature and density. We shall assume that the stage has been reached when these problems have been successfully overcome. We shall be investigating the matter within the following narrow formulation: is it possible to obtain a self-sustaining thermonuclear reaction in a mirror machine despite the continuous escape of particles through the mirrors? It is clear that such a one-sided approach to the problem can yield only the necessary, but by no means sufficient, conditions for the production of a self-sustaining thermonuclear reaction.

With our formulation of the problem, the fundamental and most difficult question that must be answered concerns the mean containment time of an ion in the trap. The first attempt to answer this question was made by Budker [1]. He employed the Landau kinetic equation, and after some simplifying assumptions he obtained a comparatively simple formula for the containment time τ_{cont}. Budker's formula was obtained by the present author in [2] by a somewhat different method. The latter paper brings out more clearly the nature of the simplifying assumptions underlying the conclusions. They are as follows:

1. It is assumed that particles escape as a result of coulomb collisions only, which change the directions of the particle velocity vectors. As soon as the direction of the velocity vector comes within the escape cone, the particle ceases to be contained by the magnetic field and escapes from the trap. Other escape mechanism are not taken into account.

2. It is assumed that the plasma consists only of electrons and identical ions. Only ion-ion scattering is taken into account. The scattering of ions by electrons is less by a factor of about $\sqrt{(m_i/m_e)\cdot(T_e/T_i)}$, and so is not to be taken into consideration.

3. The trap is assumed to be sufficiently long that the magnetic field may be taken to be uniform over the whole length except at the ends, where its intensity rises sharply.

4. Nuclear reactions are assumed to have no effect on the particle escape rate, which is valid provided the combustion rate is not too high. It will be shown below that this condition must be satisfied very well in our case.

5. Ion sources are available for injecting new ions into the trap to replace those that escape. The velocity spectrum of the sources is arranged so that a steady state with a quasi-Maxwellian velocity distribution is always maintained within the trap. By such a distribution we mean one characterized by the function $C(\theta)\exp[-(m\theta^2/2T)]$, where $C(\theta)$ depends only on the angle θ between the direction of the magnetic field and the particle velocity vector. The function $C(\theta)$ reduces to zero within the escape cone and on its surface.

6. The problem is solved in the diffusion approximation, in which the true diffusion coefficients in velocity space and the coefficients of dynamic friction are approximated by their values for a Maxwell distribution. For the diffusion approximation to be valid, the mirror ratio R must be large (ln R >> 1).

Of these simplifying assumptions the most important are No. 6 and the related No. 5. It is difficult, however, to estimate what effect they have on the final results. One must consequently view Budker's formula in an orientative light, and not as an exact relationship. For our purposes this formula is conviently written in the form

$$\tau_{cont} = 1.81\bar{\tau}_i \lambda(R), \tag{1}$$

where $\bar{\tau}_i$ is the mean ion relaxation time,

$$\bar{\tau}_i = \frac{3\sqrt{3m_i}}{8\pi nLe^4} T_i^{3/2}. \tag{2}$$

Here m_i is the ion mass, n is the plasma concentration, e is the electron charge, L is the coulomb logarithm, T_i is the ion temperature (erg). The function $\lambda(R)$ depends on the method of injecting the ions into the trap. It is best to inject perpendicular to the magnetic field, since the containment time is then a maximum. For this case Budker states that the function $\lambda(R)$ may be approximated by $\lambda(R) = \lg_{10} R$. Although this approximation was obtained for large R it is approximately valid, in fact, for any R, since in the limiting case of R = 1 this approximation yields the correct result: $\tau_{cont} = 0$. In the subsequent calculations we shall leave the function $\lambda(R)$ undefined until we come to work out the final numerical results, when we shall utilize the approximation $\lambda = \lg_{10} R$. Since ions escape mainly as a result of ion-ion scattering, we would expect that a more precise theory would also yield a proportional relationship between τ_{cont} and τ_i, i.e., we ought to get an expression of the form of Eq. (1), but with a more accurate function $\lambda(R)$. In principle $\lambda(R)$ may depend not only on the mirror ratio R, but also on any other parameters characterizing the departure of the ion velocity distribution from a quasi-Maxwellian distribution.

The containment time is given by the expression $\tau_{cont} = n/N_{esc}$, where N_{esc} is the number of ions escaping per second from unit volume of the trap. In the steady state and in the absence of nuclear reactions, N_{esc} equals N_{inj}, the number of ions injected per second into unit volume of the trap. In this case we have

$$\tau_{cont} = \frac{n}{N_{esc}}. \tag{3}$$

The latter expression will be employed even when nuclear reactions do occur. This is permissible firstly because the systems we are considering have small combusion rates, and secondly because the fast ions formed in nuclear reactions are not scattered much themselves, and have a negligible effect on the scattering of other ions.

The question of the containment time was also investigated theoretically by Judd, McDonald, and Rosenbluth [3]. Their calculations were based on the Landau kinetic equation, but without the assumption of a quasi-Maxwellian velocity distribution. A nonstationary problem without plasma sources was considered. The following expression for the containment time is given in [3]

$$\tau_{cont} \approx \frac{3}{4} \cdot \frac{m^2}{\pi nLe^4 \left\langle \frac{1}{v} \right\rangle \left\langle \frac{1}{v^2} \right\rangle} f(R). \tag{4}$$

Here $\left\langle \frac{1}{v} \right\rangle$ and $\left\langle \frac{1}{v^2} \right\rangle$ denote respectively the mean reciprocal ion velocity and the mean reciprocal ion velocity squared; the function $f(R)$ is approximated well by the expression $f(R) = \lg_{10} R$. Equation (4) suffers, however, from the same fault as Budker's formula. Its derivation is based on the arbitrary neglect of certain terms in the kinetic equation in order that this equation may be solved by the separation of variables. In the case of quasi-Maxwellian distribution, Eq. (4) reduces to Eq. (1) with $\lambda = 0.8 \lg_{10} R$. For a monoenergetic particle spectrum, Eq. (1) is also obtained with $\lambda \approx 3.3 \lg_{10} R$; in this case we must take $T_i = (2/3)\,\mathcal{E}_i$, where $\mathcal{E}_i$ is the ion kinetic energy.

The following are the main reactions of interest in the design of thermonuclear reactions

$$D + D \rightarrow He^2 + n + 3.25 \text{ MeV}; \tag{5}$$

$$D + D \rightarrow T + p + 4 \text{ MeV}; \tag{6}$$

$$T + D \rightarrow He^4 + n + 17.6 \text{ MeV}; \tag{7}$$

$$He^3 + D \rightarrow He^4 + p + 18.3 \text{ MeV}. \tag{8}$$

The rates of these reactions have been worked out often enough. The most complete information is given in the paper by B. N. Kozlov [4]. The calculated values of (σu) are given in that paper, where σ is the reaction cross section, u is the relative velocity of the reacting ions; the angular brackets denote an average over a Maxwellian velocity distribution. These quantities are functions of temperature alone. The results of the calculations were presented by B. N. Kozlov in the form of empirical formulas with suitable correction factors. Kozlov estimates the error in his calculations to be 2.5% for Eqs. (5)-(7), and 15% for Eq. (8). Table 1 shows the appropriate data obtained by the present author on the basis of Kozlov's empirical formulas. The indices 1, 2, 3 denote deuterium, tritium, and He^3 respectively. The quantities $(\sigma u)_{11p}$ and $(\sigma u)_{11n}$ refer respectively to the proton to the proton and neutron branches of the D-D reaction as a whole.

Suppose the trap contains a mixture of deuterium, tritium, and He^3 with absolute concentrations

$$n_1, n_2, n_3 \ (n_1 + n_2 + n_3 = n),$$

and relative concentrations $\alpha_1, \alpha_2, \alpha_3$ [$\alpha_i = (n_i/n)$, $\alpha_1 + \alpha_2 + \alpha_3 = 1$]. Let N_r be the number of particles which react in 1 cm^3 per second. The ratio

$$\varphi = \frac{N_r}{N_{esc.}} = \frac{N_r}{n}\tau_{cont}, \tag{9}$$

is called the combusion factor of the fuel mixture. The following expression can readily be found for this quantity

$$\varphi = (\alpha_1^2\langle\sigma u\rangle_{11} + 2\alpha_1\alpha_2\langle\sigma u\rangle_{12} + 2\alpha_1\alpha_3\langle\sigma u\rangle_{13})n\tau_{cont}. \tag{10}$$

The combustion factor is an important characteristic of a thermonuclear reactor, and it is of interest to work it out for various temperatures and for injected fuels of different percentage compositions. For this purpose it is useful to tabulate the values of the parameter $\gamma = [\lambda(R)/\varphi]$. This parameter is a completely defined function of temperature, density, and fuel composition, and depends on the density through the coulomb logarithm $L(\gamma \sim L)$. It is thus sufficient to work out γ for a single value of the density, say $n = 10^{14}$ cm^{-3}. We consider reactors of four types.

1. A reactor working on pure deuterium ($\alpha_1 = 1$; $\alpha_2 = \alpha_3 = 0$).

2. A reactor working on a mixture of equal amounts of deuterium and tritium ($\alpha_1 = \alpha_2 = 1/2$; $\alpha_3 = 0$).

3. A reactor in which the deuterium concentration is taken equal to $\alpha_1 = 1/2$, He^3 having an equilibrium concentration. The latter concentration is determined by the condition that the amount of He^3 formed in Eq. (5) must equal the amount of He^3 used up in Eq. (8), i.e.,

TABLE 1. Thermonuclear Reaction Rates [Values of (σu) are expressed in $cm^3 \cdot sec^{-1}$]

T_i, keV	$\langle\sigma u\rangle_{11p}$, $\times 10^{16}$	$\langle\sigma u\rangle_{11n}$, $\times 10^{16}$	$\langle\sigma u\rangle_{11}$, $\times 10^{16}$	$\langle\sigma u\rangle_{12}$, $\times 10^{16}$	$\langle\sigma u\rangle_{13}$, $\times 10^{16}$
20	0,024	0,0245	0,048	4,54	0,041
30	0,048	0,050	0,098	6,72	0,154
40	0,074	0,079	0,153	7,92	0,349
50	0,098	0,108	0,206	8,27	0,578
60	0,132	0,140	0,272	8,48	0,827
70	0,150	0,170	0,320	8,54	1,06
80	0,175	0,202	0,377	8,54	1,26
90	0,199	0,232	0,431	8,45	1,43
100	0,223	0,260	0,483	8,36	1,58
200	0,433	0,525	0,958	6,71	2,19
300	0,600	0,735	1,34	5,52	2,30
400	0,745	0,910	1,65	4,68	2,28
500	0,865	1,04	1,90	4,07	2,26
600	0,975	1,17	2,14	3,59	2,12
700	1,06	1,27	2,33	3,25	2,04
800	1,15	1,35	2,50	2,94	1,97
900	1,23	1,43	2,66	2,71	1,90
1000	1,30	1,50	2,80	2,50	1,85

TABLE 2. Values of Parameter $\gamma = [\lambda(R)/\varphi]$ at $n = 10^{14}$ cm^{-3}

T_i, keV	First type	Second type	Third type	Fourth type
20	$6,2\cdot10^4$	$1,17\cdot10^3$	$1,64\cdot10^3$	$5,0\cdot10^4$
30	$1,7\cdot10^4$	$4,4\cdot10^2$	$5,2\cdot10^2$	$1,12\cdot10^4$
40	$7,2\cdot10^3$	$2,4\cdot10^2$	$2,7\cdot10^2$	$4,3\cdot10^3$
50	$3,8\cdot10^3$	$1,7\cdot10^2$	$1,8\cdot10^2$	$2,3\cdot10^3$
60	$2,2\cdot10^3$	$1,25\cdot10^2$	$1,35\cdot10^2$	$1,3\cdot10^3$
70	$1,5\cdot10^3$	100	$1,05\cdot10^2$	$8,9\cdot10^2$
80	$1,05\cdot10^3$	81	87	$6,2\cdot10^2$
90	$7,8\cdot10^2$	69	74	$4,6\cdot10^2$
100	$6,0\cdot10^2$	60	64	$3,5\cdot10^2$
200	$1,1\cdot10^2$	26	28	70
300	43	16,5	18	30
400	23	12,5	13,5	18
500	14,5	9,8	10,5	12
600	9,8	8,0	8,7	9,2
700	7,3	6,8	7,4	7,3
800	5,6	5,9	6,4	6,1
900	4,4	5,1	5,6	5,2
1000	3,6	4,6	4,9	4,5

$$\alpha_3 = \frac{n_3}{n} = \frac{\alpha_1}{2} \cdot \frac{\langle \sigma u \rangle_{11n}}{\langle \sigma u \rangle_{13}} . \tag{11}$$

The third constituent is tritium, with a concentration $\alpha_2 = {}^1/_2 - \alpha_3$.

4. A reactor operating on an equilibrium mixture of deuterium, tritium, and He^3. In this case

$$\begin{aligned} \alpha_1 &= 1 - \alpha_2 - \alpha_3; \\ \alpha_2 &= \frac{\alpha_1}{2} \cdot \frac{\langle \sigma u \rangle_{11p}}{\langle \sigma u \rangle_{12}}; \\ \alpha_3 &= \frac{\alpha_1}{2} \cdot \frac{\langle \sigma u \rangle_{11n}}{\langle \sigma u \rangle_{13}} . \end{aligned} \tag{12}$$

Reactors of the latter two types were examined by Post [5].

All the above types of reactors are characterized by large values of γ (see Table 2). It follows that, as a rule, the reactors have small combustion factors φ. Indeed, it is very unlikely that a trap will be built whose mirror ratio will exceed 10 even by a single order of magnitude. Consequently, we may tentatively assume a maximum permissible mirror ratio of 10. Should the approximation $\lambda = \lg_{10} R$ be valid, then this mirror ratio would correspond to $\lambda(R) = 1$. For practicably realizable reactors it would thus be possible to take $\lambda(R) < 1$. By way of example, let us consider the case when $\lambda(R) = 1$, $n = 10^{14}$ cm^{-3}, $T = 100$ keV. We then find that the combustion factors for the above four reactor types are 1/600; 1/60; 1/64; 1/350. At lower temperatures the combustion factor is even smaller. Only at temperatures of the order of 1 MeV does the combustion factor become appreciable, when it amounts to about 20%. These results are qualitatively unchanged if the parameter λ is increased several times in magnitude.

In this manner, only a small fraction of the ions has time to react within the trap, the greater portion escaping through the mirrors without having reacted. The energy carried away by the heated and unreacted fuel mixture must clearly be utilized for some purpose or other (for example, converted into electrical energy). After the necessary purification, the unreacted fuel must be heated up and introduced once more into the trap for subsequent burning. This process must be repeated many times in order to increase the efficiency of the reactor.

The condition for a nuclear reaction to be self-sustaining that was employed in [2] is very severe. It reduces to the requirement that the combustion factor should be of the order of unity. This condition is not, however, a necessary one, and may lead to erroneous conclusions.

By itself, a small combustion factor still does not prove that it is impossible to effectuate a self-sustaining thermonuclear reaction. This question can only be answered on the basis of the energy balance. We introduce the following notation: w_{11n}, w_{11p}, w_{12}, w_{13} denote the energies released by nuclear Eqs. (5)-(8) respectively; w_c is the neutron absorption energy per neutron: $\bar{w}$ is the mean energy liberated during nuclear reactions (including the neutron absorption energy) per particle of reaction product. This quantity is readily seen to be given by

$$\bar{w} = \frac{\frac{\alpha_1}{2}\langle \sigma u \rangle_{11p} w_{11p} + \frac{\alpha_1}{2}\langle \sigma u \rangle_{11n}(w_{11n} + w_c) + \alpha_2 \langle \sigma u \rangle_{12}(w_{12} + w_c) + \alpha_3 \langle \sigma u \rangle_{13} w_{13}}{\alpha_1 \langle \sigma u \rangle_{11} + 2\alpha_2 \langle \sigma u \rangle_{12} + 2\alpha_3 \langle \sigma u \rangle_{13}} . \tag{13}$$

The energy output of the reactor can be increased by employing a moderator with as high a value of w_c as possible. Consequently, in reactors types one and four, where it is not required to reproduce tritium, sodium is utilized as a moderator (for which $w_c = 12.6$ Mev). In reactors types two and three it is required to produce tritium by means of the reaction

$$Li^6 + n \rightarrow T + He^4 + 4{,}8 \text{ MeV} .$$

In these types we shall consequently take $w_c = 4.8$ Mev. Let us consider the ideal case when all the neutrons obtained from the reaction $D + D \rightarrow n + He^3$ are used up in the production of tritium, i.e., react with Li_6 nuclei. In actual fact, losses are unavoidable on account of neutron absorption by other nuclei. A real setup must consequently make provision for neutron multiplication, for example, by means of the reaction $Be^9 + n \rightarrow 2He^4 + 2n$. Such additional reactions cannot, however, have much effect on the energy balance or on the final conclusions.

Values of $\bar{w}$ calculated from Eq. (13) are shown in Table 3. Most of the energy liberated during the nuclear reactions is carried away by neutrons. We shall term the sum of this energy and the neutron absorption energy the

TABLE 3. Mean Energy $\bar{w}$ Liberated in Reactor per Product Particle, and the Fraction of This Energy Removed by Neutrons $\bar{w}_n/\bar{w}$

T_i, keV	First type		Second type		Third type		Fourth type	
	$\bar{w}$, MeV	$\bar{w}_n/\bar{w}$, %	$\bar{w}$, MeV	$\bar{w}_n/\bar{w}$, %	$\bar{w}$, MeV	$\bar{w}_n/\bar{w}$, %	$\bar{w}$, MeV	$\bar{w}_n/\bar{w}$, %
20	5,0	81	11,2	84	11,2	85	8,55	63
60	5,1	81	11,1	84	11,1	85	8,55	62
100	5,2	82	11,0	84	11,0	83	8,55	61
300	5,3	83	10,4	84	10,1	81	8,55	60
500	5,2	83	9,7	83	9,3	76	8,55	61
700	5,2	83	9,0	83	8,5	71	8,55	61
1000	5,2	82	8,3	82	7,6	64	8,55	61

TABLE 4. Values of Function $S = (3/2) \cdot (\gamma T/\bar{w})$ for $n = 10^{14}$ cm^{-3}

T_i, keV	First type	Second type	Third type	Fourth type
20	370	3,1	4,4	175
30	152	1,8	2,1	59
40	85	1,3	1,5	30
50	56	1,15	1,25	20
60	40	1,01	1,1	13,7
70	31	0,95	1,02	10,9
80	25	0,89	0,95	8,7
90	20	0,85	0,90	7,2
100	17	0,81	0,87	6,1
200	6,3	0,72	0,80	2,5
300	3,7	0,72	0,81	1,6
400	2,7	0,73	0,85	1,25
500	2,1	0,75	0,87	1,08
600	1,7	0,78	0,88	0,97
700	1,45	0,79	0,91	0,90
800	1,28	0,81	0,94	0,85
900	1,14	0,81	0,95	0,82
1000	1,04	0,82	0,97	0,80

neutron energy. We denote by $\bar{w}_n$ the mean neutron energy per product particle. The values of the ratio $\bar{w}_n/\bar{w}$ are given in Table 3.

Charged particles carry a relatively small portion of the energy. This simplifies the discussion of the energy balance. The neutron energy can be converted into electrical energy by means of a heat cycle. In this sense it is equivalent to thermal energy. The energy carried by charged particles is small in comparison with the neutron energy. The direct conversion of charged-particle energy into electrical energy is made difficult on account of the rapid leak of the particles through the magnetic mirrors. We may thus assume during calculations that all the energy leaving the reactor is converted into electrical energy by means of a heat cycle. If even some of the energy obtained is directly converted into electrical energy with a high efficiency, this may be taken into account by replacing the efficiency η introduced below by some larger effective coefficient.

Each second N_{inj} ions of kinetic energy $(3/2)N_{inj}T$, obtained from the electrical energy with some efficiency η_k, are introduced into unit volume of the reactor. The electrical energy is, in its turn, produced from the thermal energy with some efficiency η_g. Let Q denote the total thermal energy required to produce the ion kinetic energy $(3/2)N_{inj}T$. We thus have $(3/2)N_{inj}T = \eta Q$. The total efficiency η can be written in the form $\eta = \eta_k \eta_g \eta_t$, where the coefficient η_t takes account of energy losses due to Joule heating in the windings and losses associated with the production of deuterium from water, the purification of the fuel mixture, and so on.

All the kinetic energy $(3/2)N_{inj}T = \eta Q$ introduced into the reactor leaves it in the form of the thermal energy of the unreacted fuel mixture, in the form of radiation, and also in the form of excited electrons heated up inside the trap. In addition, there is a release of nuclear energy $N_r\bar{w} = \varphi N_{inj}\bar{w}$. The total energy leaving unit volume of the reactor per second is thus $\mathcal{E} = \eta Q + \varphi N_{inj}\bar{w}$. Remembering that $\eta Q = (3/2)N_{inj}T$, we obtain on dividing throughout by Q:

$$\frac{\mathcal{E}}{Q} = \eta + \frac{2}{3} \cdot \frac{\eta\varphi\bar{w}}{T} = \eta + \frac{2}{3} \cdot \frac{\eta\lambda\bar{w}}{\gamma T}.$$

For the thermonuclear reaction to be self-sustaining we must necessarily have $(\mathcal{E}/Q) > 1$ or

$$\frac{2}{3} \cdot \frac{\lambda\bar{w}}{\gamma T} > \frac{1-\eta}{\eta}. \qquad (14)$$

On introducing the parameter

$$S = \frac{3}{2} \cdot \frac{\gamma T}{w}, \tag{15}$$

Eq. (14) takes the form

$$\lambda > S \frac{1-\eta}{\eta}. \tag{16}$$

The numerical values of the parameter S are given in Table 4 for $n = 10^{14}$ cm^{-3}. Values of S can readily be found for other densities when it is remembered that the function S depends on the density only through the coulomb logarithm L($S \sim L$).

If η were close to unity, the necessary Eq. (16) for a self-sustaining reaction could be satisfied for practicably realizable values of R. In actuality, η cannot be as large as that. Let us take, for example, $\eta_g = (1/2)$, $\eta_k \eta_t = (1/2)$, and consequently $\eta = (1/4)$ (this is a rough tentative estimate; it is very likely on the high side). We then find from Eq. (16) that $\lambda > 3S$. A reactor of the second type yields the smallest value of S, approximately 0.7. In this optimum case we must have $\lambda > 2$. Taking $\lambda = \lg_{10} R$, we obtain $R > 100$, an unrealizable condition. Thus, if the approximation $\lambda = \lg_{10} R$ is correct, it is impossible for any of the reactor types being considered to support a self-sustaining thermonuclear reaction.

Of course, the formula $\lambda = \lg_{10} R$ cannot be relied on absolutely. The non-Maxwellian nature of the ion velocity spectrum may exert an important effect. There are two ways in which this may show up. Firstly, the rates (σu) at which thermonuclear reactions occur for the true velocity distribution in the range where the cross section is a maximum may be greater than the rates corresponding to a Maxwellian ion distribution. However, calculations by Roberts and Carr [6] have shown that this effect cannot be important. Secondly, the departure of the true spectrum from Maxwellian may indirectly affect the containment time. It was shown above that Eq. (4) gives $\lambda = 3.3 \lg_{10} R$ for a monoenergetic velocity spectrum.

It is very difficult to determine λ precisely. Equations (1) and (4) yield only a rough estimate. Furthermore, in order to apply Eq. (4), the true ion velocity distribution must be known, and it is not. The existing numerical solutions of the kinetic equation are mathematically incorrect, being based on various simplifying assumptions. They also cannot give reliable values of $\lambda(R)$. It may be that the numerical coefficient in Budker's formula has to be increased several times over. This can affect the final conclusion on whether a self-sustaining nuclear reaction is possible or impossible.

Suppose, for example, that $\lambda(R) = 3 \lg_{10} R$. The permissible values of λ may then be increased by a factor of three, while the mirror ratio required is reduced by a factor of 1000. If we take once more $\eta = (1/4)$, we find from Eq. (16) for $R = 10$ that $S < 1$. For reactor types two and three this condition corresponds to $T > 70$ keV, while for type four $T > 600$ KeV. If, however, $R = 3.3$ ($\lg_{10} R = 0.5$), we find from Eq. (16) that $S < (1/2)$. This condition is not satisfied, however, by any of the reactor types.

If $\lambda = 5 \lg_{10} R$, we find for $R = 10$ that $S < (5/3)$. This condition is satisfied for reactor types two and three when $T > 40$ keV, and when $T > 300$ keV for type one. For $R = 3.3$ we find under the same conditions that $S < (5/6)$. This condition is satisfied at the limit only for type two and $T > 100$.

The following objection may be raised to the foregoing discussion. Slow ions are the most likely to escape from the trap. Consequently, in order to maintain the required temperature, one might think that instead of introducing ions of mean energy (3/2)T into the trap, the mean energy of the injected ions should be considerably less than this [(1/2)T, for instance]. However, an ion velocity distribution would then arise which would slow down the rate of thermonuclear reactions enormously. A small number of fast ions and a large group of re-injected slow ions would remain in the trap. Collisions between slow ions would scarcely ever be accompanied by nuclear reactions. Nuclear reactions would occur mainly as a result of collisions between fast and slow ions, and such collisions are rare. For the same reason there must be very little energy exchange between fast and slow ions.

We may consequently state that there is too little information at present on the containment time and on the ion velocity distribution for us to conclude categorically that particle losses as a result of coulomb collisions are sufficiently serious to preclude the possibility of a self-sustaining thermonuclear reaction in a mirror machine. The analysis carried out in the present article shows, however, that this conclusion is the most likely one. Furthermore,

the existence of a loss cone gives rise to instabilities, and this factor alone may be quite sufficient to prevent a self-sustaining thermonuclear reaction from being realized in a mirror machine.

The author would like to acknowledge his indebtedness to M. A. Leontovich, L. A. Artsimovich, V. I. Kogan, and I. N. Golovin for discussions on the problems dealt with in the present article.

LITERATURE CITED

1. G. I. Budker, In: Plasma Physics and the Problem of Controlled Thermonuclear Reactions [in Russian], Moscow Acad. Sci. USSR Press, Vol. III (1958), p. 3.
2. D. V. Sivukhin, In: Topics in Plasma Theory [in Russian], Atomic Energy Press, No. 4 (1964), p. 81.
3. D. Judd, W. McDonald, and M. Rosenbluth, End Leakage Losses from the Mirror Machine, AEC Report WASH-289, Conference on Controlled Thermonuclear Reactions, Berkeley, California (February, 1955), p. 158.
4. B. N. Kozlov, Atomnaya Énergiya, 12, 238 (1962).
5. R. Post, Nucl. Fusion. Suppl., Part 1 (1962), p. 99.
6. J. Roberts and M. Carr, AEC Report UCRL-5651-T (April, 1960).

REDUCTION IN RADIOACTIVE DISCHARGES TO THE ATMOSPHERE AND STUDY OF WATER DEAERATION PRACTICE IN THE PRIMARY LOOP OF THE VVR-M REACTOR

(UDC 621.039.586 : 539.16.04)

D. M. Kaminker, K. A. Konoplev, Yu. P. Semenov, and V. D. Trenin

Translated from Atomnaya Énergiya, Vol. 19, No. 6, pp. 517-521, December, 1965
Original article submitted February 16, 1965

The function and operating principles of the closed deaeration loop of the reactor are described, with an account of operating experience of the deaeration loop during the first two years and the results of studies of deaeration management of the primary-loop water. The deaeration system in the VVR-M reactor is reported as not being the only means for removing the detonating mixture from the primary loop water and inhibiting the formation of gas bubbles containing detonating mixture in the loop piping.

The closed loop for deaeration and combustion of detonating mixture designed and fabricated for the VVR-M reactor of the A. F. Ioffe Physics and Engineering Institute of the USSR Academy of Sciences has reduced to a mere tenth the amount of radioactive gases vented to the atmosphere.

There are three sources of radioactive discharge to the atmosphere in the VVR-M reactor [1]: the escape of radioactive gases dissolved in the primary-loop water; the discharge of air from experimental channels; the venting of radioactive gases from hot cells.

Of all the gases found in the air, the only one that makes a contribution of practical significance to radioactive discharges to the atmosphere is A^{41} (half-life ≈ 110 min) produced by neutron irradiation of the atmospheric air. N^{15} with its half-life ≈ 7.5 sec is also formed when air is irradiated, but it decays to insignificance in the time it takes to traverse the volume of active air from the point of formation to the top of the venting stack. Off-gases from experimental channel work are not significant inasmuch as the air turnover is experimental channels and in air spaces close to the core is kept low by special means. The radioactive gases discharged from hot cells made no appreciable contribution to the total in the whole five years the reactor has been in service.

The principal source of radioactive discharges to the atmosphere from the VVR-M reactor is a deaerator designed to remove products of radialysis of the primary-loop water. The deaerator also acts to remove radioactive gases from the primary-loop water, as well as radiolyzates. Gas exchange on the water surface in the reactor pressure vessel is insignificant, since the water-air contact surface area in the deaerator (with water flowing in droplets countercurrent to the air) is 40 times greater than the area of the surface in the reactor vessel. A closed deaeration loop is needed in the reactor system to effect combustion of any detonating gas formed, as part of the effort to reduce the amount of radioactivity vented to the atmosphere. Detonating gas in the primary-loop water is removed by an equal volume of air in a closed cycle, and the detonating gas is burned in one part of the deaeration loop. When uranium fission products appear in the primary-loop water, the bulk of the gaseous components become trapped within the closed deaeration loop.

When the deaeration loop is in operation (Fig. 1), the air enriched with detonating gas passes from the deaerator to an electric heater unit (each heater of 10 kW rating), is heated and then sent on to a contacting device where the detonating gas mixture is combusted by quiescent burning on platinum catalyst ≈ 7 liters in volume. The air passing through the condenser is cooled to 25-30°C, the condensate is separated off, and the air is forced back to the

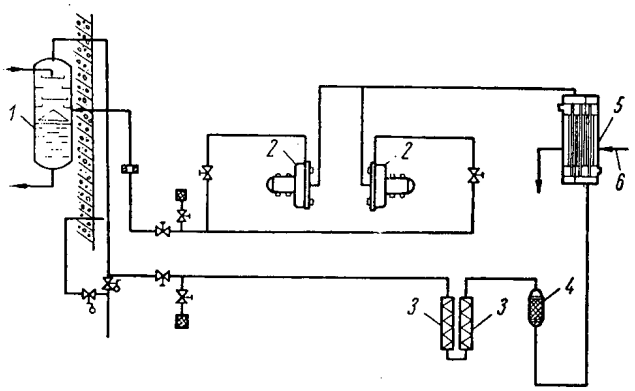

Fig. 1. Closed deaeration loop flowsheet. 1) Deaerator; 2) compressor; 3) heater; 4) phase contractor; 5) condenser; 6) coolant water input. Arrows indicate direction of air and water flow.

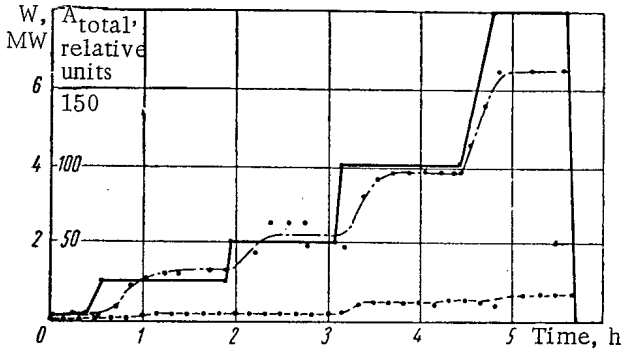

Fig. 2. Rate of discharge A of active gases to stack as as a function of reactor power output W with either the closed deaeration loop or the open deaeration loop on stream: ———) equipment capacity; —·—·—·—) rate of gas discharge in open-loop; — — — —) rate of gas discharge in closed loop.

deaerator by the compresser. The rated air flowrate in the closed deaeration loop is about 10 nm^3/h when the reactor is operating at 10 MW output, and the pressure in the loop is kept within 0.04 atm gauge.

Air arriving at the catalyst is heated to 150°C. This temperature creates favorable conditions for catalyst-aided combustion of the detonating mixture and guarantees that no moisture film will form on the catalyst and thereby lessen its effective area.

When the reactor is operated at 10 MW with the closed deaeration loop on stream, the amount of radioactive gases vented to the outside is cut down to one-tenth the amount discharged when an open deaeration loop is used (Fig. 2). No appreciable change in the specific activity of the primary-loop water or in concentration of iodine isotopes was noted when the reactor was operated with the closed deaeration loop.

The hydrogen concentration in the mixture arriving at the deaeration loop contactor is nowhere near the explosion hazard level, and does not rise above 1% when the reactor is operated at rated parameters. Combustion of the hydrogen on the catalyst was complete; the hydrogen concentration leaving the contactor is less than 0.03% (precision limit for measurements using the KhT-2M monitor). Hydrogen content in the mixture passed over the catalyst was measured periodically by sampling and gas chromatographic determinations of the hydrogen content.

Two years' operating experience with the closed deaeration loop showed that the loop equipment is reliable in operation. The biological shielding of the closed deaeration loop brings the gamma-ray dose rate down below the tolerance level.

When the closed deaeration loop is functioning in steady state, the amount of hydrogen present in the combustible mixture can be determined from the temperature differential ΔT over the catalyst bed, provided the phase contactor is well insulated thermally and a constant temperature is maintained at the contactor exit. Pure hydrogen in amounts of 0.1% of the flowrate of the gas stream over the catalyst was fed in at the entrance to the deaerator in calibrating the instrument used for measuring the temperature differential at the exit and entrance of the contactor: the absolute value of ΔT was +5.5°C. The amount of hydrogen contained in the mixture arriving at the catalyst can be estimated by using the formula

$$C'' = \frac{\Delta T}{5.5} \cdot 0.1\%. \qquad (1)$$

The error in determining C" by this formula is ±13% when $\Delta T \leq 50°C$.

The temperature differential across the contactor when oxygen is fed into the deaerator from outside remains constant, i.e., no oxygen insufficiency is observed even when the closed deaeration loop has been in on stream for nine weeks in succession.

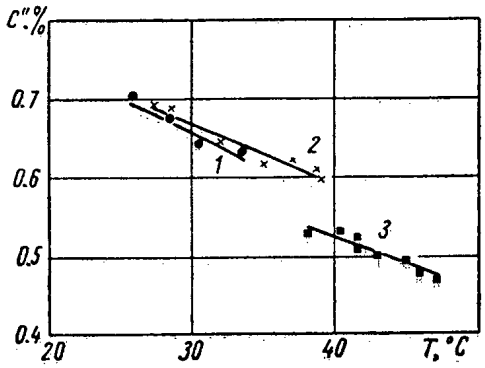

Fig. 3. Hydrogen concentration in air removed from the deaerator as a function of the temperature of the primary-loop water.

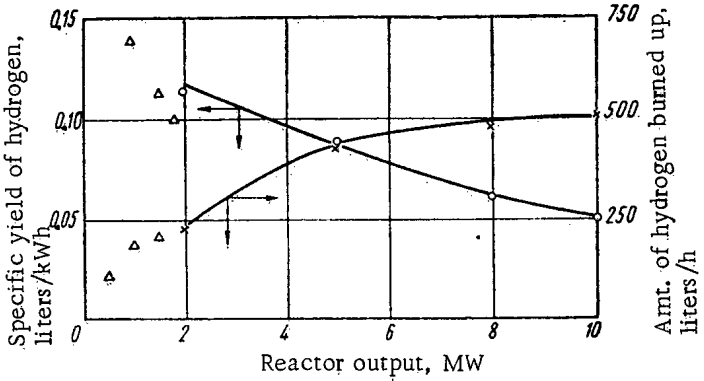

Fig. 4. The specific yield of hydrogen K from the primary-loop water and the amount of hydrogen G burned up on the catalyst bed per unit time as a function of the reactor output. Core volume V_{core} = 94.5 liters; Δ) data for the VVR-S reactor [5].

Reactor parameters	Curves 1 (●) and 2 (×)	Curves 3 (■)
Reactor power rating W, in MW	5	6.5
Water flowrate Q in primay loop, m^3/h.	1150	1450
Water flowrate to deaerator Q', m^3/h.	200	184
Air flowrate to deaerator Q", nm^3/h	115	115
Temperature t_1 ahead of contactor, °C	130	132

The following options are open for removing hydrogen dissolved in the primary-loop water: 1) formation of gas bubbles containing detonating mixture in the primary-loop piping; 2) removal from the water surface in the reactor to the V-2 ventilation process system; 3) removal in the deaerator; 4) removal by recombination in the primary-loop water. The probability of the formation of gas bubbles containing detonating mixture of hydrogen in the primary-loop piping appears to be very small, since hydrogen did not manage to accumulate even over a protracted time interval (hundreds of hours, or even longer) in a special trap placed at the intake of of the primary-loop pumps. The hydrogen concentration in the air drawn off the liquid surface in the contactor was less than 0.03%.

About 700 nliter/h hydrogen is combusted on the closed deaeration loop catalyst when the reactor is running at 8 MW output. The deaerator is designed to separate out 800 liters of hydrogen per hour.

The amount of hydrogen removed from the water surface in the reactor (surface area F_2 = 4.15 m^2) obviously must be far less than the amount of hydrogen removed in the deaerator (where the water surface area F" = 155 m^2). It is also obvious, on the other hand, that the amount of hydrogen removed from one square meter of the water surface in the reactor vessel must be slightly more than the amount of hydrogen in the same process in the deaerator, since the partial pressure of hydrogen is higher in the deaerator than above the water level in the vessel. The hydrogen concentration above the water level therefore falls in the range

$$(G \cdot 10^{-3}/Q_2)\,100\% >> H > (F_2/F") \cdot (Q"/Q_2)\,C",$$

or

$$0.06\% >> H > 0.016\%,$$

where Q_2 is the air flowrate above the water level in the reactor, in cubic meters per hour; G is the amount of hydrogen burned off on the catalyst per unit, in liters per hour. The amount of hydrogen removed from the water level in the reactor must therefore fall in the range $700 >> G_2 > 18.5$ liter/h. Radical and molecular yields of water radiolysis products are reported to be practically constant when the water temperature is 0° to 100°C [2]. More detailed investigations [3, 4] show that when water containing impurities is irradiated in a reactor the rise in water temperature has an inhibiting effect on radiolysis, by favoring recombination. This might be the reason for the lower hydrogen concentration in the mixture fed to the catalyst, a drop of 0.01% as the water temperature at the

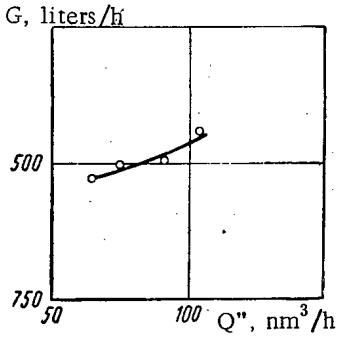

Fig. 5. Amount of hydrogen G burned up in contactor per unit time, as a function of air flowrate through the contactor: W = 7 MW; Q = 1400 m^3/h; Q' = 188 m^3/h; V_{core} = 97.7 liters; temperature of primary-loop water T = 48°C.

reactor exit rises 1°C (Fig. 3). But this effect could hardly account for the increased specific heat of the mixture, which is related to both the temperature rise and the increased moisture content. In fact, the increase in the specific heat of saturated steam as the air mixture experiences a 12°C temperature rise is about 0.4%, and the reduction in the temperature differential across the catalyst comes to 12% of the measured value.

As the reactor power rises the amount of hydrogen given off from the primary-loop water in the deaerator likewise increases, tending to a certain limit, while the yield of hydrogen per unit reactor power drops (Fig. 4). These regularities fit the data reported in [2, 5]. If we suppose that the amount of hydrogen formed in the core is proportional to the reactor output, then we may infer that the basic factor counteracting the increase in hydrogen concentration in the primary-loop water is recombination, since the amount of hydrogen liberated in the deaerator shows no increase.

We learn from Fig. 5 that the hydrogen is not completely removed from the primary-loop water in the deaerator, since the amount of hydrogen burned up on the catalyst increases as the air flowrate through the deaerator increases, and the former does not attain a limit even at peak air flowrates.

As the amount of hydrogen burned up in the closed deaeration loop drops to half (accompanying a drop in the flowrate of air through the deaerator to half), the hydrogen concentration in the primary-loop water increases but negligibly (Fig. 6). Otherwise we would observe a drop in hydrogen concentration at the entrance to the contactor and a subsequent increase, as the flowrate of air through the deaerator dropped, and after the flowrate of air through the deaerator had been restored the hydrogen concentration at the entrance to the contactor would have exceeded the initial amount. We find instead that the hydrogen concentration in the primary-loop water changes negligibly as the amount of hydrogen burned up in the closed deaeration loop drops by 40%; the excess hydrogen appears to be removed by recombination.

This suggests that the performance of the deaeration system is not the determining process hindering an increase in hydrogen content in the water or hindering the formation of gas bubbles containing detonating mixture in the primary-loop piping of the VVR-M reactor, at the hydrogen concentrations under investigation. Similar conclusions have been drawn by colleagues working at the VVR-S Polish reactor, as a result of studying radiolysis of coolant water with the reactor running at up to 2 MW [5]. The amount of hydrogen extracted from the primary-loop water in the deaerator per unit reactor power, K, is a linear function of the flowrate of water through the deaerator (Fig. 7).

The rate at which the concentration of hydrogen in the mixture flowing into the contactor drops, plotted as a function of the time elapsed after the contactor is taken off stream, gives us sufficient information to determine the

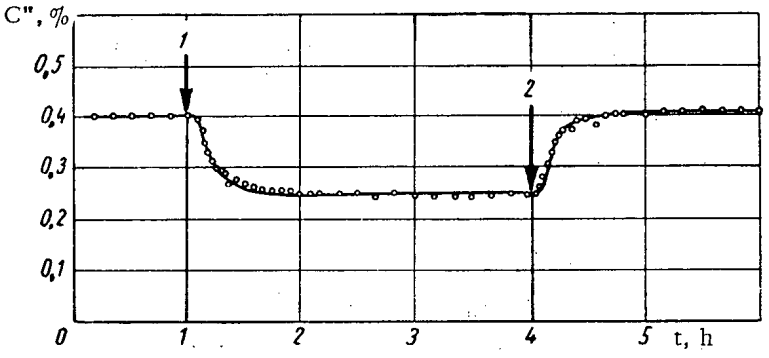

Fig. 6. Hydrogen concentration in air leaving the deaerator as a function of water flowrate through the deaerator, at constant reactor output and constant air flowrate to the deaerator: W = 5 MW; Q = 1380 m^3/h; Q' = 180–90–180 m^3/h; Q" = 100 nm^3/h; T = 47°C. 1. reduction in Q' from 180 to 9 m^3/h; 2. increase in Q' from 90 to 180 m^3/h.

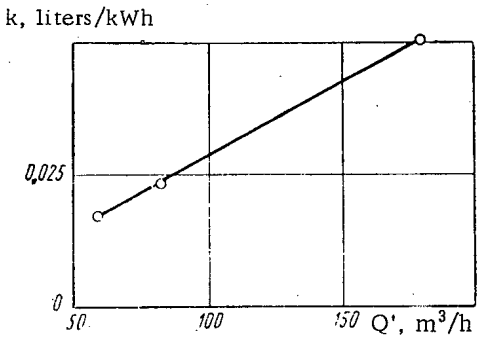

Fig. 7. Specific yield of hydrogen from primary-loop water as a function of air flowrate to deaerator: W = 8.5 MW; Q = 1550 m^3/h; Q" = 115 nm^3/h; V_{core} = 123 liters; T = 48°C.

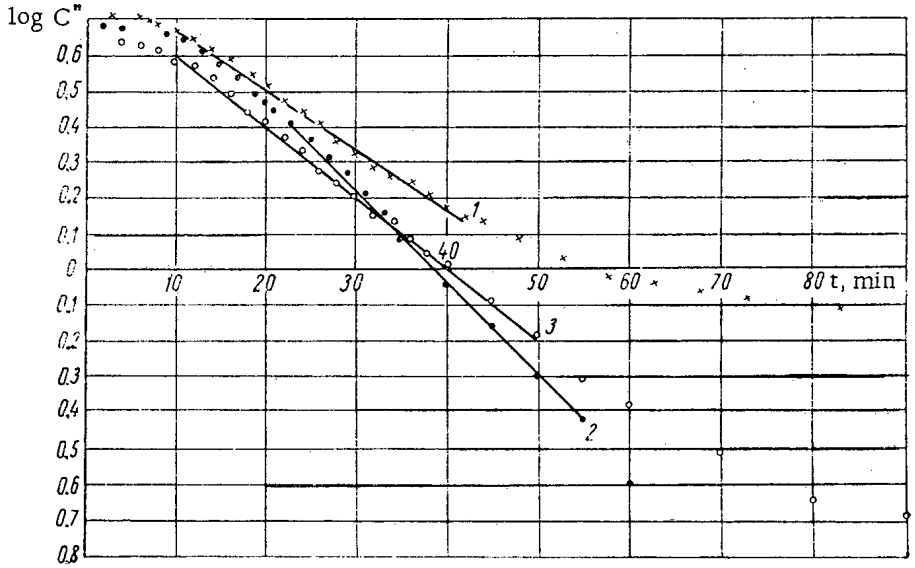

Fig. 8. Hydrogen concentration in air leaving deaerator as a function of the time t elapsed after reactor shutdown when reactor had been operating at: 1) 8.5 MW; 2) 7 MW; 3) 5 MW.

purification ratio for hydrogen removed from the primary-loop water in the deaerator, given certain simplifying assumptions. This purification factor ξ is the ratio of the amount of hydrogen burned up in the closed deaeration loop to the total amount of hydrogen present in the primary-loop water entering the deaerator. Assuming ξ to be constant with time or to be at most a weak function of the time, we can readily show that the time variation in the concentration C" of the hydrogen in the air leaving the deaerator taken as a function of the time elapsed from reactor shutdown is subject to the same law as the change in hydrogen concentration in the primary-loop water entering the deaerator, and this appears to be a natural law. In both cases we have the exponent $-\xi(Q/V)t$, where V is the volume of the primary loop.

We see in Fig. 8 that the mid-portions of the log C" = $f(t)$ curves fit closely on the straight lines, confirming the validity of the assumption that ξ is independent of the time in that region.

The nonlinearity of log C" = $f(t)$ at the beginning of the curves can be explained by the appreciable quantity of hydrogen liberated in the core immediately following the reactor shutdown, and by the slow speed of response of the measuring system. The nonlinearity when t > 40 to 60 min is due to the increased relative error in measurements of C" at low absolute values of the latter.

The average ξ read off the curves 1, 2, 3 (Fig. 8) is 0.7 ± 0.2. Under the reactor operating conditions depicted in Fig. 8 (curve 3), then, the hydrogen concentration in the primary-loop water C_1 = 0.0037 ± 0.007 nm^3 per m^3 water. A figure of 0.00445 m^3/m^3 was assigned to the hydrogen concentration in the primary-loop water entering the deaerator in the design stage.

The closed deaeration loop in the VVR-M reactor of the A. F. Ioffe Physics and Engineering Institute was designed and assembled on the recommendations and with the collaboration of E. N. Babulevich, V. V. Goncharov, and Yu. G. Nikolaev on the staff of the Institute of Atomic Energy of the USSR Academy of Sciences. The authors express their heartfelt thanks to these colleagues. The authors are also deeply indebted to staff members E. A. Volkhonskii, B. S. Razov, V. A. Solov'ev, and I. K. Yurshe of the Physics and Engineering Institute for their valuable comments in the design and run-in of the closed deaeration loop.

LITERATURE CITED

1. V. V. Goncharov et al., Proceedings of the Geneva International Conference on the Peaceful Uses of Atomic Energy (1958).
2. A. O. Allen, Radiation Chemistry of Water and Aqueous Solutions, Moscow, State Atom Press [Russian translation] (1963).

3. P. I. Dolin and B. V. Ershler, Proceedings of the Geneva International Conference on the Peaceful Uses of Atomic Energy, Moscow, Goskhimizdat, 7, (1958) p. 687.
4. G. O. Monson, Decomposition of Water. Nuclear Reactor Engineering. USAEC Materials, Moscow, Foreign Lit. Press [Russian translation] (1957).
5. A. Kostyrko, Nukleonika, 5, 133, Poland (1960).

DIFFUSION OF URANIUM IN MOLYBDENUM, NIOBIUM, ZIRCONIUM, AND TITANIUM

(UDC 621.039.542/548.526)

L. V. Pavlinov, A. I. Nakonechnikov, and V. N. Bykov

Translated from Atomnaya Énergiya, Vol. 19, No. 6,
pp. 521-523, December, 1965
Original article submitted April 2, 1965; Revised July 19, 1965

The diffusion of uranium was studied in molybdenum, niobium, zirconium, and titanium. The diffusion coefficients were determined by measuring the over-all activity of the residue of the sample, using the α-radiation of uranium enriched with the U^{235} isotope to 90%, at temperatures 1500 to 2000°C (molybdenum, niobium) and 915 to 1200°C (zirconium, titanium).

The temperature dependence of the diffusion coefficients was given by the equations

$$D^{U}_{Mo} = 7.60 \cdot 10^{3} \exp(-76\,400/RT) \text{ cm}^2/\text{sec};$$
$$D^{U}_{Nb} = 8.90 \cdot 10^{-2} \exp(-76\,800/RT) \text{ cm}^2/\text{sec};$$
$$D^{U}_{Zr} = 7.77 \cdot 10^{-5} \exp(-25\,800/RT) \text{ cm}^2/\text{sec};$$
$$D^{U}_{Ti} = 4.90 \cdot 10^{-4} \exp(-29\,300/RT) \text{ cm}^2/\text{sec}.$$

The considerable differences between the diffusion mobilities and activation energies of molybdenum and niobium on the one hand and zirconium and titanium on the other were probably due to the effects of lattice defects, for example, excess vacancies arising in zirconium and titanium during polymorphic transformations.

Earlier investigations into diffusion in systems containing uranium have mainly been concerned with self-diffusion in pure uranium and its alloys, as well as chemical and reactive diffusion [1-5]. The results of these investigations are of particular interest in developing uranium alloys and studying the character and kinetics of interactions between uranium and other metals. Comparatively little data has been published on the diffusion of uranium in pure metals at low concentration gradients. Data furnished by work on these lines may be used for estimating the penetration of uranium when small uranium-concentration gradients arise on the surface on materials in contact.

In the present investigation we studied the diffusion of uranium in molybdenum, niobium, zirconium, and titanium. The diffusion coefficients were determined by the integral-residue method [6], using the α-radiation of uranium enriched to 90% with the isotope U^{235}. We studied molybdenum (99.98% Mo; 0.001% Ti; 0.008% Fe; 0.006% Si; 0.001% W), niobium (99.55% Nb; 0.03% Cu; 0.07% Fe; 0.01% Mo; 0.11% Si), zirconium (99.61% Zr; 0.01% Cu; 0.04% Fe; 0.01% Ni), and titanium (99.62% Ti; 0.07% Fe; 0.01% Mo; 0.01% Si). The samples of these metals were first annealed at 1500°C (molybdenum, niobium) and 1000°C (zirconium, titanium). Uranium was deposited on the samples in the form of a thin layer some 0.1 μ thick by vacuum evaporation (vacuum 10^{-5} mm Hg). The diffusion annealing of the zirconium and titanium samples was carried out at 915 to 1200°C in resistance furnaces with nichrome and carborundum heaters. While being annealed, the samples were kept in a hermetically-sealed quartz ampoule previously evacuated to a residual pressure of 10^{-4} mm Hg. In order to prevent possible oxidation, the samples were covered with titanium or zirconium chips. The temperature was measured with a platinum-platino-rhodium thermocouple to an accuracy of ±5°C.

The diffusion annealing of the molybdenum and niobium samples was carried out at 1500 to 2000°C in a high-temperature vacuum furnace with a tungsten heater at a residual pressure of (3 to 5) · 10^{-5} mm Hg. In this case the temperature was measured by a tungsten-rhenium thermocouple graduated from the melting points of the pure metals. The accuracy of temperature measurement was ±10°C. The time of the diffusion annealing varied from 1

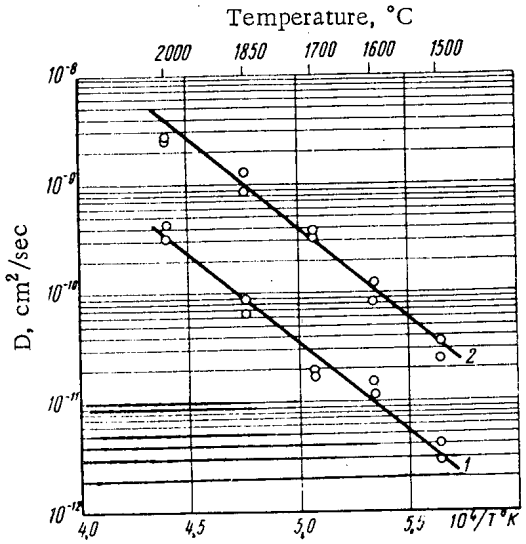

Fig. 1. Temperature dependence of the diffusion coefficient of uranium in 1) molybdenum and 2) niobium.

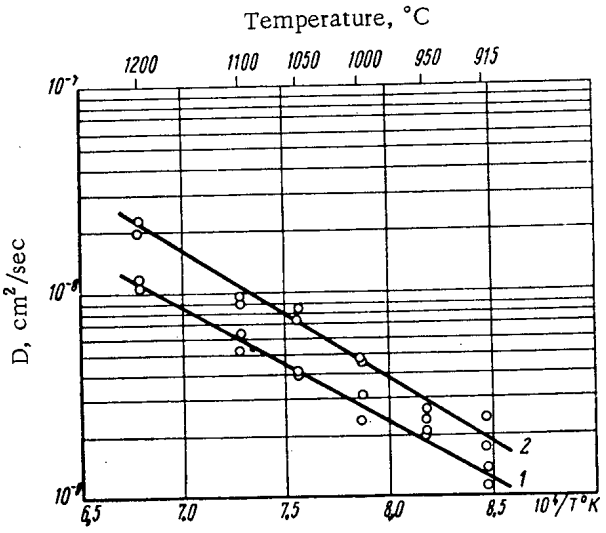

Fig. 2. Temperature dependence of the diffusion coefficient of uranium in 1) zirconium and 2) titanium.

to 20 h. The corresponding depth of penetration of the uranium was 50 to 200 μ. The thickness of the layers removed was determined from the difference between the thicknesses of the samples before and after such removal; the accuracy of this was 2 to 3 μ. The activity was measured on a B-2 radiometer with a scintillation attachment. The duration of the measurements was selected in such a way that the relative error should not exceed ±1%. Under these conditions the relative error in measuring the diffusion coefficient was approximately 12% and that in measuring the activation energy 5%.

The diffusion coefficient was determined by the integral-residue method developed by P. L. Gruzin. For α-radiation the computing equation has the form:

$$\ln I_n = A - \frac{x_n^2}{4Dt},$$

where I_n is the over-all activity of the residue of the sample after removing a layer of thickness x_n, A is a constant, D the diffusion coefficient, and t the duration of the diffusion anneal.

Figures 1 and 2 present graphs of the temperature dependence of the diffusion coefficient. The activation energies ΔH and frequency factor D_0 calculated from these graphs appear below:

Metal	Activation energy, cal/g · atom	Frequency factor, cm^2/sec
Molybdenum	76,400	$7.60 \cdot 10^{-3}$
Niobium	76,800	$8.90 \cdot 10^{-2}$
Zirconium	25,800	$7.77 \cdot 10^{-5}$
Titanium	29,300	$4.90 \cdot 10^{-4}$

We see from these data that the diffusion of uranium in molybdenum and niobium is characterized by comparatively high values of activation energy. This result corresponds to the high melting point and self-diffusion activation energy in molybdenum (T_m = 2620°C; ΔH = 92,400–115,000 cal/g · atom) [7, 8] and niobium (T_m = 2470°C; ΔH = 84,000–105,000 cal/g · atom) [9, 10]. The activation energy for the diffusion of uranium in molybdenum and niobium, however, is lower than the corresponding values for self-diffusion in these metals. This indicates that the uranium atoms are less strongly bound in the molybdenum and niobium lattices than the atoms of the main metal. This may also be correlated with the fact that alloying molybdenum and niobium with uranium leads to a fall in the melting point.

The activation energy for the diffusion of uranium in zirconium and titanium is considerably smaller than the values quoted for molybdenum and niobium. Zirconium and titanium, despite the comparatively high melting

points, have anomalously low values of activation energy for self-diffusion and the diffusion of metallic impurities. Thus for the temperature range 900 to 1200°C the experimental values of self-diffusion activation energy in β-zirconium (24,000 to 38,000 cal/g · atom) [11, 12] and β-titanium (31,200 cal/g · atom) [13] are two or three times smaller than the calculated values (70,000 to 80,000 cal/g · atom).

It follows that our own low values for the activation energy corresponding to the diffusion of uranium in zirconium and titanium are in accordance with the self-diffusion data for these metals. In our opinion, the anomalies in question are due to the influence of a polymorphic $\alpha \rightleftharpoons \beta$-transformation in zirconium and titanium; this causes atomic defects such as excess vacancies to arise. The reduction in activation energy and the rise in diffusion mobility result from this.

LITERATURE CITED

1. A. A. Bochvar, V. G. Kuznetsova, and V. S. Sergeev, In the book: Transactions of the Second International Conference on the Peaceful Use of Atomic Energy, Geneva, 1958, Contributions of Soviet Scientists, Vol. 3 [in Russian], Moscow, Atomizdat (1959), p. 370.
2. A. A. Bochvar et al., Contribution No. 333 Presented by the Soviet Union to the Third International Conference on the Peaceful Use of Atomic Energy [in Russian], Geneva (1964).
3. Y. Adda and A. Kirianenko, J. Nukl. Materials, 1, 120 (1959).
4. Y. Adda et al., C. R. Acad. Sci., 250, 536 (1960).
5. J. Philibert and Y. Adda, Colloque sur la diffusion a l'etat solide, Saclay, France (1958), p. 163.
6. P. L. Gruzin, Dokl. AN SSSR, 86, 289 (1952).
7. L. V. Pavlinov and V. N. Bykov, "Fizika metallov i metalloved.," 18, 459 (1964).
8. R. Resnik and L. Gastleman, Trans. AIME, 218, 436 (1960).
9. P. V. Gel'd and V. D. Lyubimov, Izv. AN SSSR, Otd. tekhn. and Metallurgiya i toplivo, 6, 119(1961).
10. R. Peart, D. Graham, and D. Tomlin, Acta Metallurgica, 10, 519 (1962).
11. E. B. Borisov et al., In the collection: Metallurgy and Physical Metallurgy of Pure Metals [in Russian], Moscow, Izd. AN SSSR (1958), p. 291.
12. V. S. Lyashenko, V. N. Bykov, and L. V. Pavlinov, Fizika metallov i metalloved., 8, 362 (1959).
13. I. Murdock, T. Lundy, and E. Stanslbury, Acta Metallurgica, 12, 1033 (1964).

All abbreviations of periodicals in the above bibliography are letter-by-letter transliterations of the abbreviations as given in the original Russian journal. *Some or all of this periodical literature may well be available in English translation.* A complete list of the cover-to-cover English translations appears at the back of this issue.

USE OF CONCRETES FOR HIGH-TEMPERATURE SHIELDING OF NUCLEAR REACTORS

(UDC 621.039.538.7)

V. B. Dubrovskii, N. V. Krasnoyarov, M. Ya. Kulakovskii,
B. K. Pergamenshchik, M. S. Pinkhasik, and V. I. Savitskii

Translated from Atomnaya Énergiya, Vol. 19, No. 6,
pp. 524-529, December, 1965
Original article submitted January 21, 1965; Revised July 19, 1965

The authors have studied the possibility of using chromite and chomotte heat-resistant concretes for the thermal shields of reactors. They observe neutron fluxes of various intensities (up to 10^{13} neutrons/cm^2 · sec, with spectrum similar to fission spectrum), absorbed by shields of these materials. They compute the transmission of neutrons and of fluxes of gamma quanta and the heat emission in the shielding. They calculate the temperatures in the shielding for various neutron fluxes, concrete thicknesses and cooling conditions. They perform a statistical calculation of the temperature stresses for shielding constructed of heat-resistant ferroconcrete.

It was established that nuclear reactor shields can be made from heat-resistant ferroconcrete when the neutron fluxes on the concrete are up to 10^{13} neutrons/cm^2 · sec, for temperatures up to 1000-1100°C and temperature differences of up to 900°C.

Concretes can be used for nuclear reactor shielding at high temperatures on the following conditions:

1. The concrete must possess efficient shielding properties for neutrons and gamma rays, and also retain satisfactory mechanical and thermal characteristics;

2. The temperature stresses arising in the concrete and reinforcement, and also the deformation and fissuration, must not exceed the permitted values;

3. The concrete must retain radiation stability at given integral neutron fluxes.

In connection with the tendency to increase thermal loads in the biological shielding of power reactors and dispense with thermal shielding, we studied the heat resistance of some concretes which have already been used for biological shielding [1, 2]. We determined the thermophysical characteristics, strength loss and modulus of elasticity at various temperatures for normal, barytic, magnetite, limonite, and other special concretes. Since these materials were designed to be efficient shields rather than heat-resistant materials, it was found that they are suitable for use only at 100-350°C. However, earlier studies [1, 2] did not determine all the characteristics necessary for calculating the temperature stresses.

The problem of calculating temperature stresses in concrete nuclear reactor shields has not been very completely worked out. Various authors [2-5], in making preliminary calculations of temperature stresses in ferroconcrete shields, based their work on the classical theory of elasticity [6]. On the basis of these calculations, it was recommended that temperature differences through the shielding should be limited to 30-90°C, as further increase would require so much reinforcement to take up the tension that construction would be impossible. However, these calculations cannot be regarded as reliable, because they took no account of the plastic properties of the concrete and steel or of the changes with temperature in strength, elasticity, creep rate, shrinkage and linear expansion coefficient of the concrete and reinforcement.

Calculations of the temperature stresses in the shielding by elasticity-theory methods lead to overly high results, which compel us to place between the reactor tank and the concrete shields a thermal shield to reduce the radiation flux and heat emission in the concrete. The thermal shields are made of scarce, costly materials and con-

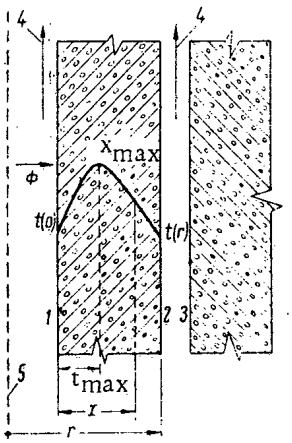

Fig. 1. Shielding system. 1, 2) Inner and outer surfaces of layer of heat-resistant concrete; 3) inner surface of layer of ordinary concrete; 4) gas cooler; 5) reactor axis. t_{max} = maximum temperature; t(r) = temperature of external surface of layer; t(o) = temperature of inner surface of layer; Φ = neutron flux; r = distance from source.

siderably complicate the construction of the reactor. These difficulties are aggravated in fast reactors, which have higher fluxes of radiation.

In this article we consider the possibility of making thermal shields of chromite and chamotte heat-resistant concretes (Fig. 1). Chromite concrete was chosen because its characteristics are satisfactory from the physical viewpoint: the presence of light oxygen nuclei, the marked inelastic deflection of neutrons and the high cross section for capture of thermal and epithermal neutrons by chromium and iron nuclei ensure efficient moderation and absorption of neutrons. The relatively high density (~ 3 g/cm^3) makes chromite concrete also an efficient material for shielding against gamma rays. Chamotte concrete has less satisfactory shielding properties, but is widely used in industry [7-10].

Tables 1 and 2 give the chemical compositions, heat resistances, strengths, thermotechnical properties etc. of the concretes according to literature and standard data [7, 11, 12]. The use of chromite and chamotte concretes in intense radiation fluxes, and thus at high temperatures, may lead to almost complete elimination of their chemically combined water. For this reason, the shielding properties of the materials were determined from the compositions given in Table 1, but with the exclusion of water.

The compositions of the radiation falling on the shielding differed markedly in different reactors, both in the leakage neutron spectrum and in the ratio between the neutron and gamma-ray fluxes. As a rule, it is the gamma radiation which is crucial from the point of view of heat emission in the shielding in thermal reactors, whereas in fast reactors it is the neutron flux (capture gamma-radiation).

In this article we calculate the heat evolution in concrete, determined by the neutron fluxes, on the assumption that gamma-ray flux incident on the shielding is equal to zero. However, from our results it is not difficult to estimate the flux of mixed radiation. For convenience, the following scheme was followed in the calculation: the neutron source was regarded as an infinite layer of pure Pu^{239} of thickness 5 cm next to which is placed the concrete under investigation. The spectrum of leakage neutrons from such a layer is close to the fission spectrum.

TABLE 1. Chemical Compositions of Chromite and Chamotte Concretes, Wt. %

Concrete	Elements										
	Si	Ca	O	Mg	Al	Fe	S	H	Cr	Na	others
Chromite	2,9	4,7	35	9,3	5,6	8,3	0,6	0,6	32	1	—
Chamotte.	20,8	7,3	53,5	0,41	12,40	0,84	0,05	1,9	—	—	2,8

TABLE 2. Properties of Chromite (Mark 400) and Chamotte Concretes

Concrete	Bulk density, t/m^3	Maximum permissible temperature, °C	Coefficient of thermal conductivity at 700°C, kcal/m · h · °C	Temp. coefficient of total linear deformation at 700°C	Modulus of elasticity at room temp., kg/cm^2	Transverse compressive strength at room temp., kg/cm^2
Chromite . . .	2,8—3,0	1700	1,35	$3,4 \cdot 10^{-6}$	$3,3 \cdot 10^5$	200
Chamotte. . .	1,8—2,0	1200	0,98	$3,5 \cdot 10^{-6}$	$2 \cdot 10^5$	200

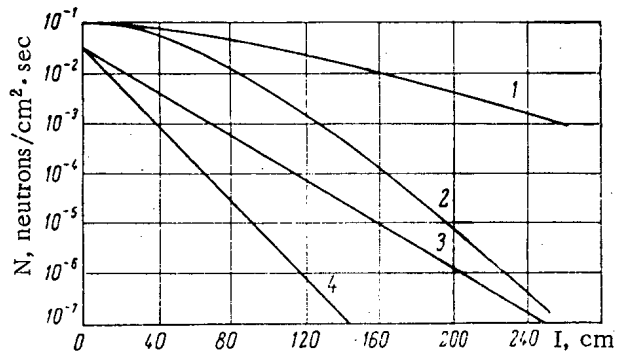

Fig. 2. Distribution of neutron fluxes in shielding. 1) Total flux in Chamotte concrete; 2) total flux in chromite; 3) fast neutrons (E > 1.4 MeV) in chamotte concrete; 4) fast neutrons (E > 1.4 MeV) in chromite concrete.

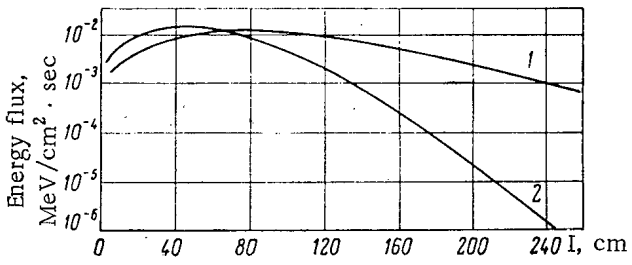

Fig. 3. Distribution of gamma-radiation fluxes in shielding, per incident neutron. 1) In chamotte concrete; 2) in chromite concrete.

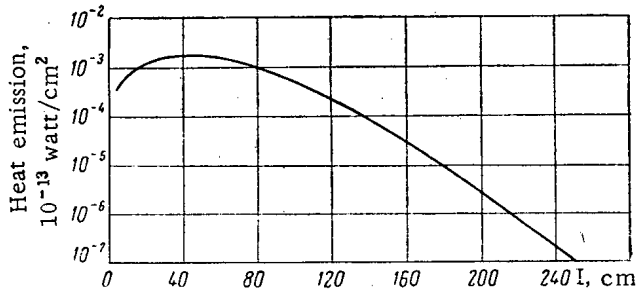

Fig. 4. Distribution of heat emission in chromite concrete shielding, per incident neutron.

The Neutron Transmission Calculations Were Performed in an 18-group Approximation[13]. The Distribution of Neutrons by Groups as Follows:

No. of group	E_{min}, MeV	No. of group	E_{min}, MeV	No. of group	E_{min}, MeV
1	1,4	7	0,025	13	$0,2 \cdot 10^{-4}$
2	0,6	8	0,01	14	$0,73 \cdot 10^{-5}$
3	0,4	9	$0,18 \cdot 10^{-2}$	15	$0,27 \cdot 10^{-5}$
4	0,2	10	$0,4 \cdot 10^{-3}$	16	$0,1 \cdot 10^{-5}$
5	0,1	11	$0,15 \cdot 10^{-3}$	17	$0,37 \cdot 10^{-6}$
6	0,05	12	$0,54 \cdot 10^{-4}$	18	$0,37 \cdot 10^{-6}$

The transmission of fast neutrons (with E > 1.4 MeV) was represented by means of the method of extraction cross section [5, 14, 15]. The extracted fast neutrons served as sources for neutrons of the lower groups. Neutron fluxes with E < 1.4 MeV were analyzed in the diffusion-age approximation [16]. Figure 2 gives the resultant distributions of neutron flux across the thickness of chromite or chamotte concretes (the total neutron flux incident on the shielding was normalized to 1 neutron /cm² · sec). From Fig. 2 we find that in traversing 200 cm of chromite concrete the total neutron flux is attenuated by a factor of 10^4, while the flux of fast neutrons is attenuated by a factor of 10^7. In the same thickness of chamotte concrete, the total neutron flux is reduced only by a factor of 20, the fast neutron flux by 10^4. Owing to the poor efficiency of chamotte concrete, it is convenient henceforward to consider only chromite concrete (relaxation length for total neutron flux 19 cm, for fast neutrons 12.2 cm, linear absorption coefficient for gamma radiation with energy 6 MeV 0.087 cm^{-1}).

From the neutron fluxes found, we determined the densities of the sources of capture gamma radiation, and calculated the densities of the sources of capture gamma-radiation, and calculated the gamma-ray flux and heat emission by the method described in [17]. The results are given in Figs. 3 and 4. It was found that a flux of 1 neutron/cm² · sec corresponds to total heat emission in chromite concrete of $\sim 1.4 \cdot 10^{-13}$ watt/cm², which is equivalent to a gamma-ray flux on the concrete of ~1 MeV/cm² · sec. This relation can be used to estimate the permissible flux of mixed radiation on chromite concrete. In calculating the temperatures, we made the following simplifying assumptions: we neglected heat loss in the vertical direction; the thermal conductivity of the chromite concrete was taken as constant throughout the temperature range and equal to 1.35 kcal/m · h · °C; the surface of the shielding was cooled by gas at 50°C at all points; the heat-transfer coefficient was taken as equal for the internal and external surfaces of the shielding layer. The temperature distribution across the thickness of the chromite concrete can be represented by the following formula:

$$t(x) = -\frac{1}{\lambda} P(x) + C_1 x + C_2,$$

where

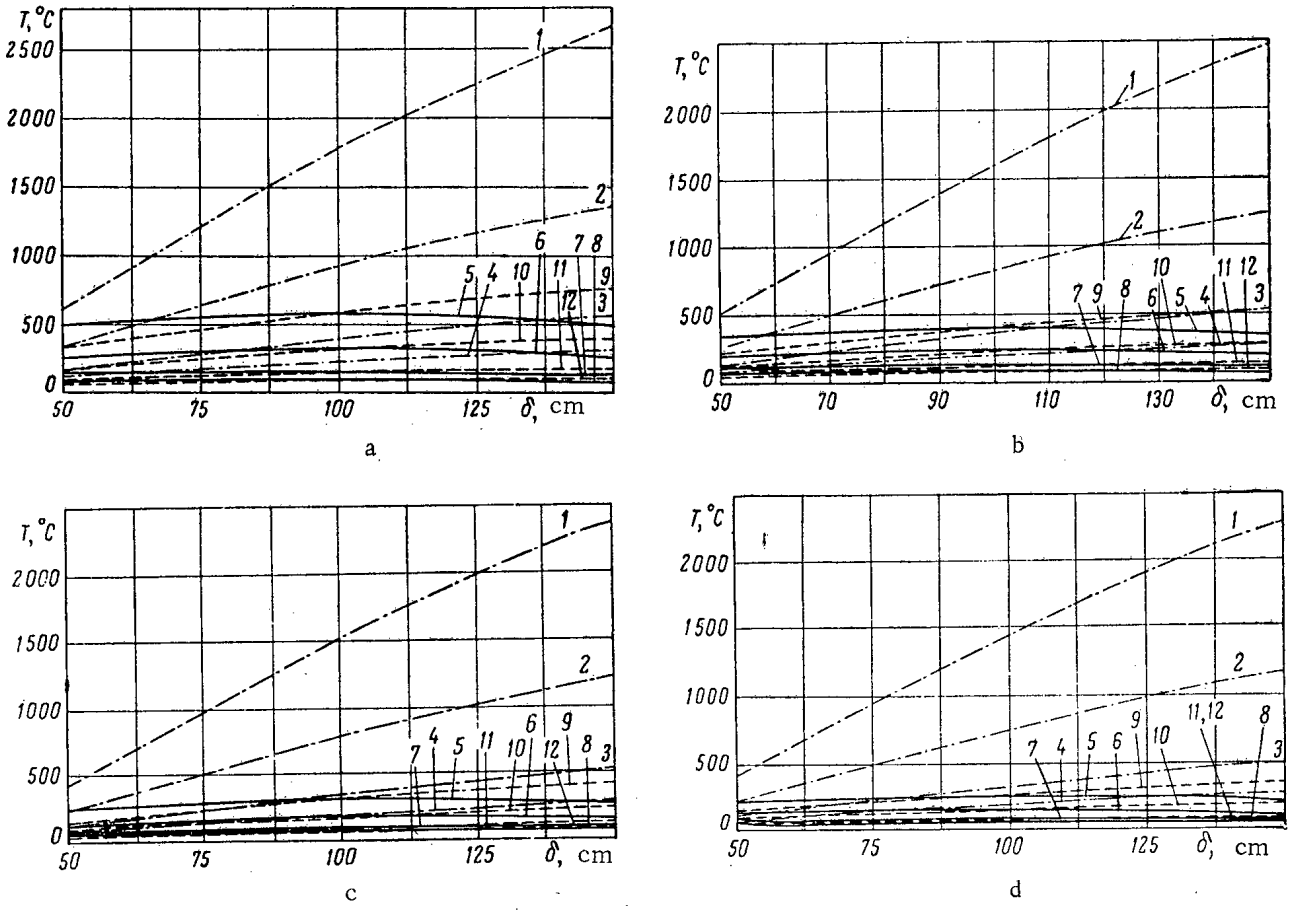

Fig. 5. Temperatures at point x_{max} and at surface of shielding layer, plotted versus neutron flux Φ, heat-transfer coefficient α, and layer thickness σ: a) α = kcal/m² · h · °C; b) α = 15 kcal/m² · h · °C; c) α = 20 kcal/m² · h · °C; d) α = 25 kcal/m² · h · °C; 1) t_{max} for flux 10^{13} neutrons/cm² · sec; 2) $5 \cdot 10^{12}$ neutrons/cm² · sec; 3) $2 \cdot 10^{12}$ neutrons/cm² · sec; 4) 10^{12} neutrons/cm² · sec; 5) t(r) for flux 10^{13} neutrons/cm² · sec; 6) $5 \cdot 10^{12}$ neutrons/cm² · sec; 7) $2 \cdot 10^{12}$ neutrons/cm² · sec; 8) 10^{12} neutrons/cm² · sec; 9) t(o) for flux 10^{13} neutrons/cm² · sec; 10) $5 \cdot 10^{12}$ neutrons/cm² · sec; 11) $2 \cdot 10^{12}$ neutrons/cm² · sec; 12) 10^{12} neutrons/cm² · sec.

$$C_1 = \frac{\frac{\alpha}{\lambda} P(\delta) + Q(\delta)}{2\lambda + \alpha\delta}; \quad C_2 = \frac{\lambda}{\alpha} C_1 + t_{gas}; \quad Q(x) = \int_0^x q(y)\,dy; \quad P(x) = \int_0^x Q(y)\,dy;$$

λis the thermal conductivity of the concrete; α is the coefficient of heat transfer; q(x) is the heat-emission distribution; and δ is the thickness of the concrete layer.

It is assumed that the velocity of the coolant gas is 2-10 m/sec. This corresponds to heat-transfer coefficients of α ≈ 10-25 kcal/m² · h · °C. The temperature in the concrete was calculated for α = 10, 15, 20, and 25 kcal/m² · h · °C, neutron fluxes of 10^{13}, $5 \cdot 10^{12}$, $2 \cdot 10^{12}$, and 10^{12} neutrons/sec · cm², and concrete thicknesses of 75, 100, 125, and 150 cm. The concrete temperatures at the point x_{max} and at the surface are given in Fig. 5; this figure enables us to calculate, for given radiation flux and coefficient of heat transfer, the thickness of chromite concrete shielding for which the temperatures of the concrete and reinforcement will not exceed the permissible values.

Nonuniform heating of a statistically indeterminate structure (as our shielding – a thick-walled cylinder – is) leads to the formation of thermal bending moments: compressive forces arise in the hotter part, tensions in the cooler parts. While the former are taken up by the concrete, in order to absorb the latter reinforcement must be applied to the cooler outer surfaces. The temperature moment in the wall of the cylinder, given a linear temperature drop, will depend on the magnitude of the drop and the rigidity of the cross section. When the temperature and

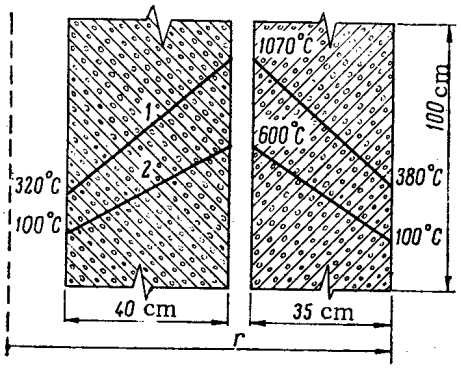

Fig. 6. Temperature distribution in shield of thickness 75 cm. 1) $\Phi = 10^{13}$ neutrons/cm^2 · sec, α = 15 kcal/m^2 · h · °C; 2) most unfavorable.

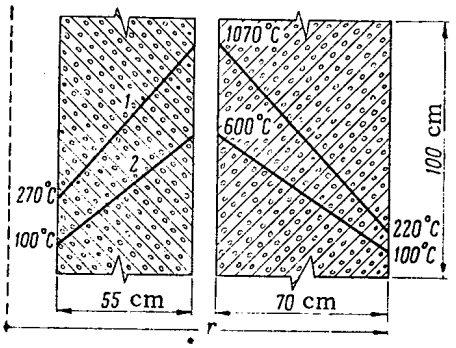

Fig. 7. Temperature distribution in shield of thickness 125 cm. 1) $\Phi = 5 \cdot 10^{12}$ neutrons/cm^2 · sec, α = 15 kcal/m^2 · h · °C; 2) most unfavorable.

TABLE 3. Reinforcement and Fissure Width in Various Types of Shielding

Scheme of calculation	Layer thickness, cm	Ring reinforcement: Diameter, mm	Ring reinforcement: Spacing, mm	Maximum width of fissures, cm	Distance between fissures, cm
1 (see Fig. 6, 1)	40	20	150	0,0065	23,3
	35	20	200	0,0069	25,7
2 (see Fig. 7, 1)	55	25	200	0,0096	35
	70	25	150	0,0125	35
3 (see Fig. 6, 2)	40	20	150	0,066	23,3
	35	20	200	0,085	25,7
4 (see Fig. 7, 2)	55	25	200	0,083	35
	70	25	150	0,063	35

the temperature drop are small, the cross section of the ferroconcrete acts as an integral whole (no cracks appear in the part under tension); the rigidity of the cross section is found from the formula

$$B = EJ,$$

where E is the modulus of elasticity of the concrete, J the moment of inertia of the cross section. At this stage the temperature moment is proportional to the temperature drop; but as the latter increases, a moment arrives when the tensile forces become so great that cracks form in the part of the concrete under tension, and the rigidity of the element falls off. With further increase in the temperature drop, there is little increase in the stresses, because the rigidity of the element rapidly falls by the growth of deformation in the compressed part of the concrete at high temperatures (at 1000°C the modulus of elasticity of heat-resistant chromite concrete is reduced by a factor of 20).

In correspondence with the analysis of ferroconcrete structures given in [18-21], we carried out a statistical calculation of two types of cylindrical shielding. We took the maximum neutron fluxes and shield thicknesses for which the temperature was close to the permissible limit for concrete (1100-1300°C) and reinforcement (500°C). Figures 6 and 7 give the temperature distributions through the thickness of the shielding and the schemes of calculation for various concrete thicknesses, neutron fluxes and heat-transfer coefficients.

To reduce the rigidity of the ring at cross section x_{max}, we provided a circular groove. Calculations on the cylinder were made only in a horizontal plane. The temperature drops for the cases given in Fig. 6 (1) and Fig. 7 (1) are not the most unfavorable from the viewpoint of temperature stresses.

Experimental studies [19] have shown that the greatest thermal stresses arise in heat-resistant ferroconcrete structures at 500-600°C; owing to plastic deformation, further increase of temperature does not lead to an increase in thermal stress. Selection of the reinforcement and testing of the stresses in the concrete were therefore performed in addition for the theoretically most unfavorable temperature distributions, as shown in Fig. 6 (2) and Fig. 7 (2).

For statistical analysis, the material used was chromite concrete Mark 400 and hot-rolled repeating-shape reinforcement Mark 2 x 13.

The characteristics of the materials and the procedure for the calculation were taken from [12]. The results are shown in Table 3.

The already-mentioned theoretical investigations lead to the following conclusions:

1. Heat-resistant concrete can be used for nuclear reactor shielding with incident neutron fluxes of up to 10^{13} neutrons/cm^2 · sec, and $t \leq 1000$-1100°C with up to 900°C temperature drop through the concrete. For practical application of heat-resistant concretes as shielding, their radiation stability must be investigated.

2. Reinforcement of concrete shielding, the stresses and deformations do not exceed the values given by existing norms.

3. Concrete made of Portland cement with chromite filler possesses excellent shielding properties, even when dehydrated.

LITERATURE CITED

1. A. N. Komarovskii, Construction of Nuclear Plants [in Russian], Moscow, Gosénergoizdat (1961).
2. J. Struct. Div., 84, 1 (1958).
3. D. Halliday, Heat Release in Concrete Reactor Shield HERE, R/p, 1963, Harwell (1956).
4. J. Lane, Nucleonics, 13, No. 6, 36 (1955).
5. B. Price, K. Horton, and K. Spinney, Shielding against Nuclear Radiation [Russian translation], Moscow, Izd. Inostr. Lit. (1959).
6. Bautechnik, No. 1, 7 (1962).
7. K. D. Nekrasov, Heat-Resistant Concrete [in Russian], Moscow, Promstroiizdat (1957).
8. K. D. Nekrasov and A. V. Zotov, Preparation of Refractory Concretes and Their Applications in Thermal Plant [in Russian], Moscow, Stroiizdat (1950).
9. K. D. Nekrasov, Experience in the Use of Heat-Resistant Concrete in Thermal Plant [in Russian], Moscow, Gosstroiizdat (1957).
10. V. I. Murashov and B. A. Al'tshuler, Construction of Thermal Plant from Heat-Resistant Ferroconcrete [in Russian], Moscow, Gosstroiizdat (1958).
11. Instructions on the Technology of Preparation and Use of Heat-Resistant Concretes [in Russian], No. CH-156-61, Moscow, Gosstroiizdat (1962).
12. A. F. Milovanov, Heat-Resistant Ferroconcrete [in Russian], Moscow, Gosstroiizdat (1963).
13. G. Marchuk, Proceeding of Seminar, Vienna (August, 1961); Physics of Fast and Intermediate Reactors, Vol. II, Vienna (1962).
14. D. L. Broder, A. A. Kutuzov, V. V. Levin, and V. V. Frolov, In symposium: Topics in the Physics of Reactor Shielding [in Russian], Moscow, Gosatomizdat (1963), p. 52.
15. B. I. Sinitsyn and S. G. Tsypin, In symposium: Topics in the Physics of Reactor Shielding [in Russian], Moscow, Gosatomizdat (1963), p. 75.
16. G. I. Marchuk, Calculation Methods for Nuclear Reactors [in Russian], Moscow, Gosatomizdat (1961).
17. Shielding of Nuclear Reactors (Symposium), Ed. by T. Rockwell [Russian translation], Moscow, Izd. Inostr. Lit. (1963).
18. V. I. Murashov, Fissure Resistance, Rigidity and Strength of Ferroconcrete [in Russian], Moscow, Mashstroiizdat (1950).
19. Investigations on Heat-Resistant Concrete and Ferroconcrete (Symposium) [in Russian], Ed. by V. I. Murashov, Moscow, Gosstroiizdat (1954).
20. Instructions on Planning of Ferroconcrete Smokestacks [in Russian], Moscow, Gosstroiizdat (1962).
21. Provisional Directions on Planning Heat-Resistant Ferroconcrete Structures No. (U-151-56/MCPMKhP), Moscow, Gosstroiizdat (1957).

NOTES ON ARTICLES RECEIVED

CALCULATING THE DIPOLE MOMENT OF A CYLINDRICAL SLUG

(UDC 621.039.51)

B. P. Kochurov

Translated from Atomnaya Énergiya, Vol. 19, No. 6,
p. 530, December, 1965
Original article submitted February 15, 1965; Note submitted September 22, 1965

In [1, 2] is given the theory of a heterogeneous reactor with cylindrical slugs of finite radius. Each slug, as well as a thermal constant, has a dipole moment which enters the determination of the squared diffusion length and neutron age for the radial and axial directions. The dipole moment can be calculated for an individual slug without reference to the general theory.

Consider a cylindrical slug with axis along the Z axis in an infinite moderator. Let us suppose that the neutron distribution outside the slug has constant gradient along the X axis. From Boltzmann's equation it follows that the vector $g_x = \int (\mu_x + x\Sigma_{tr3}) \times \mu \; N(\mathbf{r}, \mu) d\mu$, characterizing the "dipole flux," satisfies some equation of continuity, and in particular, in the moderator div $\mathbf{g}_X = 0$. Hence it follows that the dipole moment P for the radial direction is equal to the flux of vector $\mathbf{g}_X$ through the surface of the slug:

$$P = \int_{S_0} g_x \, dS_0.$$

In the absence of scattering in the slug, the angular neutron distribution in this integral is equal to

$$N(\mathbf{r}_{S_0}, \mu) = \frac{1}{4\pi} \int N_0(\mathbf{r}') \, e^{-\Sigma \tilde{R}} \, dR,$$

where the integration is carried out along a ray in the moderator. In calculating P, the diffusion distribution is taken as $N_0(\mathbf{r}')$. For a slug with scattering, we introduce the capture probability Γ, which is calculated by the method of successive collisions on the assumption that the angular distribution of neutrons incident on the slug is the same as that in an undisturbed medium. The formula for P contains the relative value Γ/Γ_c, where Γ_c is the value of Γ for a slug without scattering. Finally, the dipole moment P is expressed in terms of certain tabulated functions. For a blank or black slug, simpler formulas are derived. For a blank slug, the formula for the dipole moment is similar that that of Benoist [3] (which was derived by a totally different method) and is practically the same as Carter's result in [4]. For black slugs, a physically valid limiting transition is made for large and small slugs. As shown by comparison, the above method is more accurate than the P_2 approximation of the method of spherical harmonics.

LITERATURE CITED

1. A. D. Galanin and B. P. Kochurov, Atomnaya Énergiya, 15, 107 (1963).
2. R. Bednazh and B. P. Kochurov, Nukleonika, IX, 439 (1964).
3. P. Benoist, Rapport SPM No. 759, Saclay (1963).
4. C. Carter and R. Jarvis, J. Nucl. Energy, 15, 133 (1961).

REDUCTION IN THE THERMAL NEUTRON FLUX CAUSED BY A HOLLOW CHANNEL IN THE REFLECTOR

(UDC 621.039.512.45)

A. S. Kochenov

Translated from Atomnaya Énergiya, Vol. 19, No. 6,
pp. 530-531, December, 1965
Original article submitted July 19, 1965; Note submitted September 15, 1965

An integral equation, the solution of which can be found by using the method of successive approximations, is used for calculating the thermal neutron flux at the center of the bottom of a cylindrical channel with the radius R. In the first approximation, it is assumed that the thermal neutron "sources" outside the channel are distributed in the same manner as if the channel were filled with the reflector material.

If the thermal neutron flux does not change over the transverse cross section of a channel filled with the reflector material, and the distribution

$$\Phi(x)=\Phi(0)\,e^{-x/L}, \tag{1}$$

where x is the distance from the channel bottom, holds along the channel, the relative flux reduction can be found with an accuracy to ~3% from the following expression:

$$\frac{\Phi_1'(0)}{\Phi(0)}=\frac{1+J}{2}. \tag{2}$$

Here, $\Phi_1'(0)$ is the thermal neutron flux at the center of the bottom of a hollow channel;

$$J=R/L\left\{\frac{\pi}{2}[H_1(R/L)-N_1(R/L)]-1\right\}, \tag{3}$$

where H_1 is the Struve function, and N_1 is the Neumann function. The solutions of the equations for channels with square and triangular cross sections indicate that, if the equivalent (with respect to the channel area) radius is introduced, and thus obtained results virtually coincide with the data for a cylinder.

J Values in Dependence on the R/L Ratio

R/L	J calculated by means of (3)	J calculated by means of (4)	$\Delta J = J - J_L$*
0,0	1,000	1,000	0,000
0,2	0,846	0,821	0,003
0,4	0,740	0,695	0,011
0,6	0,657	0,638	0,019
0,8	0,592	—	0,026
1,0	0,538	—	0,032

* The J value was calculated by means of expression (3); J_L is the contribution to J due to neutrons scattered in a layer with the thickness L.

For a narrow channel where R/L << 1, we obtain with an accuracy to the $(R/L)^4$

$$J=1-R/L+\frac{1}{2}\left(\frac{3}{2}-C\right)(R/L)^2+\frac{1}{3}(R/L)^3, \tag{4}$$

where C = 0.5772 is the Euler constant. The thus obtained J values in dependence on the R/L ratio are given in the table.

Equation (2) holds for narrow channels (R/L<<1). Investigating the limiting processes, we can write the interpolation expression for any R/L value:

$$\frac{\Phi'(0)}{\Phi(0)}\gtrsim J. \tag{5}$$

If the distribution of the thermal neutron flux is symmetric with respect to the channel axis, we have

$$\frac{\Phi'(0)}{\Phi(0)} \approx \frac{\Phi(0)_R}{\Phi(0)} J, \tag{6}$$

where $\Phi(0)_R$ is the thermal neutron flux at the bottom of a channel filled with the reflector material at the distance R from the channel axis.

APPLICABILITY OF VARIOUS APPROXIMATIONS OF THE METHOD OF SPHERICAL HARMONICS FOR CALCULATING THE TRANSMISSION OF NEUTRONS THROUGH SHIELDS

(UDC 539.125.52)

N. A. Artem'eva, K. K. Popkov, S. M. Rubanov,
and L. S. Shkorbatova

Translated from Atomnaya Énergiya, Vol. 19, No. 6,
pp. 531-532, December, 1965
Original article submitted June 15, 1965; Note submitted September 20, 1965

We investigated the accuracy of various approximations of the method of spherical harmonics by comparing the experimental data on the space-energy distributions of neutron fluxes in different media, obtained by means of multigroup calculations in the P_1-, P_2-, and P_3-approximations as well as in the age-diffusion approximation. The calculations in the P_1-, P_2-, and P_3-approximations were performed according to the 18-group method, which differed from the 21-group method [1] by the fact that the first four groups were combined into one. The seven-group method [2] that was used for calculations in the age-diffusion approximation was characterized by the fact that the first group (neutrons with an energy exceeding 1.5 MeV) was assigned in correspondence with experimental data or on the basis of the results of calculations performed with higher approximations.

Shield compositions including water, graphite, boron carbide, iron, lead, and also their homogeneous and heterogeneous mixtures were considered. These materials have different neutron and physical characteristics, which gives reason for assuming the generality of the results obtained. We analyzed the accuracy of describing the effective relaxation lengths of fast neutrons, the spectra of moderated neutrons, and the factors of thermal neutron accumulation in shielding media in different approximations of the polynomial method.

The following conclusions were reached on the basis of the investigations performed:

1. In using the method of spherical harmonics for determining the space-energy distribution of neutrons in the shield, we can limit our considerations to the P_3-approximation.

2. The P_1-approximation method without an allowance for the spatial distribution of the fast group can be used only for calculating shields with small thicknesses (not exceeding 5 to 8 mean free paths lengths).

If the leading neutron group is assigned in correspondence with experimental data or on the basis of calculations in higher approximations, the basic functionals of the shield can be determined with satisfactory accuracy by means of simple approximations (up to the age-diffusion approximation).

3. For compositions consisting of heavy and medium atoms, the shield functionals are determined by intermediate-energy neutrons. Because of the lower scattering anisotropy in these media, satisfactory results can also be obtained by using the P_2-approximation.

4. Near the boundaries in heterogeneous compositions, the P_2- and P_3-approximations secure satisfactory agreement in the description of fast-neutron flux distributions (for thicknesses smaller than 100 cm, discrepancies between the results do not exceed 50-70%); the agreement is even better for moderated and thermal neutrons.

LITERATURE CITED

1. G. I. Marchuk, Methods for Calculating Nuclear Reactors [in Russian], Moscow, Gosatomizdat (1961).
2. D. L. Broder et al., Atomnaya Énergiya, 12, 129 (1962).

CALORIMETRIC DOSIMETRY OF GAMMA RADIATION FROM NUCLEAR REACTORS

(UDC 536.629)

V. M. Kolyada and V. S. Karasev

Translated from Atomnaya Énergiya, Vol. 19, No. 6,
p. 532, December, 1965
Original article submitted July 29, 1965

The effect of radiation from nuclear reactors on materials and biological specimens depends on the energy spectrum, the intensity, and the absorbed dose of neutron and gamma radiations. Measurements of the gamma radiation energy spectrum by means of spectrometers are usually performed at the exits from horizontal channels. This yields only incomplete information on the gamma radiation from the core, since the intensity of the low-energy region of the spectrum ($E_\gamma < 1-1.5$ MeV), which accounts for a considerable share of the absorbed dose, is neglected in this case.

The proposed method is based on analyzing the data from calorimetric measurements of the doses absorbed in specimens with different dimensions, made of heavy materials, for which the neutron component can be neglected. After measuring the effective coefficients of absorption of the gamma radiation energy μ_α^{eff}/ρ for the materials under consideration (lead, tungsten, and tin), we can determine the gamma radiation intensity I_γ at the location where the specimens are irradiated and the reactor's gamma radiation spectrum in the 0-1.5 MeV energy range (Fig. 1), which, together with the results obtained in measuring the spectrum at the exit from the horizontal channel, is used for calculating the dependence of the effective mass absorption coefficient of the gamma radiation energy μ_α^{eff}/ρ on the charge Z of atomic nuclei (Fig. 2).

This information makes it possible to calculate the absorbed dose D_γ of gamma radiation from the reactor in any material whose composition is known with an error not exceeding 10%.

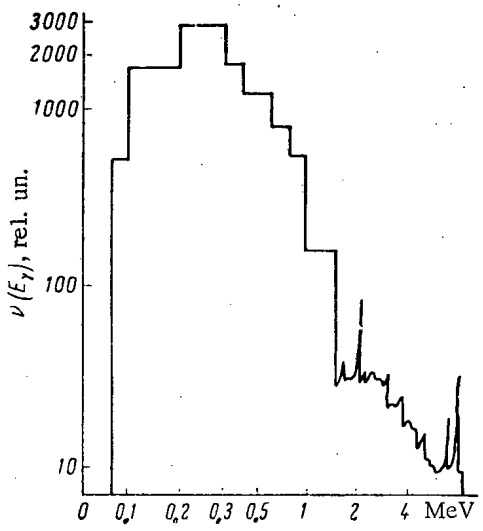

Fig. 1. Energy spectrum of gamma radiation from the VVR-M reactor ($I\nu = \int_0 \nu(E)\,EdE$ = 63.5 W/cm² for a reactor power level of 10 MW.

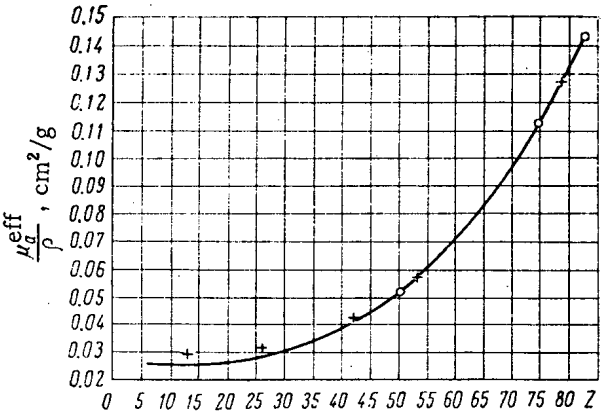

Fig. 2. Dependence of the effective mass absorption coefficient of the reactor's gamma radiation energy on Z. ○) Experiment; +) calculation.

DETERMINATION OF THE SURFACE RELIEF OF MATERIALS BY MEANS OF REFLECTED GAMMA RADIATION

(UDC 621.039.84)

P. L. Gruzin, V. N. Afanas'ev, and V. O. Gaiduchik

Translated from Atomnaya Énergiya, Vol. 19, No. 6,
p. 533, December, 1965
Original article submitted July 15, 1965

We investigated experimentally a method for determining the surface relief of friable materials which is based on producing on this surface a sharply defined gamma irradiated region and determining its coordinates by means of a finely collimated receiver which records the gamma quanta scattered in the surface layer of the material.

The experimental device consisted of two collimated Co^{60} sources with an activity of 14 Ci each and a mobile receiver which included an 80 × 40 mm NaI scintillation detector and a multichannel lead collimator. The materials investigated were iron ore and metallurgical coke.

As a result of this investigation, we checked the accuracy in determining the coordinates of the complex surface relief at distances of 1-5 m between the source and receiver levels and the surface. The coordinates of the relief points were determined with respect to the shape of the curve of intersection between the boundary of the irradiated region and the receiver's visibility region.

We estimated the mean absorption coefficient of the gamma quanta reflected from the surfaces of the materials. We also investigated the degree and the form of blurring of the irradiated section's boundary in the case where a steel collimator was used in the source. Moreover, we determined the fluxes of particles emerging from 1 cm^2 of the reflector's surface in a range of distances between the sources and the surface from 1 to 4 m for both materials under investigation.

RULES FOR DEPOSITING ARTICLES

Translated from Atomnaya Énergiya, Vol. 19, No. 6,
p. 533, December, 1965

Articles are deposited either on the authors' request or in accordance with the decision of the Editorial Board of the journal.

Detailed abstracts of the deposited articles will be published in the journal, while the complete articles will be kept at the Editor's Office and sent COD to readers on request. The volume of an abstract should not exceed two pages of typewritten text, while the volume of the text to be deposited should not exceed 20 to 22 pages. On the authors' request, diagrams, tables, the basic equations, etc., can be included in the abstract.

An abstract will be published no later than three to four months after the article has been received at the Editor's Office (if the article is deposited on the authors' request) or after the authors have agreed to deposit if (if this decision has been brought by the Editorial Board).

Deposited articles are regarded as scientific publications and are taken into consideration in the defense of dissertations.

The articles submitted for deposition must be presented by the authors in their final form, and they must be suitable for photographic reproduction. The text must be typed on a typewriter with a fresh black ribbon; the equations must be written with India or black ink; the drawings must be made on Whatman or tracing paper, inserted in the text and pasted on the paper, and provided with captions.

The price of a single copy of a deposited article is 40 k. In ordering copies of the deposited articles, reference must be made to the registration number of the article given at the end of the abstract.

Orders should be sent to the Editorial Office of the journal at the following address: 18 Kirov Street, Center, Moscow.

ON THE OSCILLATION DECREMENTS IN ACCELERATORS IN THE PRESENCE OF ARBITRARY ENERGY LOSSES

(UDC 621.384.6)

A. A. Kolomenskii

Translated from Atomnaya Énergiya, Vol. 19, No. 6,
pp. 534-535, December, 1965
Original article submitted May 25, 1965

In accelerators, particles experience energy losses caused by various effects (ionization and bremsstrahlung on residual gases, magnetic bremsstrahlung, etc.). These losses and their compensation by the high-frequency accelerating field lead to the following consequences: 1) oscillations (betatron and synchrotron) are excited as a result of the discrete nature of the losses, while the excitation mechanism recalls the excitation of oscillations in an oscillator under the action of noise; 2) the energy losses, on the average, produce a force which may play the role of positive or negative friction acting on the oscillations. Until now, this problem was considered only for one particular case – the loss due to magnetic bremsstrahlung in the relativistic motion of electrons (see, for instance, [1], Ch. 5).

The present article provides the expressions for the decrements of betatron and synchrotron oscillations in the presence of arbitrary energy losses. These expressions, which hold for any particle energy, make it possible to estimate the magnitude and the sign of the friction connected with the losses and also the efficiency of any method of artificial oscillation damping.

We shall abstract ourselves from the above-mentioned oscillation excitation connected with loss fluctuations. This excitation basically depends on the actual conditions, in particular, the fluctuation distribution function.

Let the instantaneous energy loss P depend on the total particle energy E, the magnetic field B at the point in question, the radial coordinate x (along the normal to the equilibrium orbit), and the generalized azimuth θ:

$$P = P(E, B, x, \theta).$$

For determining the oscillation decrements, we shall consider the equation of motion of particles:

$$\frac{d}{dt}(m\mathbf{v}) = \frac{e}{c}[\mathbf{vB}] + e\mathcal{E} - \frac{P}{v^2}v, \tag{1}$$

where the last term represents the damping force connected with the energy losses, $\mathbf{v}$ and m are the velocity and the total particle mass, respectively, and $\mathcal{E}$ is the electric field. Equation (1) holds if the direction of the dissipative force is in opposition to the velocity direction.

From Eq. (1), we can obtain linearized equations describing the motion in the symmetry plane of a cyclic accelerator in the vicinity of the equilibrium orbit (see [1], Ch. 5, paragraph 2):

$$\frac{d^2x}{d\theta^2} + \left(\Gamma_1 + \frac{\Gamma}{\beta^2}\right)\frac{dx}{d\theta} + \frac{K^2}{K_0^2}(1-n)\,x = \frac{K}{K_0^2}\cdot\frac{\varepsilon}{E_s}\,; \tag{2}$$

$$\frac{1}{E}\cdot\frac{d\varepsilon}{d\theta} = -\frac{eV\sin\varphi_s}{2\pi E}\eta - \Gamma(\theta)\left[\left(\frac{\partial \ln P}{\partial \ln E} - \frac{1-\beta^2}{\beta^2}\right)\frac{\varepsilon}{E} + \left(1 - n\frac{\partial \ln P}{\partial \ln B} + \frac{1}{K}\cdot\frac{\partial \ln P}{\partial x}\right)Kx\right], \tag{3}$$

where $K = K(\theta)$ is the curvature of the orbit, $2\pi/K_0$ is the length of the orbit, $n = (1/KB) \cdot (\partial B/\partial x)$ is the field index, $\beta = (v/c)$; $\varepsilon = E - E_s$; $\eta = \varphi - \varphi_s$, where φ_s and E_s are the equilibrium values of the phase and the energy, respectively, q is the multiplicity of acceleration, ω is the angular frequency, V is the amplitude of the accelerating voltage, and

$$\frac{d\eta}{d\theta} = q\left(Kx - \frac{\Delta\beta}{\beta}\right); \quad \Gamma = \frac{P}{\omega E}; \quad \Gamma_1 = \frac{1}{E}\cdot\frac{dE_s}{d\theta}. \tag{4}$$

The closed perturbed orbit $x_0(\theta)$ is described by the expression

$$x_0(\theta) = \frac{\psi(\theta)}{K_0}\cdot\frac{\varepsilon}{E}, \tag{5}$$

where $\psi(\theta)$ is the known periodic function of the orbit.

By means of Eqs. (2)-(5), using the methods applied in [1] (see Ch. 5, paragraph 3, or Appendix D), we can find the expressions for the decrement $\langle\zeta_x\rangle$ of radial betatron oscillations and the decrement $\langle\zeta_s\rangle$ of synchrotron oscillations, connected with energy losses:

$$\langle\zeta_x\rangle = \frac{1}{2}\left\langle\Gamma\left(\frac{1}{\beta^2} - F\right)\right\rangle; \tag{6}$$

$$\langle\zeta_s\rangle = \frac{1}{2}\left\langle\Gamma\left(\frac{\partial \ln P}{\partial \ln E} - \frac{1-\beta^2}{\beta^2} + F\right)\right\rangle, \tag{7}$$

where $\langle\ \rangle$ denotes averaging with respect to θ;

$$F = \frac{K\psi}{K_0}\left[\left(1 - n\frac{\partial \ln P}{\partial \ln B}\right) + \frac{1}{K}\cdot\frac{\partial \ln P}{\partial x}\right]. \tag{8}$$

From Eqs. (6) and (7), we find the sum of decrements

$$\sigma = \langle\zeta_x\rangle + \langle\zeta_s\rangle = \frac{1}{2}\left\langle\Gamma\left(1 + \frac{\partial \ln P}{\partial \ln E}\right)\right\rangle, \tag{9}$$

which characterizes the rate of change in the over-all phase volume of oscillations during the process of motion. The found Eq. (9) indicates that this rate is determined only by the dependence of losses on the energy E. If the lost power P decreases with an increase in D faster than E^{-1}, then, $\sigma < 0$, which corresponds to an increase in the total phase volume, for which simultaneous damping of betatron and synchrotron oscillations cannot be secured. This can be ensured if P decreases more slowly than E^{-1}, and even more so if P increases with E.

As an example, we shall provide approximate estimates of the σ value for certain particular cases.

1. Ionization losses lead to the buildup of oscillations for $\beta < (1/\sqrt{2})$:

$$P \sim \frac{1}{\beta}, \quad \sigma \approx \frac{1}{2}\left\langle\Gamma\frac{2\beta^2-1}{\beta^2}\right\rangle. \tag{10}$$

2. Bremsstrahlung losses lead to the buildup of oscillations for $\beta < (1/2)$:

$$P \sim \beta E^2, \quad \sigma \approx \frac{1}{2}\left\langle\Gamma\frac{4\beta^2-1}{\beta^2}\right\rangle. \tag{11}$$

3. The loss due to magnetic relativistic bremsstrahlung ($\beta = 1$)

$$P \sim E^2, \quad \sigma = \frac{3}{2}\langle\Gamma\rangle \tag{12}$$

leads, as is known, to the damping of oscillations, which is of great importance for the operation of electron accelerators and accumulators.

The calculation of the root-mean-square amplitudes of the oscillations excited as a result of losses due to ionization, bremsstrahlung, etc. with an allowance for the friction described by Eqs. (6) and (7) will be presented in another paper.

LITERATURE CITED

1. A. A. Kolomenskii and A. N. Lebedev, Theory of Cyclic Accelerators [in Russian], Moscow, Fizmatgiz (1962).

UNIFORM IRRADIATION OF THE SURFACE OF SPECIMENS WITH PULSED ELECTRON BEAMS

(UDC 539.107)

Yu. S. Ryabukhin, A. G. Vasil'ev, and A. N. Belyakov

Translated from Atomnaya Énergiya, Vol. 19, No. 6,
pp. 535-537, December, 1965
Original article submitted August 26, 1964; Revised July 20, 1965

In recent years, electron accelerators have been used to an ever increasing extent as radiation machines [1, 2] (for modifying the properties of polymer parts, sterilization, etc.). In connection with this, uniform irradiation of the surface of specimens with pulsed electron beams constitutes an important problem. We shall consider here the conditions of uniform irradiation of flat specimens.

We shall assume that the area of the surface to be irradiated is much larger than the area of the stationary beam, the beam axis is perpendicular to the surface, the current distribution in the beam is symmetric relative to the beam axis, and the pulse duration is so short that the "spot" on the surface due to a pulse is practically "unblurred" as the specimen moves relative to the beam (or vice versa). Consider an infinite plane in which the centers of the spots due to pulses form a rectangular lattice with the parameters a and b (Fig. 1). The D(x, y) function which determines the dose at the point whose coordinates are x, y depends on the current distribution over the beam's cross section and the lattice parameters a and b. If the deviation of electrons from the beam axis obeys the normal Gaussian law

$$I = I_{\max} e^{-r^2/2\sigma^2}, \tag{1}$$

(where I_{max} is the current density at the beam axis, I is the current density at the distance r from the beam axis in the plane of the spot, and σ is the standard deviation of electrons from the beam axis), then, the function D(x, y) in the shaded rectangle (see Fig. 1) is given by the following expression

$$D(x, y) = C\left(\sum_{n=-\infty}^{\infty} e^{-\frac{(na-x)^2}{2\sigma^2}}\right)\left(\sum_{m=-\infty}^{\infty} e^{-\frac{(mb-y)^2}{2\sigma^2}}\right), \tag{2}$$

where C is a constant determined by the I_{max} value and other irradiation conditions.

Without bothering to calculate the various numerical distribution parameters, we shall consider a quantity which characterizes the irradiation nonuniformity, ε, i.e., the ratio of the minimum dose D_{min} to the maximum dose D_{max}. It is obvious that the dose is at a minimum at the point whose coordinates x = 0.5 a; y = 0.5 b and that it is at a maximum at the point whose coordinates are x = y = 0. If we denote

$$e^{-a^2/2\sigma^2} = q_1; \quad e^{-b^2/2\sigma^2} = q_2, \tag{3}$$

the expression for ε can be written thus:

$$\varepsilon = \frac{2q_1^{0{,}25}(1+q_1^2+q_1^6+q_1^{12}+\ldots)\,2q_2^{0{,}25}(1+q_2^2+q_2^6+q_2^{12}+\ldots)}{(1+2q_1+2q_1^4+2q_1^9+\ldots)(1+2q_2+2q_2^4+2q_2^9+\ldots)} = \frac{\vartheta_2(q_1)\,\vartheta_2(q_2)}{\vartheta_3(q_1)\,\vartheta_3(q_2)}, \tag{4}$$

where ϑ_2 and ϑ_3 are the so-called theta-functions. The ratio of squares of these functions can be expressed in terms of a certain angle α:

$$\frac{\vartheta_2^2}{\vartheta_3^2} = \sin\alpha, \tag{5}$$

while the α values are tabulated; the α values are found with respect to the assigned log q value in the table [3].

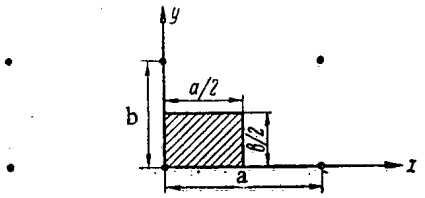

Fig. 1. Rectangular lattice formed by spot centers on the surface.

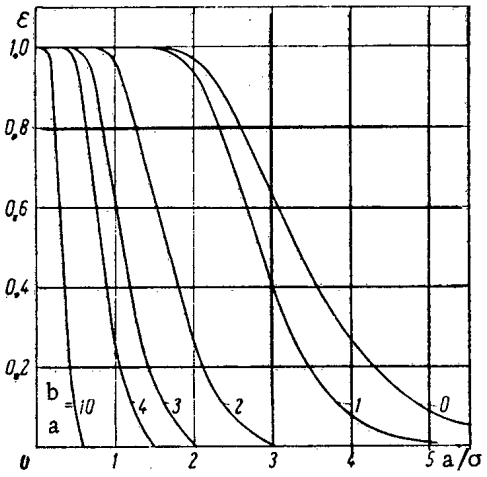

Fig. 2. Ratio of the minimum dose to the maximum dose (the figures on the diagram pertain to the b/a value for each curve).

By substituting Eq. (5) in Eq. (4), we finally obtain

$$\varepsilon = (\sin \alpha_1 \cdot \sin \alpha_2)^{1/2}. \tag{6}$$

If a = b, we have $\varepsilon = \sin \alpha$; if (b/a) = 0, then $\varepsilon = \sin^1/_2 \alpha$.

If the dose value is given, i.e., if the concentration of spots on the surface is assigned, the best radiation uniformity will be secured for a = b.

Figure 2 shows the dependence of ε on a/σ, calculated by means of Eq. (6) for different relationships between a and b. It is important that, as b/a varies from 0 to 1 (for b ≤ a), the ε values are virtually equal to unity if the larger side of the rectangular lattice exceeds σ by a factor not larger than 1.6 (see Fig. 2). If this a/σ ratio has been secured, further adjustment of the lattice with the aim of bringing the a and b values closer to each other will hardly improve the degree of uniformity. Furthermore, it should be noted that the irradiation uniformity is not worse than 95% in the (a/σ) < 1.95 range and not worse than 90% in the (a/σ) < 2.10 range for any ratio of sides.

Let us determine the conditions which the basic parameters characterizing the irradiation process must satisfy if the latter is to be uniform. We shall base our considerations on the fact that it is sufficient to satisfy the requirement (a/σ) ≤ 2 in most cases of practical importance (a is the larger side of the rectangular cell). In this case, the condition ε ≥ 0.94 is satisfied for any ratio of the cell sides.

Assume that I_0 is the total beam current (μA), t is the irradiation time (sec), S is the area of the surface to be irradiated (cm^2), and (dE/dz) is the mass stopping power of electrons in the material of the specimen to be irradiated* (MeV g^{-1} cm^{-2}). Then, the mean dose absorbed in the surface layer is

$$D = \frac{0.1 \left(\frac{dE}{dz}\right) I_0 t}{S} \text{ Mrad}. \tag{7}$$

By taking into account the inequality (a/σ) ≤ 2 and considering that S = abft (f is the repetition frequency of beam pulses (sec^{-1}), we find from Eq. (7) the requirement which the total beam current must satisfy:

$$I_0 \leqslant 40 \frac{b}{a} \frac{D}{\left(\frac{dE}{dz}\right)} f\sigma^2. \tag{8}$$

* For materials with a small value of the atomic number Z (in particular, for organic materials), the dE/∂z value is virtually equal to ionization losses, which, for thin films, where multiple scattering can be neglected, are calculated by usin the Bethe equation [4].

Equation (8) makes it possible to solve in a rather simple manner the question of the applicability range of a certain accelerator for the required radiation processes. It is obvious from Eq. (8) that the maximum allowable current of the accelerator beam is the higher, the larger the f, D, and σ values and the closer the lattice cell to a square cell. Uniform irradiation with large currents can be secured by:

1) increasing the repetition frequency f (within a reasonable range);

2) increasing the σ value. This method is advisable in the case where the accelerator's repetition frequency is insufficient for uniform irradiation. A larger σ value can be secured by increasing the distance between the accelerator's exit window and the specimen to be irradiated (beam divergence), defocusing the beam, or using scattering foils. Beam scanning can also be used for increasing the transverse cross section of the beam;

3) providing a square "lattice" on the surface.

In the above considerations of irradiation uniformity, it was assumed that the shape of the electron beam was Gaussian. We investigated the shapes of the electron beams of several industrial linear accelerators. Measurements have shown that the beam shape deviated from a Gaussian shape: for large r values, the curves obtained decayed more slowly than the corresponding Gaussian curves. However, the actual curves can be approximated by superimposing two Gaussian curves; the above considerations of uniform irradiation conditions can readily be extended to this case.

If the spot centers are to form a rectangular lattice on the surface (see Fig. 1), the beam must move relative to the specimen according to the principle of line scanning. For this, it is sufficient to move the specimen in a suitable manner in front of the beam: the specimen then intersects the beam at the velocity v and is shifted through the distance δ (the spacing between lines) beyond the limits of the beam. Considering that a = δ and b = (v/f) in Eq. (7) and taking into account S = abft, we obtain the expression for calculating the mean absorbed dose:

$$D = 0{,}1\frac{\left(\frac{dE}{dz}\right) I_0}{\delta v} \text{ Mrad.} \tag{9}$$

In practice, it is more convenient to use a different irradiation variant. The specimens to be irradiated are arranged on the surface of a cylindrical drum with a sufficiently large radius, which rotates in front of the beam while simultaneously moving along its axis through the distance δ per revolution. Considering, in this case, that v = 2πnR in Eq. (9), where n is the number of drum revolutions per second, while R is the rotation radius of the specimen's surface, we obtain the following for the mean surface dose:

$$D = \frac{0.1}{2\pi} I_0 \frac{dE}{dz} \cdot \frac{1}{R\delta n} \text{ Mrad.} \tag{10}$$

Another variant of practical importance consists in passing once in front of the beam a strip with the width H at the velocity v. If the beam does not perform scanning, we can write the following on the basis of the above theory:

$$\varepsilon = \frac{D_{\min}}{D_{\max}} = q_1 \sin^{1/2}\alpha_2 = q_1 \frac{\vartheta_2(q_2)}{\vartheta_3(q_2)}, \tag{11}$$

where $q_1 = e^{-H^2/8\sigma^2}$; and $q_2 = e^{-b^2/2\sigma^2}$.

The dose will be at a minimum at the end of the specimen at a point equidistant from the spot centers. For sufficiently large σ values, this variant can also secure satisfactory uniformity of irradiation. Let us find the mean absorbed dose in irradiating a strip whose length is much larger than σ. For this, it is sufficient to substitute in Eq. (7) the current I_1 of the beam's portion falling on the strip for the total beam current I_0. Noting that $I_{max} = (I_0/2\pi\sigma^2)$ and $r^2 = x^2 + y^2$ in Eq. (1), we find

$$I_1 = I_{\max} \int_{-H/2}^{H/2} e^{-x^2/2\sigma^2} dx \int_{-\infty}^{\infty} e^{-y^2/2\sigma^2} dy = I_0 \Phi\left(\frac{H}{2\sigma}\right), \tag{12}$$

where

$$\Phi(\xi)=\frac{2}{\sqrt{2\pi}}\int_0^{\xi} e^{-t^2/2}\,dt,$$

is the probability integral, the values of which are found from tables. By substituting in Eq. (7) the values I_1 and $(S/t) = Hv$, we obtain

$$D=0.1\left(\frac{dE}{dz}\right)I_0\frac{\Phi\left(\frac{H}{2\sigma}\right)}{Hv}\ \text{Mrad}. \qquad (13)$$

In conclusion, the authors hereby extend their thanks to A. Kh. Breger for his participation in the discussion of this project.

LITERATURE CITED

1. A. Kh. Breger, Nuclear Radiation Sources and Their Application in Radiation-Chemical Processes [in Russian], Moscow, Izd. VINITI (1960).
2. K. Wright, Introduction Electron Beam Technology, J. Wiley, New York–London (1962).
3. E. Janke and F. Emde, Tables of Functions with Equations and Curves [Russian translation], Moscow, Fizmatgiz (1959).
4. Radiation Dosimetry, Edited by J. Hine and G. Brownell [Russian translation], Moscow, Izd. Inostr. Lit. (1958).

OPTIMUM CONTROL OF THERMAL PROCESSES IN NUCLEAR REACTORS

(UDC 621.039.56)

I. M. Kurbatov, M. P. Leonchuk, and A. S. Trofimov

Translated from Atomnaya Énergiya, Vol. 19, No. 6,
pp. 537-540, December, 1965
Original article submitted February 13, 1965

Paper [1] was concerned with the problem of optimum-speed control of transient thermal processes in nuclear reactors, where control was effected by varying the coolant discharge $G(\tau)$, while the reactor's power level changed in accordance with a linear law, which often constitutes the determining condition of the transient process:

$$q(\tau)=\begin{cases}\dfrac{q^*}{\tau^*}\tau, & 0\leqslant\tau\leqslant\tau^*;\\ q^*, & \tau>\tau^*.\end{cases} \tag{1}$$

The investigation of the dynamic properties of the thermal simulator of a nuclear reactor as an element of a control system is continued in the present article. As in [1], the effect of the other elements of the power plant (the heat exchangers, the circulation pump, the power level control system, etc.) on the transient processes in the reactor is neglected.

Two problems are posed in the present article. The first consists in determining, for the assigned linear dependence $q(\tau)$, the discharge $G(\tau)$ which would secure under transient conditions the least deviation from a linear dependence $\theta(\tau, 1)$ of the outlet temperature:

$$\theta^*(\tau)=\begin{cases}\dfrac{\bar{\theta}}{\tau^*}\tau, & 0\leqslant\tau\leqslant\tau^*;\\ \bar{\theta}, & \tau>\tau^*,\end{cases}$$

i.e., the problem consists in determining the minimum of the functional

$$\psi=\int_0^\infty \frac{N}{2}\left[\theta(\tau, 1)-\theta^*(\tau)\right]^2 d\tau. \tag{2}$$

This condition makes it possible to determine the optimum rate of changing the power level of the plant.

In the other problem, it is assumed that the variation of $q(\tau)$ can be arbitrary. The regulating parameters (the functions $G(\tau)$ and $q(\tau)$ are found from the condition for the minimum time of the transient process. Such a formulation of the problem is perhaps the most comprehensive one for a check of the potential possibilities of the reactor dynamics.

I. We shall assume that the thermal processes in the reactor channel are described by means of a system of partial differential equations [2]:

$$\left.\begin{aligned}&\frac{\partial\theta}{\partial\tau}+G(\tau)\frac{\partial\theta}{\partial z}=Ku+(1-G)\,\eta(z), && 0\leqslant z\leqslant 1;\\ &\frac{\partial u}{\partial\tau}+\xi\frac{\partial\theta}{\partial\tau}+K\psi u=\psi\eta(z)\,q(\tau), && 0\leqslant\tau,\end{aligned}\right\} \tag{3}$$

with the following boundary conditions:

$$\tau=0;\quad \theta=u=0;\quad z=0;\quad \theta=\theta_+(\tau);\quad [\theta_+(\tau)=0].$$

In this case, it is necessary that the control functions under transient conditions satisfy the limitations

$$\begin{aligned} 0 < G_{\min} \leqslant G(\tau) \leqslant G_{\max}; \\ q_{\min} \leqslant q(\tau) \leqslant q_{\max}, \end{aligned} \tag{4}$$

and that the solution of the system satisfy the limitations

$$\theta_{\min} \leqslant \theta(\tau, 1) \leqslant \theta_{\max}, \tag{5}$$

$$\left| \frac{\partial \theta(\tau, 1)}{\partial \tau} \right| \leqslant \beta. \tag{6}$$

It is also necessary that the parameters arrive at a new steady state corresponding to the reactor's static characteristics:

$$\left.\begin{aligned} \overline{G}(T)\,\overline{\theta}(T, z) = [1 - \overline{G}(T) + q^*] \int_0^z \eta(z)\,dz; \\ \overline{\theta}(T, 1) = \overline{\theta} = \text{const}; \\ K\overline{u}(T, z) = q^* \eta(z) \text{ for } T \to \infty. \end{aligned}\right\} \tag{7}$$

(For a finite T value, Eq. (7) must be satisfied with the assigned degree of accuracy. In Eqs. (4)-(7), $G_{\min}$, $G_{\max}$, $q_{\min}$, $q_{\max}$, $\theta_{\min}$, $\theta_{\max}$, β, and $\overline{\theta}$ are constants which are determined by the reactor's parameters and the operating conditions.) In our calculations, the energy release distribution $\eta(z)$ along the reactor's height was used in the following form:

$$\eta(z) = 1.21 \cos \frac{2}{3} \pi (z - 0{,}5).$$

The problem was solved by using the method described in [3].

II. We shall now give the algorithm for the solution of the second problem.

1. By approximating the partial differential equations by a system of ordinary differential equations (the method of straight lines), we arrive at the problem of optimum control involving the solution of ordinary differential equations:

$$\frac{dy}{d\tau} = f(y, G, q\ \tau), \tag{8}$$

where $y = (y_1, \ldots, y_n)$ are the values of θ and u on the straight lines, while $y(0) = y_0$ and $Y(T) = y_T$ (y_0 and y_T are given).

2. In order to take into account the limitations of Eq. (6), we shall use the method penalty functions [1], and we shall add the following equation to Eq. (1):

$$\frac{dy_{n+1}}{d\tau} = \begin{cases} \frac{N_0}{2} \left[\frac{dy_n}{d\tau} \pm \beta \right]^2, & \text{if } \left| \frac{\partial \theta(\tau, 1)}{\partial \tau} \right| \geqslant \beta; \\ 0, & \text{if } \left| \frac{\partial \theta(\tau, 1)}{\partial \tau} \right| \leqslant \beta, \end{cases} \tag{8'}$$

where $y_{n+1}(0) = y_{n+1}(T) = 0$ and $\theta(\tau, 1) = y_n$.

Thus, we arrive at the fast-operation problem with the Eqs. (8) and (8') for $\tau = T$.

3. We shall use the Pontryagin maximum principle in order to solve the problem [4]. For this, we shall write the Hamiltonian $H = fp$, where

$$\dot{p} = -\frac{\partial f}{\partial y} p, \tag{9}$$

According to the maximum principle, the optimum control functions are determined from the condition for the maximum of H for

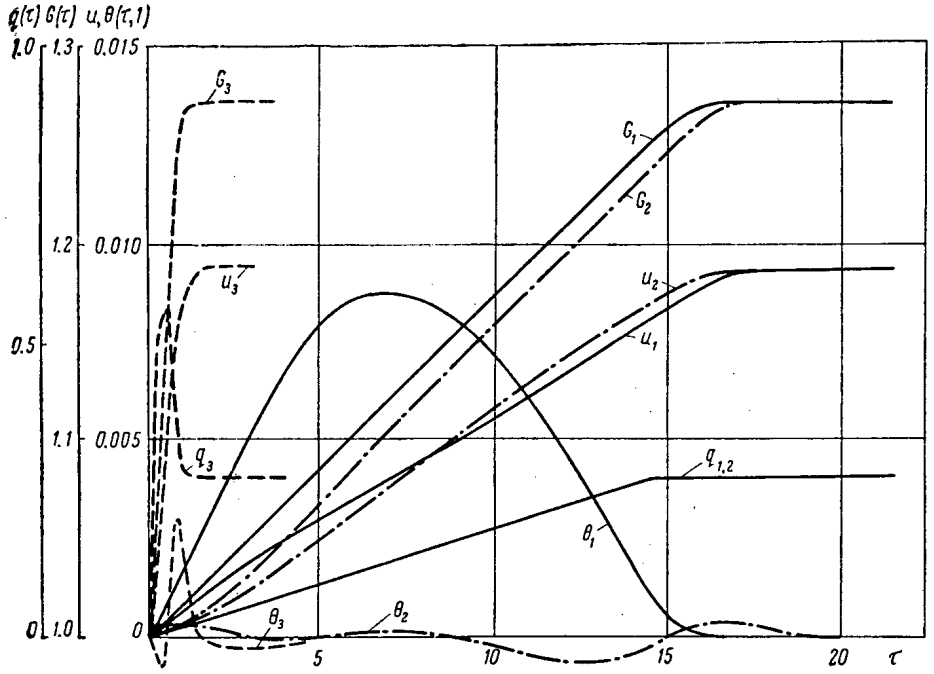

Fig. 1. Rise of the reactor's power level for $q^* = 0.277$ and $\overline{\theta}$.

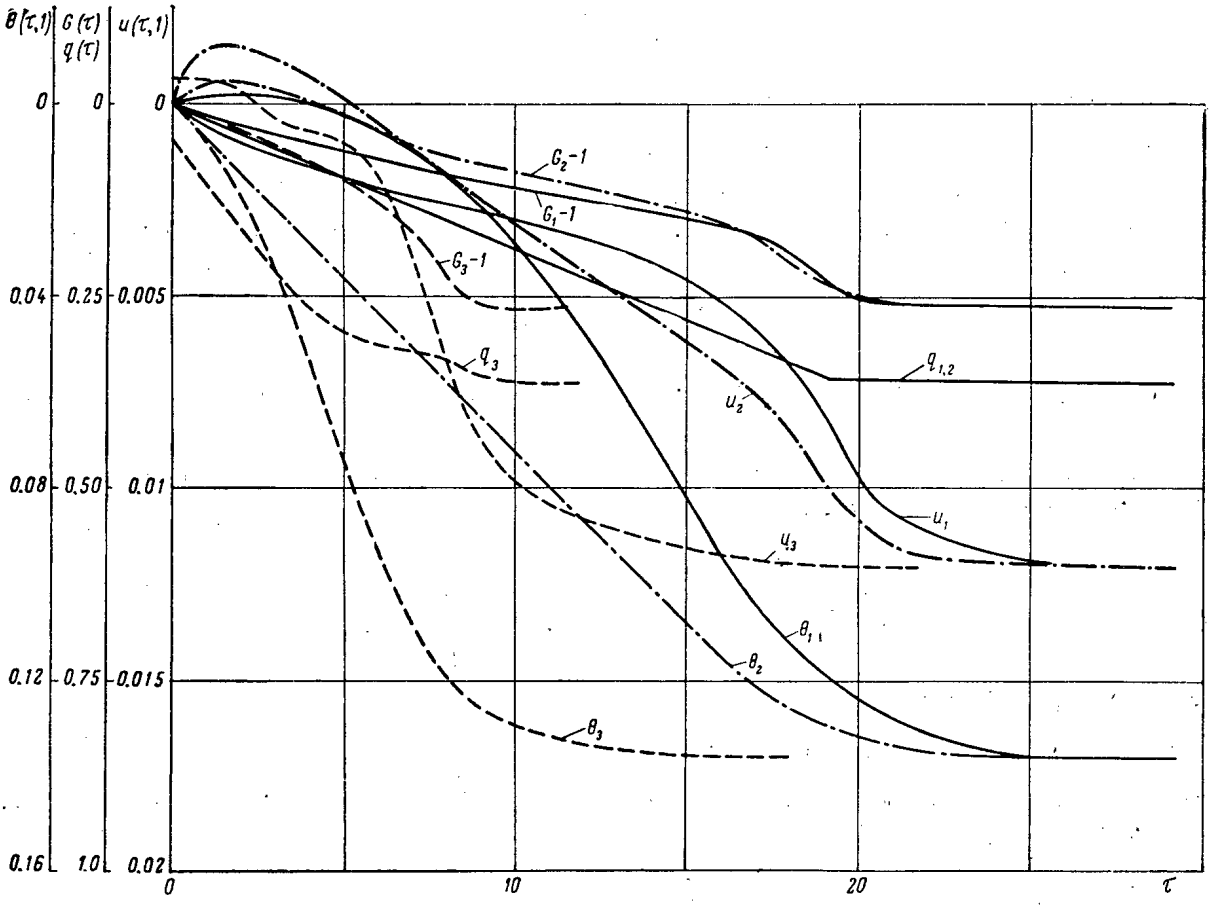

Fig. 2. Drop of the reactor's power level for $q^* = -0.361$ and $\overline{\theta} = -0.137$.

$$(G, q) \in \overline{Q}. \tag{10}$$

The $\overline{Q}$ region has been defined in [4].

4. We shall assign a certain value $T = T_0$, for which we shall determine the minimum of the following functional by using the method of successive approximations:

$$I(G, q) = \sum_{i=1}^{n+1} \frac{N_i}{2} [y_i(T_0) - y_{iT}]^2: \tag{11}$$

a) We shall assign $[G^0(\tau), q^0(\tau)] \in \overline{Q}$, solve the Cauchy problem for the limits from 0 to T_0, and determine $\partial I/\partial y$ from Eq. (11) for $\tau = T_0$;* b) by using $\partial I/\partial y$ as the boundary conditions for the conjugate Eq. (9) for $\tau = T_0$ and solving Eq. (9) for the limits from T_0 to 0, we find along the solution of Eqs. (8), (8'), and (9)

$$\frac{\partial H}{\partial G}, \frac{\partial H}{\partial q}, \max_{0 \leqslant \tau \leqslant T_0} \left| \frac{\partial H}{\partial G} \right| \text{ and } \max_{0 \leqslant \tau \leqslant T_0} \left| \frac{\partial H}{\partial q} \right|;$$

c) on the basis of Eq. (10), we shall formulate a method of successive approximations by using the gradient of the H function:

$$G^{(k+1)} = G^{(k)} + \frac{\lambda_1}{\max_{\tau} |\partial H^{(k)}/\partial G|} \cdot \frac{\partial H^{(k)}}{\partial G};$$

$$q^{(k+1)} = q^{(k)} + \frac{\lambda_2}{\max_{\tau} |\partial H^{(k)}/\partial q|} \cdot \frac{\partial H^{(k)}}{\partial q},$$

where λ_1 and λ_2 are the step values, while k is the iteration number; in this, $[G^{(k+1)}(\tau), q^{(k+1)}(\tau)] \underline{\in} \overline{Q}$. The criteria for the optimicity of the control $(G, q) \in \overline{Q}$ for I are

$$\max_{\tau} \left| \frac{\partial H}{\partial G} \right| = 0(\varepsilon) \text{ and } \max_{\tau} \left| \frac{\partial H}{\partial q} \right| = 0(\varepsilon),$$

where ε is the assigned accuracy.

5. Furthermore, in dependence on min I, we assume that $T_1 = T_0 + \Delta T$ for min $I \geq \varepsilon$ or that $T_1 = T_0 - \Delta T$ for min $I < \varepsilon$, and we repeat the process.

6. The step values λ_1 and λ_2 are first chosen arbitrarily. If the maximum values of $\partial H/\partial G$ or $\partial H/\partial q$ do not change their sign in iteration, the corresponding λ values are doubled, while, with every change in the sign of dH/dG or dH/dq, we use $\lambda^{(k+1)} = \frac{\lambda^{(k)}}{2}$ in the next operation.

We shall introduce a new phase coordinate for solving the first problem:

$$\frac{dy_{n+2}}{d\tau} = \frac{N}{2} [\theta(\tau, 1) - \theta^*(\tau)]^2, \tag{8"}$$

where $y_{n+2}(0) = 0$, and, instead of Eq. (11), we shall consider

$$I_1 = \frac{N_{n+2}}{2} y_{n+2}^2 + \sum_{i=1}^{n+1} \frac{Ni}{2} (y_i - y_{iT})^2. \tag{11'}$$

Figures 1 and 2 show the curves of the optimum processes of raising or reducing the power level of a reactor with the parameters given in [1]. The curves were calculated for the choice of two controls with respect to G and q (curves marked by the index 3) as well as for a linear law of power level variation (with two definitions: for the minimum time of the transient process – curves marked by the index 1 – and for the minimum deviation of the out-

* The T_0 value can be determined by solving Eqs. (8) and (8'), where Eq. (5) for the assigned $G^0(\tau)$ and $q_0(\tau)$ is violated.

let temperature from the linear dependence determined by the reactor's static characteristics – curves with the index 2). It is obvious from the diagrams that the last two reactor control methods differ only slightly from each other with respect to speed: the time of transient conditions is basically determined by the time of change in the reactor's power level. The curves of the control function (the discharge G) are also similar to each other and fairly monotonic. However, the regulation method based on two control modes is much more efficient, since the reactor's dynamic properties can be fully utilized in this case, while the transient process time can be considerably reduced (it is seen in Fig. 1 that the control time is reduced by a factor of 10 in comparison with other control methods). An analysis of the temperature curve indicates that $\theta(\tau, 1)$ in this case almost always follows the boundary of one of the limitations.

The last two control methods can be more readily realized, since the discharge curves are smoother.

LITERATURE CITED

1. M. P. Leonchuk, A. S. Trofimov, and I. M. Kurbatov, Zh. Vychisl. Matematiki i Matem. Fiziki, 5, 558 (1965).
2. B. F. Gromov and A. S. Trofimov, Inzh.-Fiz. Zh., No. 8, 31 (1964).
3. M. P. Leonchuk, Zh. Vychisl. Matematiki i Matem. Fiz., No. 4, 1112 (1964).
4. L. S. Pontryagin et al., Mathematical Theory of Optimal Responses [in Russian], Moscow, Fizmatgiz (1964).

CONDITIONAL SEPARATION OF SPATIAL AND ANGULAR VARIABLES IN SOLVING THE TRANSPORT EQUATION FOR NEUTRONS

(UDC 621.039.51.12 : 539.125.52)

V. V. Khromov and I. S. Slesarev

Translated from Atomnaya Énergiya, Vol. 19, No. 6,
pp. 540-542, December, 1965
Original article submitted March 17, 1965; Revised September 20, 1965

The method of conditional separation of variables was used in [1] to solve the two-dimensional spatial diffusion problem. The basic idea of the method can also be used to get an approximate solution to the transport equation for neutrons; it should be efficient in analysis of small, so-called "nondiffusion" systems for which the ordinary methods give large errors.

Let us consider the application of the method of conditional separation of variables by solving a partial problem as an example: namely, to determine the spatial-angular distribution in a plane-parallel plate in the one-velocity approximation. We shall use the following form of the transport equation, derived in [2] for a symmetrical scattering indicatrix:

$$-\frac{\partial}{\partial x}\cdot\frac{\mu^2}{\Sigma}\cdot\frac{\partial}{\partial x}u(x,\mu)+\Sigma u(x,\mu)$$
$$-(\Sigma_s+\nu_f\Sigma_f)\int_0^1 u(x,\mu)\,d\mu=0. \qquad (1)$$

The weak scattering anisotropy is easily taken care of by introducing the mean of the cosine of the scattering angle $\bar{\mu}_0$.

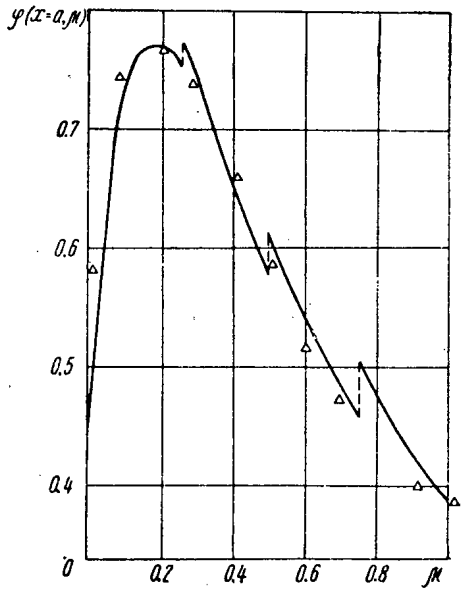

Angular distribution of neutrons at edge of plate, $\varphi(a, \mu)$. ———) Our results; △) results of [3].

Percentage Error of Various Approximate Methods for Calculating Critical Size of One-Dimensional Plate without Reflector

C	Method of conditional separation of variables			P_1	P_5	S_2	S_8
	$K=1$	$K=2$	$K=4$				
2,0	−6,3	−1,4	−0,03	45,9	9,9	31,8	0,93
1,8	−4,4	−0,69	+0,05	39,7	6,9	26,7	0,57
1,6	−2,2	+0,30	+0,13	32,7	4,2	21,0	0,5
1,4	−0,26	+0,20	+0,18	24,8	2,1	14,8	0,23

Equation (1) can be solved with boundary conditions at the interface between the plate and a vacuum and has the form

$$u+\frac{\mu}{\Sigma}\cdot\frac{\partial u}{\partial x}\Big|_{x=a}=0;\quad u-\frac{\mu}{\Sigma}\cdot\frac{\partial u}{\partial x}\Big|_{x=-a}=0, \tag{2}$$

where a is the semithickness of the plate.

The range of variation of μ is divided into K intervals of arbitrary length $\Delta\mu_k$, and the range of variation of x into I intervals Δx_i. The phase space of (x, μ) will then be divided into u(x, μ) regions. In each region (i, k) the function $u(x, \mu)$ can be approximately written as

$$u_{i,k}(x,\mu)=v_i(x)\,m_k(\mu). \tag{3}$$

Introduce new functions

$$x_{i,k}=v_i(x)\int\limits_{\Delta\mu_k} m_k(\mu)\,d\mu; \tag{4}$$

$$M_{i,k}=m_k(\mu)\int\limits_{\Delta x_i} v_i(x)\,dx. \tag{5}$$

From Eq. (1) we easily obtain a system of equations in the new functions X(x) and M(μ). To do this, we integrate it w.r.t. μ over the range $\Delta\mu_k$ and w.r.t. x over the range Δx_i. We thus get

$$-\frac{d}{dx}D_{i,k}\frac{d}{dx}X_{i,k}(x)+\Sigma_i X_{i,k}(x)=(\Sigma_s+\nu_f\Sigma_f)_i\Delta\mu_k\sum_{k=1}^{K}X_{i,k}(x); \tag{6'}$$

$$M_{i,k}(\mu)\left[1+\frac{\varkappa^r_{i,k}}{2}\cdot\frac{\mu^2}{\Sigma_i}(\operatorname{sign}\varkappa^r_{i,k}-1)+\frac{\varkappa^e_{i,k}}{2}\cdot\frac{\mu^2}{\Sigma_i}(\operatorname{sign}\varkappa^e_{i,k}+1)\right]-M_{i-1,k}(\mu)\frac{\varkappa^r_{i-1,k}}{2}\cdot\frac{\mu^2}{\Sigma_{i-1}}(\operatorname{sign}\varkappa^r_{i-1,k}-1)-$$
$$-M_{i+1,k}(\mu)\frac{\varkappa^r_{i+1,k}}{2}\cdot\frac{\mu^2}{\Sigma_{i+1}}(\operatorname{sign}\varkappa^e_{i+1,k}+1)=(\Sigma_s+\nu_f\Sigma_f)_i\int\limits_{x\Delta_i}\sum_{k=1}^{K}X_{i,k}(x)\,dx. \tag{6''}$$

Here

$$D_{i,k}=\frac{1}{\Sigma_i}\frac{\int\limits_{\Delta\mu_k}\mu^2M_{i,k}\,d\mu}{\int\limits_{\Delta\mu_k}M_{i,k}\,d\mu}; \tag{7}$$

$$\operatorname{sign} A=\begin{cases} 1 & \text{for} \quad A>0; \\ 0 & \text{for} \quad A=0; \\ -1 & \text{for} \quad A<0; \end{cases}$$

$$\varkappa_{i,\,k}^{\Gamma}(e)=\frac{\nabla X_{i,\,k}}{\int\limits_{\Delta x_1} X_{i,\,k}(x)\,dx}, \tag{8}$$

where the gradient is chosen on the right (left) boundary of the region i, k. In deriving Eq. (6") we used the property of continuity of $\frac{1}{\Sigma}\,\Omega\,\nabla u$ for transition across the boundary.

Thus Eq. (1) reduces approximately to the system of two equations (6' and 6"), one of which is a simple algebraic equation.

Equations (6') and (6") are solved by the method of successive approximations. The solution can be begun, for instance, with Eq. (6'), assigning an isotropic angular distribution $M_{i,k}$ = const for calculating $D_{i,k}$ and the value of the source on the right hand side.

Equation (6') is quasi-diffusional, with a diffusion coefficient such that it is expressed in fractionally linear form by solving (6") and leads us to expect a rapid convergence of the iteration process. The boundary conditions for Eq. (6') are easily obtained by integrating the initial boundary conditions w.r.t. μ [2]. The required function $u(x, \mu)$ is synthesized as follows:

$$u_{i,\,k}(x,\,\mu)=M_{i,\,k}(\mu)\,X_{i,\,k}(x)\,\frac{1}{\int\limits_{\Delta x_i} x_{i,\,k}(x)dx}. \tag{9}$$

Similarly we can write down and solve the multigroup transport equation, but for this purpose we need to write the equation in a vector matrix form.

Let us consider the method of conditional separation of spatial and angular variables, taking as an example the calculation of the critical dimension and neutron distribution in a plane one-dimensional reactor, in the one-velocity approximation (below we shall compare this method with existing methods for P_n and S_n, and also with the method given in [3]).

The table gives the relative errors in calculating the critical the semithickness a_{cr} for a plate with various values of $C = (\Sigma_s + \nu_f\Sigma_f)/\Sigma$, calculated by various methods.

The magnitude of the error was calculated from the formula $[(a_{cr} - a^0_{cr})/a^0_{cr}] \cdot 100\%$, where a^0_{cr} is the exact value of the critical semithicknesses. In using the method of conditional separation of variables, the number of intervals of μ was changed from K = 1 to K = 4 (equal intervals), I = 1.

The figure shows the angular distribution at the edge of the plate (emergent radiation) $\varphi(a, \mu)$, found from the function $u(x, \mu)$. The results obtained by conditional separation of variables with K = 4 and I = 1 are compared with the data of [3].

From experience of the calculations, and also from physical considerations, it is clear that the method of separation of variables is markedly more accurate only in the case when the range of variation of x (I > 1) is subdivided near the boundary of a zone with different physical properties.

In conclusion, we would note that the above method can be realized with an electronic computer even on a basis of programs for reactors using the diffusion approximation.

LITERATURE CITED

1. V. V. Khromov et al., In symposium: Some Topics in Reactor Physics and Engineering [in Russian], Moscow, Atomizdat (1965).
2. V. S. Vladimirov, Izv. AN SSSR, Ser. Matemat., 21 (1957).
3. G. Metsis, Nucl. Sci. and Eng., 17, 55 (1963).

DETERMINATION OF URANIUM (VI) IN CARBONATE SOLUTIONS BY ABSORPTION IN THE SHORT-WAVE UV-REGION

(UDC 661.879: 167.2)

T. S. Dobrolyubskaya

Translated from Atomnaya Énergiya, Vol. 19, No. 6,
pp. 542-544, December, 1965
Original article submitted June 2, 1964; Revised July 29, 1965

Absorption spectra of uranyl solutions appear at $\lambda \sim 500$ mμ and reach into the UV-region [1, 2]; continuous absorption begins at 330 mμ. In the visible region the absorption spectra have banded structures.

The authors of [3-8] developed methods for determining uranium (VI), based on absorption of uranyl solutions in the visible region of the spectrum. Later, the UV-region was used for spectrophotometric determinations of uranium (VI). The authors of [9] describe a method of determining uranium (VI) in which the absorption of a uranyl-tributyl phosphate complex at 250 mμ is measured; in another method, it is determined by absorption of a uranyl chloride complex in concentrated HCl at 246 mμ [10]. Other methods have also been developed.

The aim of the present work is to determine the character of the absorption spectrum of uranium (VI) in carbonate solutions in the short-wave UV, the emphasis being on quantitative determination of uranium in these solutions with admixtures of DBP, TBP and synthine.

According to [11-13], solutions of this composition are formed when uranium and plutonium are separated from fission products by extraction with TBP (in the given case DBP is formed by radiation decomposition of TBP).

The solutions were prepared as follows: 1 g of uranium chips (99.7% uranium) was dissolved by heating in nitric acid, the solution was evaporated almost to dryness and the uranyl nitrate thus obtained dissolved in water. This solution contained 1 g/liter uranium. Solutions with lesser uranium concentrations (0.2, 0.25, 0.5, and 0.75 g/liter) were made by dilution.

Dry soda (A.R. grade) was added to the solution, its concentration ranging from 0 to 50 g/liter. The absorption spectra of the solutions were measured in the range 205-340 mμ in a Hitachi (Japan) automatic spectrophotometer, using quartz cells (solution layer 0.1 and 0.05 mm) and water as comparison. Figure 1 gives the absorption spectra of two solutions: 1) uranyl nitrate with 0.2 g/liter uranium; 2) uranium (VI) in a carbonate solution with 0.2 g/liter uranium; and 50 g/liter soda (layer thickness 0.1 mm).

In the wavelength range used in our work the absorption spectra of uranyl solutions contain only one band, with a maximum at ~ 213 mμ, and the characteristic structure of these solutions' absorption spectra in the visible region is absent. Another feature is the sharp increase in the short-wave UV region in comparison with the visible region. The molar extinction coefficient of uranium (VI) in a carbonate solution at 213 mμ, ε_{213}, is ~ 7200, and for the visible region at 449 mμ (the main absorption maximum in this region [7]) ε_{449} is ~ 48 (absorption at 449 mμ was measured in the same spectrophotometer, using a glass cell and layer thickness 5 cm).

The high value of the molar extinction coefficient in this case enables us to develop a method for quantitative determination of uranium (VI) in carbonate solutions.

Figure 2 shows the absorption spectrum of a soda solution of concentration 20 g/liter, containing no uranium; the layer thickness was 0.05 mm. The absorption spectrum again has only one broad band. It was found that in the concentration range of these measurements (0-30 g/liter Na_2CO_3) the optical density increases with the concentration (the measurements were performed at wavelength 213 mμ). For a solution with uranium concentration 1 g/liter the correction for adsorption when the soda content is changed from 10 to 30 g/liter is ±5 rel. %.

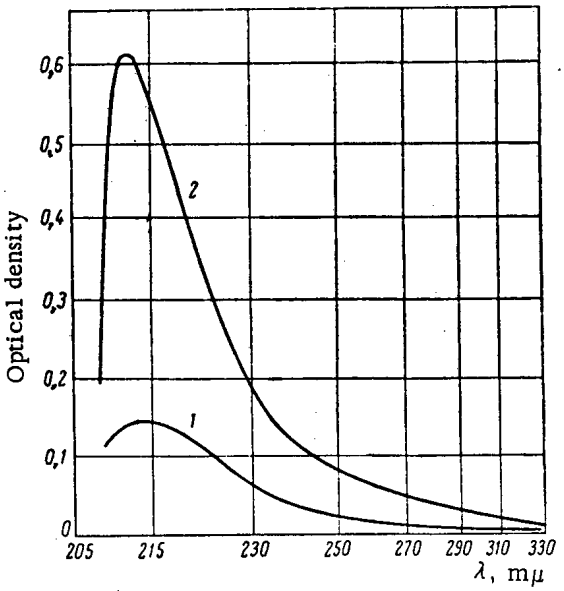

Fig. 1. Absorption spectra of solutions: 1) uranyl nitrate; 2) uranium (VI) in sodium carbonate solution.

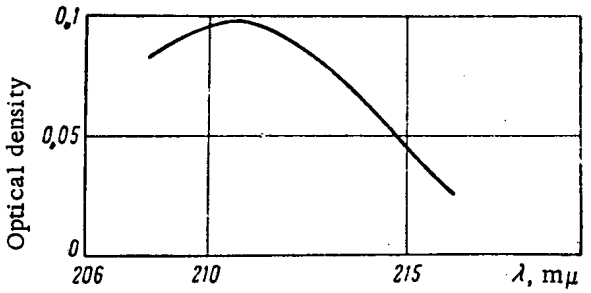

Fig. 2. Absorption spectrum of a soda solution.

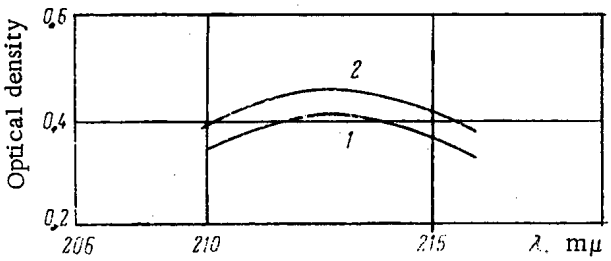

Fig. 4. Influence of additions of a solution of TBP in synthine on absorption of uranyl carbonate complex: 1) uranium content in the solution 1 g/liter, soda content 20 g/liter, DBP 30 mg/liter; 2) the same composition saturated with TBP solution in synthine.

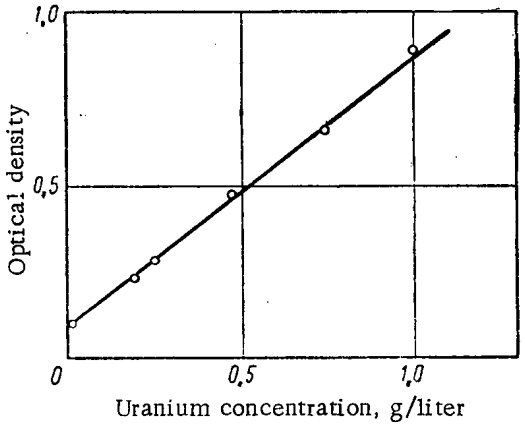

Fig. 3. Calibration curve for determining uranium (VI) in carbonate solutions.

Figure 3 gives a calibration curve for determining uranium (VI) in carbonate solutions by absorption of the uranyl carbonate complex at 213 mμ (soda concentration 20 g/liter, layer thickness 0.05 mm). In the uranium concentration range of these measurements (0-1 g/liter) the optical density is proportional to the uranium concentration.

The measurements of uranium (VI) absorption in carbonate solutions at 213 mμ were used for determining uranium in carbonate solutions containing DBP, TBP, and synthine, prepared in our laboratory. With regard to the influence of DBP on absorption of the uranyl carbonate complex in the short-wave UV-region, it was found that addition of small amounts (300-400 mg/liter) of DBP to carbonate solutions of uranium reduces absorption very slightly. This reduction was also noted in [14] when DBP was added to uranyl nitrate solutions.

To determine the influence of additions of TBP (dissolved in synthine) on absorption of a uranyl carbonate complex, we used solutions containing 1 g/liter uranium, 20 g/liter Na_2CO_3, 300 mg/liter DBP; these solutions were saturated with a TBP solution in synthine (20% TBP and 80% synthine, both reagents being used without further purification). Figure 4 shows the influence of additions of a TBP solution in synthine on absorption of a uranyl carbonate complex (layer thickness 0.05 mm). The optical density of uranyl carbonate solutions saturated with a TBP solution in synthine at 213 mμ is 15-17% greater than that of unsaturated solutions, mainly due to absorption of synthine.

According to [15], the solubility of a mixture of TBP and synthine in carbonate solutions of uranium is low, but sufficient to be taken into account when determining uranium by absorption of a uranyl carbonate complex. The correction for absorption, due to the presence of the organic phase in the solution, must be constant (at constant TBP/synthine ratio and the same temperature) and is excludable by plotting calibration curves for solutions pre-saturated with a TBP solution in synthine.

Due to the marked difference between the molar extinction coefficients of uranium (VI) in carbonate solutions at 213 and 449 mμ, the sensitivity of spectrophotometric determinations of uranium (VI) by absorption in the short-wave UV-region must be much higher than that for the visible region.

The following conclusions may be drawn:

1. At the wavelengths used in this work (205-340 mμ) the absorption spectrum of uranium in carbonate solutions has a single broad band with a maximum at 213 mμ.

2. The results may be used for quantitative determination of uranium (VI) in carbonate solutions containing DBP, TBP and synthine (the method being based on measurement of absorption at 213 mμ).

The author thanks her colleague, G. D. Yatsun, for measuring the absorption spectra.

LITERATURE CITED

1. G. Dicke and A. Duncan, Spectroscopic Properties of Uranium Compounds, New York (1949), p. 71.
2. V. L. Levshin, Photoluminescence of Liquids and Solids [in Russian], Moscow, Gostekhteorizdat (1951), p. 202.
3. T. Scott and P. Dixon, Analyst, 70, 462 (1945).
4. L. Silverman and L. Mouday, Analyt. Chem., 28, 45 (1956).
5. A. Bacon and G. Milner, Analyst, 81, 456 (1956).
6. B. Wessling and M. DeSesa, Analyt. Abstrs., 5, 497 (1958).
7. Analytical Chemistry of Uranium, Ed. by D. I. Ryabchikov and M. M. Senyavin [in Russian], Moscow, Izd. AN SSSR (1962), p. 104.
8. V. K. Markov et al., Methods of Determining Uranium [in Russian], Moscow, Atomizdat (1964), p. 221.
9. B. Paige, M. Elliot, and J. Rein, Analyt. Chem., 29, 1029 (1957).
10. C. Callahan, Analyt. Chem., 33, 1660 (1961).
11. F. S. Martin and J. L. Miles, Chemical Processing of Nuclear Fuel [Russian translation], Moscow, Metallurgizdat (1961), p. 113.
12. Chemistry of Nuclear Fuel, Reports of Foreign Scientists to the International Conference on the Peaceful Uses of Atomic Energy [Russian translation], Moscow, Goshkimizdat (1956), p. 187.
13. A. Kerst and M. Helpern, Inorgan. Nucl. Chem., 20, 115 (1961).
14. T. S. Dobrolyubskaya, Zh. Analit. Khim., 20, 470 (1965).
15. V. B. Shevchenko and B. N. Sudarnikov, Technology of Uranium [in Russian], Moscow, Gosatomizdat (1961), p. 220.

STATISTICAL CHARACTERISTICS OF FUNCTIONAL COUNT-RATE METERS

(UDC 539.16.08)

V. M. Skatkin

Translated from Atomnaya Énergiya, Vol. 19, No. 6,
pp. 544-546, December, 1965
Original article submitted August 7, 1965

Owing to the currently extending applications of continuous monitoring of radioactive radiation, the need has arisen for functional count-rate meters. In these meters, the output voltage (or current) is proportional to the result of an algebraic process which is continuously performed on the input count rates. Examples are logarithmic meters, sum meters, difference and ratio meters.

Owing to the statistical nature of the signals at the input, the output voltage of a count-rate meter fluctuates. The magnitude of the fluctuations is usually characterized by the relative statistical error $\delta = \sigma/\bar{u}$, where σ is the root mean square deviation, $\bar{u}$ the mean voltage. To calculate these characteristics, use is made of the method in [1], comprising summation of the dispersions of the charges transmitted to the integrating capacitance in nonoverlapping time intervals. However, this method cannot always be used to calculate the dispersion of the output voltage of a functional count-rate meter, owing to the statistical relation between the values of the transmitted charges.

We note that the output voltage (and its square) of most functional meter circuits working in steady conditions is a stationary random function of time, which is a Markov random process (cf., e.g., [2]). For such a function it is easy to derive an expression for the mean value of the derivative; since the function is stationary, we can equate this to zero, and from the equation thus obtained determine $\bar{u}$ (and similarly $\overline{u^2}$), and then calculate $\sigma^2 = u^2 - \bar{u}^2$ and $\delta = \delta/\bar{u}$. (The method of calculating the dispersion by determining the mean of the derivatives was used in [3].)

By this method let us determine the mean value and dispersion of the output voltage of the circuit shown in the diagram. The statistical characteristics of the above functional count-rate meters can be determined from the equations obtained as partial cases. Keys K_1 and K_2 are acted on by pulses statistically distributed in time with mean succession frequencies n_1 and n_2, respectively. By switching of the dosing element, each input pulse causes the voltage on the integrating capacitance C_0 to alter by $(V_i - u)C_i/C_0$, where $C_i = C_{Di}C_0/(C_{Di} + C_0)$, if we are using a charging circuit with a dosing capacitance C_{Di}, or $C_i = \tau/R_i$, if we are using a circuit which charges via resistance R_i in time τ (see figure, dashed lines), where $i = 1, 2$.

If the output voltage is u(t) at time t [the square of the output voltage being $u^2(t)$], then at time $t + \Delta t$ it can, with various probabilities p, take one of the following values:

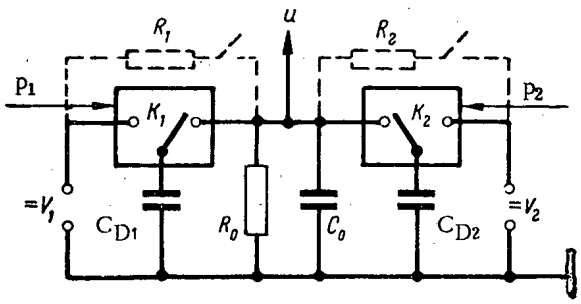

Equivalent circuit of count-rate meter.

Values of Relative Statistical Error for Functional Count-Rate Meters with Various Circuits

Type of functional count-rate pulse	Value of parameters	$\bar{u}$	δ	Ref.
Linear meter	$n_2=0$; $u \ll V_1$	$V_1 n_1 R_0 C_1$	$(1/2\, n_1 R_0 C_0)^{1/2}$	[4, 5]
Sum and difference (lower sign) meters	$V_1=\pm V_2=V$; $u \ll V$	$VR_0(C_1 n_1 \pm C_2 n_2)$	$\frac{(C_1^2 n_1 + C_2^2 n_2)^{1/2}}{(2R_0C_0)^{1/2}\ (C_1 n_1 \pm C_2 n_2)}$	[5]
Ratio meters	$V_2=0$; $R_0=\infty$; $C_1=C_2=C$	$V_1 \frac{n_1}{n_1+n_2}$	$\left(\frac{n_2}{n_1}\cdot\frac{C}{2C_0-C}\right)^{1/2}$	[6]
	$V_2=0$; $R_0=\infty$; $C_1,\ C_2 \ll C_0$; $u \ll V_1$	$V_1 \frac{C_1 n_1}{C_2 n_2}$	$\left[\frac{C_2}{2C_0}\left(1+\frac{n_2}{n_1}\right)\right]^{1/2}$	[7]
Logarithmic meters	$n_2=0$; $C_1 \ll C_0$	$\frac{V_1 n_1 R_0 C_1}{1+n_1 R_0 C_1}$	$\left[\frac{1}{2n_1 R_0 C_0 (1+n_1 R_0 C_1)}\right]^{1/2}$	[4, 5]

$$u^k(t+\Delta t)=\begin{cases}\left[u(t)\left(1-\dfrac{\Delta t}{R_0C_0}\right)\right]^k & p_0=1-(n_1+n_2)\Delta t;\\ \left\{u(t)+[V_1-u(t)]\dfrac{C_1}{C_0}\right\}^k & p_1=n_1\Delta t;\\ \left\{u(t)+[V_2-u(t)]\dfrac{C_2}{C_0}\right\}^k & p_2=n_2\Delta t,\end{cases}$$

where p_0 is the probability of absence of pulses in time Δt, p_1 and p_2 the probabilities of arrival of one "left" pulse or one "right" pulse. Hence at time $t + \Delta t$ the mean value of the function ($k = 1$), on condition that at time t it is $u(t)$, can be found from the expression

$$u(t+\Delta t)=u(t)\left(1-\frac{\Delta t}{R_0C_0}\right)[1-(n_1+n_2)\,\Delta t]$$
$$+\left\{u(t)+[V_1-u(t)]\frac{C_1}{C_0}\right\}n_1\Delta t$$
$$+\left\{u(t)+[V_2-u(t)]\frac{C_2}{C_0}\right\}n_2\Delta t.$$

Transfer $u(t)$ to the l.h.s., divide by Δt and go to the limit when $\Delta t \to 0$. Average over-all values of $u(t)$, and equating the expression obtained to zero, we get

$$u=\frac{R_0(C_1V_1n_1+C_2V_2n_2)}{1+R_0C_1n_1+R_0C_2n_2}.$$

Using the expression for the mean of the square of the function ($k = 2$) at time $t + \Delta t$, it is easy to use the same method to determine $\overline{u^2}$, and thus also σ^2. Finally, we get

$$\sigma^2=\frac{C_1C_2n_1n_2\left\{\frac{2}{R_0}[V_1^2C_1+V_2^2C_2-(C_1+C_2)V_1V_2]+C_1C_2(n_1+n_2)(V_1-V_2)^2\right\}+\frac{1}{R_0^2}(C_1^2V_1^2n_1+C_2^2V_2^2n_2)}{\left[2\frac{C_0}{R_0}+C_1(2C_0-C_1)n_1+C_2(2C_0-C_2)n^2\right]\left(\frac{1}{R_0}+C_1n_1+C_2n_2\right)^2}.$$

The table gives expressions for $\bar{u}$ and $\sigma = \sigma/\bar{u}$, obtained from the latter two equations for given values of the parameters, and also cites references in which the circuits are described.

LITERATURE CITED

1. Schiff and Evans, Rev. Scient. Instrum., 7, 546 (1936).
2. V. S. Pugachev, Theory of Random Functions [in Russian], Moscow, Fizmatgiz (1962).
3. V. I. Gol'danskii, A. V. Kutsenko, and M. I. Podgoretskii, Statistics of Meters for Recording Nuclear Particles [in Russian], Moscow, Fizmatgiz (1959).
4. V. Price, Recording Nuclear Radiation [Russian translation], Moscow, Izd. Inostr. Lit. (1960).
5. L. S. Gorn and B. I. Khazanov, Radiation-Intensity Recorders [in Russian], Moscow, Atomizdat (1965).
6. R. Hindel, Rev. Scient. Instrum., 33, 1343 (1962).
7. B. L. Kiselev, N. V. Ryzhov, and V. M. Skatkin, Avtorskoe Svidetel'stvo, No. 166937 (1964).

CORROSION RESISTANCE OF STRUCTURAL MATERIALS IN BORON-CONTAINING SOLUTIONS

(UDC 620.193.4 : 621.039.546)

V. N. Belous, A. I. Gromova, É. T. Shapovalov, and V. V. Gerasimov

Translated from Atomnaya Énergiya, Vol. 19, No. 6, pp. 546-549, December, 1965
Original article submitted March 17, 1965; Revised July 29, 1965

Boron has a large neutron capture cross section in the low energy region [1], and boron-containing solutions can therefore serve as neutron shields and reactor controls.

In the USA, boric acid is used for cold and hot shutdowns of the Yankee reactor and for protection during fuel recharging [2]. In emergencies, boric acid is added to water in the first loop of a water boiler reactor [3] and to the R-3 heavy-water heat reactor [4]. At the Indian Point atomic power station, boric acid is used as an additional fine control throughout the service life of the active zone [5].

The use of aqueous solutions of boron in nuclear engineering has raised the question of the resistance of structural materials like OKh18N10T steel, carbon steel, AMg-5 aluminum alloy, titanium and lead in boron-containing solutions.

It is noteworthy that the authors of [6] indicate that boric acid has an inhibiting effect on zirconium at 500°C.

The aim of the present work is to obtain comparative data on the corrosion behavior of the above-mentioned structural materials at temperatures below 100°C, and to study crevice and contact corrosion.

For this work we used solutions of boric acid, sodium and ammonium tetraborates, because these are the most closely studied compounds of boron and are also readily soluble and noncorrosive.

Boron-containing solutions of two concentrations (Table 1) were prepared from dimineralized water of the following composition: Cl^- = 0.06 mg/liter; SO_4 = 3.5 mg/liter; Fe = 0.136 mg/liter; dry residue = 4.1 mg · equiv/liter; pH = 5.95.

TABLE 1. Characteristics of the Initial Solutions at Room Temperature

Solution group	Solution characteristics	Boric acid	Sodium tetraborate	Ammonium tetraborate
1	Boron, g/liter	7,32	4,85	4,85
	pH *	5,5	9,75	9,4
	Oxygen, mg/liter	Not determ.	3,4	4,4
2	Boron, g/liter	2,44	2,5	2,49
	pH *	6,75	9,45	9,25
	Oxygen, mg/liter	3,4	5,1	8,6

* Solutions saturated with air.

TABLE 2. Corrosion Rates of Materials in Deaerated Boron-Containing Solutions, $g/m^2 \cdot day$.

Solution	Boron content g/liter	Temp., °C	Time, h	Material				
				OKh18N10T steel	VT-1-2-alloy	AMg-5 alloy	S-1 lead	20 steel
Boric acid	7,32	20*	100	0,012	0,036	0,06	3,6	1,8
			300	0,004	0,012	0,05	3,060	1,4
			500	0,003	0,006	0,018	2,65	1,29
	7,32	20	100	0,024	0,048	0,12	1,32	1,68
			500	0,009	0,012	0,0156	0,43	0,57
	7,32	100	100	0,036	0,036	0,036	0,84	—
			500	0,019†	0,036†	0,264†	0,29	—
	2,5	100	300	0,008	0,008	0,104	1,38	—
			500	0,002	0,002	0,08	0,37	—
Sodium tetraborate	4,85	20*	100	0,012	0,012	0,24	0,72	0,024
			300	0,008	0,008	0,344	0,87	0,004
			500	0,006	0,21		0,62	0,012
	4,85	20	100	0,036	0,048	0,27	0,48	0,048
			500	0,007	0,012	0,18	0,16	0,007
	4,85	100	100	0,024	0,012	6,4	1,76	—
			500	0,019†	0,036†	1,4†	0,15	—
	2,5	100	300	0,012	0,008	0,78	0,9	—
			500	0,004	0,004	0,6	0,34	—
Ammonium tetraborate	4,85	20*	100	0,0012	0,012	0,29	0,72	0,024
			300	0,0022	0,008	0,212	1,08	0,008
			500	0,009	0,006	0,17	0,61	0,014
	4,85	20	100	0,036	0,036	0,24	0,46	0,084
			500	0,007	0,012	0,19	0,34	0,007
	4,85	100	100	0,024	0,072	4,5	1,1	—
			500	0,019	0,019	3,9†	0,16	—
	2,5	100	300	0,021	0,008	0,82	0,5	—
			500	0,009	0,007	0,63	0,23	—

* Solutions saturated with air.
† After 400 h.

Specimens of the different materials were tested in quartz ampoules in deaerated solutions at 100°C and in deaerated and air-saturated solutions at room temperature. The solutions were deaerated with argon. Contact and contact-crevice corrosion was studied in boric acid solutions of the first group, the test duration being 100 h.

We studied contact and contact-crevice corrosion of the following pairs of materials: OKh18N10T steel-lead; VT-1-2 alloy-lead; AMg-5 alloy-lead. The gap between specimens in contact-crevice corrosion tests was 0.1 mm.

The corrosion rate of all the specimens was determined by weighing the specimens after removal of the corrosion products. In the case of titanium and steel the corrosion products were removed by 1 N sulfuric acid containing 4M inhibitor (5 ml/liter) with cathode treatment with direct current, density 0.25 amp/dm^2; for aluminum alloy, the corrosion products were boiled in a solution containing 35 g/liter phosphoric acid and 75 g/liter chromium trioxide; in the case of lead, the corrosion products were removed by immersing the specimens in a saturated ammonium acetate solution at room temperature.

As would be expected, stainless steel had a high corrosion resistance in all three solutions at 20 and 100°C. No specimen showed any sign of corrosion.

The corrosion rate of steel increases slightly with the boron content in the solution (from 2.5 to 7.32 g/liter for boric acid, and from 2.5 to 4.85 g/liter for sodium tetraborate solutions) (Table 2).

TABLE 3. Ratio of the Amount of Metal Passing into Solution to the Loss of Metal by Corrosion, %

Solution	Temp., °C	Time, h	Material and test metal				
			OKh18N10T steel (Fe)	20 steel (Fe)	VT-1-2 alloy (Ti)	AMg-5 alloy (Al)	Lead (Pb)
Boric acid	20 *	300	22,9	13,3	Traces	14,7	8,6
		500	53	13,3	»	22,9	Not det.
	20	100	18,4	8,1	»	3,9	Not det.
		500	8	7,15	»	16,9	31
	100	100	15,8	Not det.	»	7,1	Not det.
Sodium tetraborate	20 *	300	13,5	2,8	»	5,1	Not det.
		500	16,6	7,5	»	Not det.	7,6
	20	100	5,38	2,6	»	1,62	3,5
		500	1,88	6,8	»	7,15	4,7
	100	100	10,8	Not det.	»	Not det.	Not det.
Ammonium tetraborate	20 *	300	9	17	»	3,14	31
		500	10,7	14,1	»	Not det.	16,3
	20	100	4	1,5	»	2,2	3,78
		500	4,7	4,6	»	0,695	2,45
	100	100	14,2	Not det.	»	Not det.	Not det.

* Solution saturated with air.

TABLE 4. Corrosion Rates of Materials during 100 h Tests in Boric Acid at 100°C

Material	Contact material	Corrosion rate, g/m² · day	
		contact corrosion	contact-service corrosion
OKh18N10T steel	Lead	0,032	0,048
VT-1-2 alloy	»	0,016	0,06
AMg-5 alloy	»	0,16	0,20
Lead	OKh18N10T steel	1,6	1,08
	VT-1-2 alloy	1,28	1,4
	AMg-5 alloy	0,99	0,78

Alloy VT-1-2 also has a high corrosion resistance in these solutions. The surface of the specimens showed no visible sign of corrosion, and the corrosion rate is comparable with that of OKh18N10T steel.

The corrosion of 20 Steel depends largely on the medium; in boric acid saturated with air this material corrodes at the steady potential in the active state.

In boric acid the corrosion rate slackens a little with time, even at 20°C, this retardation depending on the oxygen content in the solution. In alkaline solutions (ammonium and sodium tetraborate) 20 Steel behaves like stainless steel. After 100 h the corrosion rate of 20 Steel is still markedly higher than that of OKh18N10T steel, but after 500 h the rates are virtually the same. 20 Steel displayed no sign of pitting corrosion, even in solutions containing 3.4 and 4.4 mg/liter O_2 in sodium and ammonium tetraborate respectively.

Corrosion of AMg-5 alloy is uniform but the alloy's resistance depends on the pH.

In boric acid, aluminum alloy has a satisfactory corrosion resistance although much below that of stainless steel.

The alloy behaves in practically the same way in solutions of sodium and ammonium tetraborate, the corrosion rate being nearly tenfold higher than in boric acid. A white flocculent precipitate appeared after tests at 100°C.

The corrosion resistance of lead differed in all three solutions, although the differences were not very great. At 20°C the presence of oxygen increases the corrosion rate somewhat. As regards the corrosion kinetics, the absence of a distinct relation between corrosion and time is noteworthy. Although the corrosion products are retained

on the specimen (there was no crumbling of these products in any case), they do not screen it efficiently. Evans [7] shows that we should distinguish three types of influence of water on lead: 1) the solution process gives a transparent liquid containing dissolved lead salts; 2) a turbid liquid is formed if the lead compounds are present as suspensions; 3) a tight skin is formed and this gradually reduces the influence of water on the metal. In the case studied, corrosion of the first and third types probably occurs.

Chemical analysis of the solutions showed that in experiments on steels more Fe passed into solution in acid media than in alkaline media (Table 3). In the case of AMg-5 alloy the amount of soluble corrosion products formed in acid media is greater than in alkaline media, despite the lower corrosion rate in the former. Practically no titanium passes into solution (cf. Table 3).

The amount of lead passing into solution is considerable in all solutions.

The materials studied corrode uniformly on contact with lead; in all the pairs of materials studied (Table 4) (with the exception of AMg-5 alloy-lead in tetraborate solutions) this metal is the anode.

In every case the corrosion rate of lead increases somewhat on contact with steels, titanium, and aluminum alloy. A further increase in the corrosion rate of lead, due to the presence of the crevice, is only noted in the case of contact with titanium (cf. Table 4).

The currents from the pairs were less than 5 $\mu A/cm^2$ when contact was made, and then decreased to 1 $\mu A/cm^2$.

Aluminum alloy in contact with lead in tetraborate solutions is an exception; in these conditions, aluminum is the anode. But if we bear in mind that in tetraborate solutions aluminum dissolves in the active state, contact with a more positive metal will lead to increasingly higher corrosion rates of aluminum with increasing cathode area.

LITERATURE CITED

1. Nuclear Reactors, Doc. Atomic Energy Commission of the USA, 3 [Russian translation], Moscow, IL (1956).
2. W. Schupp et al., Proc. of the Second International Conference on the Peaceful Uses of Atomic Energy (Geneva, 1958), Selected Reports of Foreign Scientists, 4 [Russian translation], Moscow, Atomizdat (1959), p. 248.
3. W. Zinn et al., Ibid, p. 297.
4. P. Margen et al., Ibid, p. 417.
5. G. Milne et al., Ibid, p. 275.
6. C. Britton and J. Wanklyn, J. Nucl. Materials, 5, 326 (1962).
7. H. R. Evans, Corrosion, Passivity, and Protection of Metals [Russian translation], Moscow–Leningrad, Metallurgizdat (1941).

II ALL-UNION CONFERENCE ON LOW TEMPERATURE PLASMA GENERATORS

L. P. Kudrin

Translated from Atomnaya Énergiya, Vol. 19, No. 6,
pp. 559-561, December, 1965

A conference devoted to physical and applied aspects of low-temperature plasma was held in June 1965 at Novosibirsk. Representatives of several dozen organizations in Moscow, Leningrad, Minsk, Novosibirsk, Alma-Ata, Kiev, and other cities throughout the nation were in attendance. A total of 115 papers were presented.

Three main topics dominated the agenda of the conference: 1) electric arc generators of low-temperature plasmas and their characteristics; 2) generation and properties of plasma and plasma research techniques; 3) applications of low-temperature-plasma generators.

The conference was a demonstration of the notable advances scored in the field of the relatively "old" physics and engineering of plasma (gas discharge, plasma diagnostic techniques) as well as of the progress made in the younger sciences (plasma chemistry, plasma metallurgy). A large number of the experimental papers made fresh and major contributions to the understanding of plasma physics and contributed to the development of industrial plasma facilities. The conference took note at the same time of the lag in theoretical research, which has yet to catch up with experimental research in the field. Electronic computer calculations are not being exploited properly in the work. The development of theoretical research in the field is greatly hampered by the lack of data on kinetic and thermodynamic properties of low-temperature plasma. Still discouragingly meager is information on the cross sections of elementary processes in plasma, particularly on scattering cross sections of slow electrons scattered by atoms and molecules. The thermodynamics of a nonideal plasma where the thermal energy is comparable to the coulomb energy at the mean interparticle distance has not been subjected to theoretical study at all, and even experimental studies have only scratched the surface. The same applies to the kinetic coefficients of low-temperature plasma. The insufficiencies of physics research in this area severely affect the quality of engineering calculations and stress the difficulties encountered in designing concrete plasma devices.

The conference took note of advances in engineering calculations based on similitude theory. The efficiency and power reserves of low-temperature-plasma generators have been improved considerably and plasmotrons requiring no current stabilization have been built. But the pace of this work still lags far behind the demands of industry.

In a resolution adopted, the conference took note of the need for further research on the thermodynamical and kinetic properties of low-temperature plasma, the need to devise standard techniques in the diagnostics of the physical characteristics of plasma, in studying the chemical diagnostics of plasma of involved chemical composition, and in designing new procedures for the diagnostics of nonequilibrium plasma.

The conference focused its attention on the importance of developing power supplies for high-level plasmotrons, on the study of the interaction between the electric arc and an external electric target, on the study of arc stability and the stability of a gas discharge plasma, on the study of possible uses of microwave discharge plasma in chemical processes, the study of heat transfer between a low-temperature plasma and materials being processed, and a number of other salient topics. The conference resolution pointed out the inadequate coordination of research work on low-temperature plasmas.

The large number of papers presented at the conference dealt with physical techniques in the diagnostics of low-temperature plasma. The experiments included measurement of the plasma temperature, the electron concentration, of optical characteristics, and measurement of atomic constants.

All the papers submitted could not be covered in this brief survey. Remarks will be made on some of them.

S. G. Zaitsev, T. V. Zazhenova, Yu. S. Lobastyi, and Yu. S. Lazareva [ÉNIN (Krzhizhanovskii Institute of Power Engng)] proposed a method for measuring electron concentration by absorption of radio waves and by optical refraction; they tested out their method on an argon plasma. Since the refractive index of light is determined pri-

mary by electrons in the optical region and $(n_e-1) \approx N_e\lambda^2$, the electron density N_e can be determined in the region $N_e < N_e^{max} = 10^{15}$ cm^{-3} (here N_e^{max} is determined by the strength of the source) in order to measure the refractive index of the electronic component $n_e(\lambda)$ by the spectrally inverted interference pattern.

A. M. Trokhan [ITiPM, Novosibirsk (Institute of Theoretical and Applied Mechanics)] submitted a paper on cold plasma diagnostics using electron beams. He measured the structure and velocity of the beam, the electron density, and some of the plasma parameters. Trokhan's experiment stands out in the inventiveness of his approach and the elegance of its conception. The flowspeed of the cold plasma (nitrogen) was measured to within 1% accuracy by the fluorescent additive method. The electron concentration was measured by the bremsstrahlung intensity of the electron beam, which produced hard x-rays. This procedure can be useful for measuring the density distribution, as well as point-wise density fluctuations. The temperature of the jet was measured to within 10% by the Doppler broadening of the lines.

G. A. Kasabov (I. V. Kurchatov Institute of Atomic Energy, Moscow) reported an experimental determination of oscillator strengths in cesium. The shifts and Stark broadening of the spectral lines of this Cs atoms in low-temperature plasma were measured ($T_e \simeq 2380$°K). The spectral line shifts were found to be strongly affected by the electron temperature. The electron temperature was measured as independent of whether or not thermodynamic equilibrium had been established. The absolute intensity of the recombination afterglow, the absolute intensity of the spectral lines were measured, the inverted spectrum and the absorption line widths were recorded. Agreement with calculations based on the oscillator strengths was within 10%.

A. A. Ovsyannikov and L. S. Polak measured the temperature distribution over the length of a plasmotron jet, as described in "Optical pyrometry of plasma jets" (INKhS, Moscow), and also measured the distribution over the transverse section of the jet. Temperature measurements in terms of relative and absolute line intensity (of copper) yield surprisingly different values in the argon jet. Temperature measurements in terms of the intensity of the continuum or the width of the H_β line (Saha formula conversion) show that temperature determination by copper lines gives a result too high, other methods referred to give a value too low. One of the conclusions in the paper is that copper line measurements of T cannot be performed in the region T > 5000 to 6000°K (the results yielded by the method are far too low in that region).

Of the few theoretical papers, one deserving of special mention was presented by K. N. Ul'yanov (V. I. Lenin All-Union Electrical Engng. Inst.) on a study of the effect of radiation yield on departures from thermodynamic equilibrium in a plasma. The one-dimensional kinetic equation containing a radiation term was solved. The electron velocity distribution function was derived and balance formulas were derived by integrating the kinetic equation. The problem was solved in the ideal-plasma approximation, so that the solution arrived at is valid for electron densities $N_e \leq 10^{16}$ cm^{-3}. A paper by G. L. Iosel'son (Kharkov State Inst. of Measures and Measuring Instruments) reported electron temperature measurements based on thermal radio-frequency emission with automatic corrections for deviations from black-body radiation. The method proposed makes measurements of T_e to values ≈ 1 eV possible, using already available equipment (electron temperatures to 10 eV can be measured). The measurements were performed in a rather rarefied plasma ($N_e \simeq 10^{12}$ to 10^{14} cm^{-3}), unfortunately.

Other papers submitted at the second session included "Contribution on the use of the tungsten lines 4659 A, 4680 A for plasma jet temperature determinations," by N. G. Zabudkina and L. A. Tonkonoga (Polytechnic Inst., Alma-Ata), "Determination of the collision cross section of alkali metals with low-energy electrons" by V. A. Popov (ÉNIN), "Calculations of a cylindrical arc with radiative transport of energy taken into account" by V. N. Vetlutskii, A. T. Onufriev, and V. G. Sevost'yanenko (Novosibirsk Inst. of Theoret. and Applied Mechanics), and "On spectral techniques in plasma temperature measurements" by A. L. Rudnitskii, as well as some others.

The discussion was very helpful in pointing out the explicit advantages of spectroscopic techniques in plasma diagnostics. Unfortunately, there were no papers presented on laser diagnostics of low-temperature plasma at this conference.

Some of the papers at the first session dealt with criteria-based generalizations of low-temperature plasma parameters using simulitude theory. Interesting papers in this line were "Criterial generalization of the characteristics of eddy-current plasmotrons" by G. Yu. Dautov and M. F. Zhukov (Novosibirsk Inst. of Th. and Appl. Mech.), and a paper by N. M. Belyanin (TsIAM, Moscow). Generalized voltage-current characteristics arrived at in this work facilitate theoretical analysis. The discussion unfolding at the panel sessions revealed, however, that the theory of similitude elaborated to date is still far from complete and incapable of contributing effectively in the synthesis of new plasma devices.

Papers on the synthesis of diagnostic devices were presented. One example is an excellent standard instrument for measuring the temperature of a low-temperature plasma by the relative intensities of cesium lines (Kondyb, Kharkov). This instrument is now on display at the Exposition of Achievements of the National Economy, by the way.

Several important papers were presented at the third session, on applications (industrial included) of low-temperature plasma. "Anisotropy of a low-temperature plasma and optimized MHD generators" by A. S. Plashanov (ÉNIN), "Heat transfer between a lithium plasma and a solid" by E. K. Chekalin and V. S. Shumanov (ÉNIN), and "Effect of solid particulate impurities on electrical conductivity of a high-temperature nitrogen jet" by V. Straupmane and N. Zake (Power Engng. Inst., Riga) should be singled out.

Plasmotrons are being widely used in plasma metallurgy. The conference discussed the use of plasmotrons in high-speed continuous melting of some materials (V. M. Turulin, Cement Machinery Research Inst.), the production of semiconducting and refractory materials in low-temperature plasma (G. Ya. Umarov, S. E. Ermetov, F. R. Karimov, Physics and Engng. Inst., Tashkent), development and research work on electric-arc gas heaters for direct production of iron in pilot-plant operation, and plasma cutting and trimming of ferrous rolled shapes (N. P. Belenko, I. I. Morev, B. S. De, Polytechnic Inst., Alma-Ata), tungsten production by plasma metallurgy (N. N. Rykalin, Metallurg. Inst., Moscow), the design of electric-arc low-temperature plasma generators for rock drilling operations, etc.

The conference also demonstrated advances in plasma chemistry. L. S. Polak and V. S. Shchipachev (INKhS) submitted a report "Production of fixed nitrogen from air and water in a plasma jet, and process optimization," while F. G. Vurzel' and L. S. Polak submitted "Production of unsaturated liquid and gaseous hydrocarbons in a plasma jet." The practical significance of these papers is obvious.

Taken as a whole, the splendidly organized conference (organized under the auspices of the Institute of Theoretical and Applied Mechanics – Siberian Division of the USSR Academy of Sciences) made an important contribution to the understanding of low-temperature plasma physics, and yielded important practical results on both experimental techniques and on industrial applications of low-temperature plasma.

The proceedings of the conference will be published in the periodical "Teplofizika bysokikh temperatur" [High-Temperature Physics] issued by The Academy of Sciences of the USSR.

INDEX

SOVIET ATOMIC ENERGY

Vols. 18 and 19, 1965

SOVIET ATOMIC ENERGY
Vols. 18 and 19, 1965

(A Translation of Atomnaya Énergiya)

E

F

G

I

K

L

M

N

O

P

R

S

T

U

V

W

Y

Z

SOVIET ATOMIC ENERGY

A translation of **ATOMNAYA ÉNERGIYA**
A publication of the Academy of Sciences of the USSR

Volume 18, Number 1 January, 1965

CONTENTS

Annual Subscription: $95 **Single Issue: $30** **Single Article: $15**

CONTENTS (continued)

SOVIET ATOMIC ENERGY

A translation of **ATOMNAYA ÉNERGIYA**
A publication of the Academy of Sciences of the USSR

Volume 18, Number 2 February, 1965

CONTENTS

Annual Subscription: $95 **Single Issue: $30** **Single Article: $15**

CONTENTS (continued)

SOVIET ATOMIC ENERGY

A translation of **ATOMNAYA ÉNERGIYA**
A publication of the Academy of Sciences of the USSR

Volume 18, Number 3 March, 1965

CONTENTS

Annual Subscription: $95 **Single Issue: $30** **Single Article: $15**

CONTENTS (continued)

CONTENTS (continued)

SOVIET ATOMIC ENERGY

A translation of **ATOMNAYA ÉNERGIYA,**
a publication of the Academy of Sciences of the USSR

Vol. 18, No. 4 April, 1965

CONTENTS

Annual Subscription: $95 **Single Issue: $30** **Single Article: $15**

CONTENTS (continued)

SOVIET ATOMIC ENERGY

A translation of **ATOMNAYA ÉNERGIYA,**
a publication of the Academy of Sciences of the USSR

Volume 18, Number 5 May, 1965

CONTENTS

Annual Subscription: $95 **Single Issue: $30** **Single Article: $15**

CONTENTS (continued)

SOVIET ATOMIC ENERGY

A translation of **ATOMNAYA ÉNERGIYA,**
a publication of the Academy of Sciences of the USSR

Volume 18, Number 6 June, 1965

CONTENTS

Annual Subscription: $95 **Single Issue: $30** **Single Article: $15**

CONTENTS (continued)

ATOMNAYA ENERGIYA

SOVIET ATOMIC ENERGY

A translation of **ATOMNAYA ÉNERGIYA,**
a publication of the Academy of Sciences of the USSR

Volume 19, Number 1 July, 1965

CONTENTS

Annual Subscription: $95 **Single Issue: $30** **Single Article: $15**

CONTENTS (continued)

CONTENTS (continued)

SOVIET ATOMIC ENERGY

A translation of **ATOMNAYA ÉNERGIYA,**
a publication of the Academy of Sciences of the USSR

Volume 19, Number 2 August, 1965

CONTENTS

Annual Subscription: $95 **Single Issue: $30** **Single Article: $15**

CONTENTS (continued)

SOVIET ATOMIC ENERGY

A translation of **ATOMNAYA ÉNERGIYA,**
a publication of the Academy of Sciences of the USSR

Volume 19, Number 3 September, 1965

CONTENTS

Annual Subscription: $95 **Single Issue: $30** **Single Article: $15**

CONTENTS (continued)

SOVIET ATOMIC ENERGY

A translation of **ATOMNAYA ÉNERGIYA,**
a publication of the Academy of Sciences of the USSR

Volume 19, Number 4 October, 1965

CONTENTS

Annual Subscription: $95 **Single Issue: $30** **Single Article: $15**

CONTENTS (continued)

SOVIET ATOMIC ENERGY

A translation of **ATOMNAYA ÉNERGIYA,**
a publication of the Academy of Sciences of the USSR

Volume 19, Number 5 November, 1965

CONTENTS

Annual Subscription: $95 **Single Issue: $30** **Single Article: $15**

CONTENTS (continued)

CONTENTS (continued)

NOTE

The Table of Contents lists all material that appears in Atomnaya Énergiya. Items originally published in English or generally available in the West are not included in the translation and are shown in brackets. Whenever possible, the English-language source containing the omitted items is given.

SOVIET ATOMIC ENERGY

A translation of **ATOMNAYA ÉNERGIYA,**
a publication of the Academy of Sciences of the USSR

Volume 19, Number 6 December, 1965

CONTENTS

Annual Subscription: $95 **Single Issue: $30** **Single Article: $15**

CONTENTS (continued)

SOVIET JOURNALS AVAILABLE IN COVER-TO-COVER TRANSLATION

This list includes all Russian journals which—to the publisher's knowledge—were available in cover-to-cover translation on June 30, 1965, or for which definite and immediate plans for cover-to-cover translation had been announced by that date. The list reflects only *current* publication arrangements, but the date and issue listed for first publication refer to translations available from any source. Thus, earlier volumes of a translation journal may have been published by an organization other than that listed as the current publisher, and possibly under a different title (and, for *Doklady Akademii Nauk SSSR*, in a different arrangement of sections).

Five bits of information are furnished, separated by bullets:

1. The abbreviation(s) by which the journals are most frequently referred to in Russian bibliographies (if the name of the journal is customarily spelled out, no abbreviation is given).
2. The transliterated full name of the journal.
3. The full name of the translation journal (in bold type).
4. The year, volume (in parentheses), and issue of first publication of the translation (parentheses are empty if the Russian journal does not use volume numbers).
5. The current publisher of the translation [AGI—American Geological Institute, AGU—American Geophysical Union, AIP—American Institute of Physics, CB—Consultants Bureau, CH—Clearing House for Federal Scientific and Technical Information, CS—The Chemical Society (London), FP—Faraday Press, IEEE— Institute of Electrical and Electronic Engineers, ISA—Instrument Society of America, PP—Pergamon Press].

For convenience in locating bibliographic references the journals are listed in alphabetical order of the *abbreviated* titles.

AÉ • Atomnaya énergiya • **Soviet Journal of Atomic Energy** • 1956(1)1 • CB

Akust. zh. • Akusticheskii zhurnal • **Soviet Physics—Acoustics** • 1955(1)1 • AIP

Astrofiz. • Astrofizika • **Astrophysics** • 1965(1)1 • FP

Astr(on). zh(urn). • Astronomicheskii zhurnal • **Soviet Astronomy—AJ** • 1957(34)1 • AIP

Avtomat. i telemekh. • Avtomatika i telemekhanika • **Automation and Remote Control** • 1956(27)1 • ISA

Avto(mat). svarka • Avtomaticheskaya svarka • **Automatic Welding** • 1959(12)1 • British Welding Research Association

Avtometriya • **Autometry** • 1965(1)1 • CB

Biokhim. • Biokhimiya • **Biochemistry** • 1956(21)1 • CB

Byul. éksp(erim). biol. (i med.) • Byulleten' éksperimental'noi biologii i meditsiny • **Bulletin of Experimental Biology and Medicine** • 1959(41)1 • CB

DAN (SSSR) • *see* Doklady AN SSSR

Defektoskopiya • **Soviet Defectoscopy** • 1965(1)1 • CB

Diff. urav. • Differentsial'nye uravneniya • **Differential Equations** • 1965(1)1 • FP

Dokl(ady) AN SSSR; DAN (SSSR) • Doklady Akademii Nauk SSSR • The translation of Doklady is published in various journals, according to subject matter. The sections of Doklady contained in each of the translation journals are listed in parentheses.

Doklady Biochemistry (biochemistry) • 1957(112)1 • CB

Doklady Biological Sciences Sections (anatomy, cytology, ecology, embryology, endocrinology, evolutionary morphology, parasitology, physiology, zoology) • 1957(112)1 • CB

Doklady Biophysics (biophysics) • 1957(112)1 • CB

Doklady Botany (botany, phytopathology, plant anatomy, plant ecology, plant embryology, plant physiology, plant morphology) • 1957(112)1 • CB

Doklady Chemical Technology (chemical technology) • 1956(106)1 • CB

Doklady Chemistry (chemistry) • 1956(106)1 • CB

Doklady Earth Sciences Sections (geochemistry, geology, geophysics, hydrogeology, lithology, mineralogy, paleontology, permafrost, petrography) • 1959(124)1 • AGI

Doklady Physical Chemistry (physical chemistry) • 1957(112)1 • CB

Doklady Soil Science (soil science) • 1964(154)1 • Soil Science Society of America

Soviet Mathematics—Doklady (mathematics) • 1960(130)1 • American Mathematical Society

Soviet Oceanography (oceanology) • 1959(124)1 • AGU

Soviet Physics—Doklady (aerodynamics, astronomy, crystallography, cybernetics and control theory, electrical engineering, energetics, fluid mechanics, heat engineering, hydraulics, mathematical physics, mechanics, physics, technical physics, theory of elasticity • 1956(106)1 • AIP

Élektrokhimiya • **Soviet Electrochemistry** • 1965(1)1 • CB

Élektrosvyaz' • combined with Radiotekhnika in **Telecommunications and Radio Engineering** • 1957(16)1 • IEEE

Élektrotekh. • Élektrotekhnika • **Soviet Electrical Engineering** • 1965 (36)1 • FP

Éntom(ol). oboz(r). • Éntomologicheskoe obozrenie • **Entomological Review** • 1958(37)1 • Entomological Society of America

Fiz. goreniya i vzryva • Fizika goreniya i vzryva • **Combustion, Explosion, and Shock Waves** • 1965(1) • FP

Fiziol(ogiya) rast. • Fiziologiya rastenii • **Soviet Plant Physiology** • 1957(4)1 • CB

Fiz.-khim. mekh(anika) mater(ialov); FKhMM • Fizikokhimicheskaya mekhanika materialov • **Soviet Materials Science** • 1965(1)1 • FP

Fiz. met. i metallov.; FMM • Fizika metallov i metallovedenie • **Physics of Metals and Metallography** • 1957(5)1 • Acta Metallurgica

Fiz.-tekhn. probl. razr. polezn. iskopaem. • Fizikotekhnicheskie problemy razrabotki poleznykh iskopaemykh • **Soviet Mining Science** • 1965(1)1 • CB

Fiz. tv(erd). tela; FTT • Fizika tverdogo tela • **Soviet Physics—Solid State** • 1959(1)1 • AIP

FKhMM • *see* Fiz.-khim. mekhanika materialov

FMM • *see* Fiz. met. i metallov.

FTT • *see* Fiz. tverd. tela

Geliotekh. • Geliotekhnika • **Applied Solar Energy** • 1965(1)1 • FP

Geol. nefti i gaza • Geologiya nefti i gaza • **Petroleum Geology** • 1958 (2)1 • Petroleum Geology, Box 171, McLean, Va.

Geomagnet. i aéronom. • Geomagnetizm i aéronomiya • **Geomagnetism and Aeronomy** • 1961(1)1 • AGU

Inzh.-fiz. zh. • Inzhenerno-fizicheskii zhurnal • **Journal of Engineering Physics** • 1965(8)1 • FP

Inzh. zh. • Inzhenernyi zhurnal • **Soviet Engineering Journal** • 1965(5)1 • FP

Iskusstv. sputniki Zemli • Iskusstvennye sputniki Zemli • **Artificial Earth Satellites** • 1958(1)1 • CB [superseded by Kosmich. issled.]

Izmerit. tekhn(ika) • Izmeritel'naya tekhnika • **Measurement Techniques** • 1958(7)1 • ISA

Izv. AN SSSR, o(td.) kh(im.) n(auk) (*or* ser. khim.) • Izvestiya Akademii Nauk SSSR: Otdelenie khimicheskikh nauk (*or* Seriya khimicheskaya) • **Bulletin of the Academy of Sciences of the USSR: Division of Chemical Science** • 1952(16)1 • CB

Izv. AN SSSR, ser. fiz(ich). • Izvestiya Akademii Nauk SSSR: Seriya fizicheskaya • **Bulletin of the Academy of Sciences of the USSR: Physical Series** • 1954(18)3 • Columbia Technical Translations

Izv. AN SSSR, ser. fiz. atm. i okeana • Izvestiya Akademii Nauk SSSR: Seriya fiziki atmosfery i okeana • **Izvestiya, Atmospheric and Oceanic Physics** • 1965( )1 • AGU

Izv. AN SSSR, ser. fiz. zemli • Izvestiya Akademii Nauk SSSR: Seriya fiziki zemli • **Izvestiya, Physics of the Solid Earth** • 1965( )1 • AGU

Izv. AN SSSR, ser. geofiz. • Izvestiya Akademii Nauk SSSR: Seriya geofizicheskaya • **Bulletin of the Academy of Sciences of the USSR: Geophysics Series** • 1957(7)1 • AGU [superseded by Izv. AN SSSR, ser. fiz. atm. i okeana and Izv. AN SSSR, ser. fiz. zemli]

Izv. AN SSSR, ser. geol. • Izvestiya Akademii Nauk SSSR: Seriya geologicheskaya • **Bulletin of the Academy of Sciences of the USSR: Geologic Series** • 1958(23)1 • AGI

Izv. AN SSSR, ser. neorgan. mat(er). • Izvestiya Akademii Nauk SSSR: Seriya neorganicheskie materialy • **Inorganic Materials** • 1965(1) 1 • CB

Izv. AN SSSR, tekhn. kiber(netika) • Izvestiya Akademii Nauk SSSR: Tekhnicheskaya kibernetika • **Engineering Cybernetics** • 1963(1)1 • IEEE

Izv. v(yssh.) u(ch.) z(av.) aviats. tekh. • Izvestiya vysshikh uchebnykh zavedenii. Aviatsionnaya tekhnika • **Aviation Engineering** • 1963(6)1 • CH

Izv. v(yssh.) u(ch.) z(av.) fiz. • Izvestiya vysshikh uchebnykh zavedenii. Fizika • **Soviet Physics Journal** • 1965(8)1 • FP

Izv. v(yssh.) u(ch.) z(av.) geodez. i aérofot. • Izvestiya vysshikh uchebnykh zavedenii. Geodeziya i aérofotos"emka • **Geodesy and Aerophotography** • 1959(4)1 • AGU

Izv. v(yssh.) u(ch.) z(av.) priborostr. • Izvestiya vysshikh uchebnykh zavedenii. Priborostroenie • **Izvestiya VUZOV. Instrument Building** • 1962(5)1 • CH

Izv. v(yssh.) u(ch.) z(av.) radiofiz. • Izvestiya vysshikh uchebnykh zavedenii. Radiofizika • **Izvestiya VUZOV. Radiophysics** • 1958(1)1 • CH

Izv. v(yssh.) u(ch.) z(av.) radiotekhn(ika) • Izvestiya vysshikh uchebnykh zavedenii. Radiotekhnika • **Izvestiya VUZOV. Radio Engineering** • 1959(2)1 • CH

Izv. v(yssh.) u(ch). z(av.) tekh. teks. prom. • Izvestiya vysshikh uchebnykh zavedenii. Tekhnologiya tekstilnoi promyshlennosti • **Technology of the Textile Industry, USSR** • 1960(4)1 • The Textile Institute (Manchester)

Kauch. i rez. • Kauchuk i rezina • **Soviet Rubber Technology** • 1959 (18)3 • Maclaren and Sons Ltd.

Khim. getero(tsik). soed. • Khimiya geterotsiklicheskikh soedinenii • **Chemistry of Heterocyclic Compounds** • 1965(1)1 • FP

Khim. i neft. mash(inostr). • Khimicheskoe i neftyanoe mashinostroenie • **Chemical and Petroleum Engineering** • 1965( )1 • CB

Khim. i tekhnol. topliv i masel • Khimiya i tekhnologiya topliv i masel • **Chemistry and Technology of Fuels and Oils** • 1965( )1 • CB

Khim. prirod. soed. • Khimiya prirodnykh soedinenii • **Chemistry of Natural Compounds** • 1965(1)1 • FP

Kib. • Kibernetika • **Cybernetics** • 1965(1)1 • FP

Kinet. i katal. • Kinetika i kataliz • **Kinetics and Catalysis** • 1960(1)1 • CB

Koks i khim. • Koks i khimiya • **Coke and Chemistry, USSR** • 1959( )8 • Coal Tar Research Assn. (Leeds, England)

Kolloidn. zh(urn). • Kolloidnyi zhurnal • **Colloid Journal** • 1952(14)1 • CB

Kosmich. issled. • Kosmicheskie issledovaniya • **Cosmic Research** • 1963(1)1 • CB

Kristallog. • Kristallografiya • **Soviet Physics—Crystallography** • 1957 (2)1 • AIP

Liteinoe proiz(-vo). • Liteinoe proizvodstvo • **Russian Castings Production** • 1961(12)1 • British Cast Iron Research Association

Mag. gidrodin. • Magnitnaya gidrodinamika • **Magnetohydrodynamics** • 1965(1)1 • FP

Mekh. polim. • Mekhnika polimerov • **Polymer Mechanics** • 1965(1)1 • FP

Metalloved. i term. obrabotka metal.; MiTOM • Metallovedenie i termicheskaya obrabotka metallov • **Metal Science and Heat Treatment** • 1958(6)1 • CB

Metallurg • **Metallurgist** • 1957( )1 • CB

Mikrobiol. • Mikrobiologiya • **Microbiology** • 1957(26)1 • CB

MiTOM • *see* Metalloved. i term. obrabotka metal.

Ogneupory • **Refractories** • 1960(25)1 • CB

Opt. i spektr.; OS • Optika i spektroskopiya • **Optics and Spectroscopy** • 1959(6)1 • AIP

Osnovan. fund. i mekh. gruntov • Osnovaniya fundamenty i mekhanika gruntov • **Soil Mechanics and Foundation Engineering** • 1964 ( )1 • CB

Paleon. zh(urn). • Paleontologicheskii zhurnal • **Journal of Paleontology** • 1962( )1 • AGI

Plast. massy • Plasticheskie massy • **Soviet Plastics** • 1960(8)7 • Rubber and Technical Press, Ltd.

PMM • *see* Prikl. matem. i mekhan.

PMTF • *see* Zhur. prikl. mekhan. i tekhn. fiz.

Pochvovedenie • **Soviet Soil Science** • 1958(53)1 • Soil Science Society of America

Poroshk. met. • Poroshkovaya metallurgiya • **Soviet Powder Metallurgy and Metal Ceramics** • 1962(2)1 • CB

Priborostroenie • **Instrument Construction** • 1959(4)1 • Taylor and Francis, Ltd.

Pribory i tekhn. éksp(erimenta); PTÉ • Pribory i tekhnika éksperimenta • **Instruments and Experimental Techniques** • 1958(3)1 • ISA

Prikl. biokhim. i mikrobiol. • Prikladnaya biokhimiya i mikrobiologiya • **Applied Biochemistry and Microbiology** • 1965(1)1 • FP

Prikl. matem. i mekh(an).; PMM • Prikladnaya matematika i mekhanika • **Applied Mathematics and Mechanics** • 1958(22)1 • PP

Probl. pered. inform. • Problemy peredachi informatsii • **Problems of Information Transmission** • 1965(1)1 • FP

Probl. severa • Problemy severa • **Problems of the North** • 1958( )1 • National Research Council of Canada

PTÉ • *see* Pribory i tekhn. éksperimenta

Radiokhim. • Radiokhimiya • **Soviet Radiochemistry** • 1962(4)1 • CB

Radiotekh. • Radiotekhnika • combined with Élektrosvyaz' in **Telecommunications and Radio Engineering** • 1961(16)1 • IEEE

Radiotekhn. i élektron(ika) • Radiotekhnika i élektronika • **Radio Engineering and Electronic Physics** • 1961(6)1 • IEEE

Stal' • **Stal' in English** • 1959(19)1 • The Iron and Steel Institute

Stanki i instr. • Stanki i instrument • **Machines and Tooling** • 1959 (30)1 • Production Engineering Research Association

Stek. i keram. • Steklo i keramika • **Glass and Ceramics** • 1956(13)1 • CB

Svaroch. proiz(-vo). • Svarochnoe proizvodstvo • **Welding Production** • 1959(5)4 • British Welding Research Association (London)

Teor. i éksperim. khim. • Teoreticheskaya i éksperimental'naya khimiya • **Theoretical and Experimental Chemistry** • 1965(1)1 • FP

Teor. veroyat. i prim. • Teoriya veroyatnostei i ee primenenie • **Theory of Probability and Its Application** • 1956(1)1 • Society for Industrial and Applied Mathematics

Teploénergetika • **Thermal Engineering** • 1964(11)1 • PP

Teplofiz. vys(ok). temp. • Teplofizika vysokikh temperatur • **High Temperature** • 1963(1)1 • CB

Tsvet. metally • Tsvetnye metally • **The Soviet Journal of Nonferrous Metals** • 1960(33)1 • Primary Sources

Usp. fiz. nauk; UFN • Uspekhi fizicheskikh nauk • **Soviet Physics—Uspekhi** • 1958(66)1 • AIP

Usp. khim.; UKh • Uspekhi khimii • **Russian Chemical Reviews** • 1960(29)1 • CS

Usp. mat. nauk; UMN • Uspekhi matematicheskaya nauk • **Russian Mathematical Surveys** • 1960(15)1 • Cleaver-Hume Press, Ltd.

Vest. Akad. med. nauk SSSR • Vestnik Akademii meditsinskikh nauk SSSR • **Vestnik of USSR Academy of Medical Sciences** • 1962(17)1 • CH

Vest. mashinostroeniya • Vestnik mashinostroeniya • **Russian Engineering Journal** • 1959(39)4 • Production Engineering Research Association

Vest. svyazi • Vestnik svyazi • **Herald of Communications** • 1954(14)1 • CH

Vysoko(molek). soed(ineniya) • Vysokomolekulyarnye soedineniya (SSSR) • **Polymer Science (USSR)** • 1959(1)1 • PP

Yadernaya fizika • **Soviet Journal of Nuclear Physics** • 1965(1)1 • AIP

Zashch(ita) met(allov) • Zashchita metallov • **Protection of Metals** • 1965(1)1 • CB

Zav(odsk). lab(oratoriya); ZL • Zavodskaya laboratoriya • **Industrial Laboratory** • 1958(24)1 • ISA

ZhÉTF pis'ma redaktsiyu • **JETP Letters** • 1965(1)1 • AIP

Zh(ur). anal(it). khim(ii); ZhAKh • Zhurnal analiticheskoi khimii • **Journal of Analytical Chemistry** • 1952(7)1 • CB

Zh(ur). éks(perim). i teor. fiz.; ZhÉTF • Zhurnal éksperimental'noi i teoreticheskoi fiziki • **Soviet Physics—JETP** • 1955(28)1 • AIP

Zh(ur). fiz. khimii; ZhFKh • Zhurnal fizicheskoi khimii • **Russian Journal of Physical Chemistry** • 1959(33)7 • CS

Zh(ur). neorg(an). khim.; ZhNKh • Zhurnal neorganicheskoi khimii • **Russian Journal of Inorganic Chemistry** • 1959(4)1 • CS

Zh(ur). obshch. khim.; ZhOKh • Zhurnal obshchei khimii • **Journal of General Chemistry of the USSR** • 1949(19)1 • CB

Zh(ur). org. khim.; ZhOrKh(im) • Zhurnal organicheskoi khimii • **Journal of Organic Chemistry of the USSR** • 1965(1)1 • CB

Zh(ur). prikl. khim.; ZhPKh • Zhurnal prikladnoi khimii • **Journal of Applied Chemistry of the USSR** • 1950(23)1 • CB

Zh(ur). prikl. mekhan. i tekhn. fiz. • Zhurnal prikladnoi mekhaniki i tekhnicheskoi fiziki • **Journal of Applied Mechanics and Technical Physics** • 1965( )1 • FP

Zh(ur). prikl. spektr. • Zhurnal prikladnoi spektroskopii • **Journal of Applied Spectroscopy** • 1965(2)1 • FP

Zh(ur). strukt(urnoi) khim.; ZhSKh • Zhurnal strukturnoi khimii • **Journal of Structural Chemistry** • 1960(1)1 • CB

Zh(ur). tekhn. fiz.; ZhTF • Zhurnal tekhnicheskoi fiziki • **Soviet Physics—Technical Physics** • 1956(26)1 • AIP

Zh(ur). vses. khim. ob-va im. Mendeleeva • Zhurnal vsesoyuznogo khimicheskogo obshchestva im. Mendeleeva • **Mendeleev Chemistry Journal** • 1965(10)1 • FP

Zh(ur). vychis. mat. i mat. fiz. • Zhurnal vychislitel'noi matematika i matematicheskoi fiziki • **USSR Computational Mathematics and Mathematical Physics** • 1962(1)1 • PP

ZL • *see* Zavodsk. laboratoriya

SIGNIFICANCE OF ABBREVIATIONS MOST FREQUENTLY ENCOUNTERED IN SOVIET PERIODICALS

FIAN	Phys. Inst. Acad. Sci. USSR.
GDI	Water Power Inst.
GITI	State Sci.-Tech. Press
GITTL	State Tech. and Theor. Lit. Press
GONTI	State United Sci.-Tech. Press
Gosenergoizdat	State Power Press
Goskhimizdat	State Chem. Press
GOST	All-Union State Standard
GTTI	State Tech. and Theor. Lit. Press
IL	Foreign Lit. Press
ISN (Izd. Sov. Nauk)	Soviet Science Press
Izd. AN SSSR	Acad. Sci. USSR Press
Izd. MGU	Moscow State Univ. Press
LEIIZhT	Leningrad Power Inst. of Railroad Engineering
LET	Leningrad Elec. Engr. School
LETI	Leningrad Electrotechnical Inst.
LETIIZhT	Leningrad Electrical Engineering Research Inst. of Railroad Engr.
Mashgiz	State Sci.-Tech. Press for Machine Construction Lit.
MEP	Ministry of Electrical Industry
MES	Ministry of Electrical Power Plants
MESEP	Ministry of Electrical Power Plants and the Electrical Industry
MGU	Moscow State Univ.
MKhTI	Moscow Inst. Chem. Tech.
MOPI	Moscow Regional Pedagogical Inst.
MSP	Ministry of Industrial Construction
NI ZVUKSZAPIOI	Scientific Research Inst. of Sound Recording
NIKFI	Sci. Inst. of Modern Motion Picture Photography
ONTI	United Sci.-Tech. Press
OTI	Division of Technical Information
OTN	Div. Tech. Sci.
Stroiizdat	Construction Press
TOE	Association of Power Engineers
TsKTI	Central Research Inst. for Boilers and Turbines
TsNIEL	Central Scientific Research Elec. Engr. Lab.
TsNIEL-MES	Central Scientific Research Elec. Engr. Lab.-Ministry of Electric Power Plants
TsVTI	Central Office of Economic Information
UF	Ural Branch
VIESKh	All-Union Inst. of Rural Elec. Power Stations
VNIIM	All-Union Scientific Research Inst. of Metrology
VNIIZhDT	All-Union Scientific Research Inst. of Railroad Engineering
VTI	All-Union Thermotech. Inst.
VZEI	All-Union Power Correspondence Inst.

Note: Abbreviations not on this list and not explained in the translation have been transliterated, no further information about their significance being available to us —Publisher.

Mass Spectrometry

Theory and Applications

By R. Jayaram
Geophysical Institute, University of Alaska

The first half of this unique book provides a lucid and thorough introduction to the principles of mass spectrometers. The second half features the applications of nonmagnetic mass spectrometers to upper atmospheric research, describing problems in the performance of satellite experiments and instruments for the direct study of the ion and neutral atom composition of the upper atmosphere. Other topics include composition studies using rocket- and satellite-borne mass spectrometers, the IGY rocket measurements of Arctic atmosphere composition above 100 km, an emission current regulator for rf mass spectrometers, a theory to determine ionic masses in rf spectrometers in flight, a two stage single frequency rf analyzer for exosphere research, the results of Soviet experiments with rf mass spectrometers, composition studies with quadrupole and time-of-flight mass spectrometers, a quadrupole mass spectrometer for D and lower E region composition measurements, a conventional magnetic mass spectrometer designed for an aeronomy satellite, and particular experimental and engineering problems.

OF INTEREST TO: researchers and students in physics involved in mass spectrometry, atmospheric physics and space physics researchers, and instrumentation specialists working on analytical problems with special reference to mass spectrometry.

Approx. 220 pages 1966 $12.50

PLENUM PRESS 227 West 17th Street, New York, New York 10011
A DIVISION OF PLENUM PUBLISHING CORPORATION